MSc by Research Cardiovascular Science - Thesis

PROJECT REPORT

Using Mouse and Cellular Models to Investigate the *ACTN2* M228T Variant in the Heart and its Link to Cardiac Disease

Kirsty Wadmore

14th October 2021

UNIVERSITY OF BIRMINGHAM | INSTITUTE OF CARDIOVASCULAR SCIENCES

Acknowledgments:

I would like to thank my supervisor Katja Gehmlich for all her help with my project and for helping me co-write and publish my first review.

I would also like to thank Dr Sophie Broadway-Stringer and Dr Jasmeet Reyat for all their help with laboratory techniques and understanding.

Finally, I would like to say a special thank you to Amar Azad and Max Cumberland for supporting and helping me throughout my project.

Table of Contents

Figures/tables:

Figures:

Tables:

Abbreviations:

1. Actin alpha 1 (ACTA1)
2. Actin binding domain (ABD)
3. Activin A (AA)
4. Angiotensin-converting enzyme inhibitor (ACE-I)
5. Arrhythmogenic right ventricular cardiomyopathy (ARVC)
6. Atrial fibrillation (AF)
7. Body weight to tibia length ratio (BW/TL)
8. Bone morphogenic protein 4 (BMP4)
9. Bovine serum albumin (BSA)
10. Cardiac troponin T (CTNT)
11. Cardiomyopathies (CMs)
12. Cardiovascular disease (CVD)
13. Cardiovascular magnetic resonance imaging (CMRI)
14. CHIR99021 (CHIR)
15. Clustered regularly interspaced short palindromic repeats (CRISPR)
16. Cyclin-dependent kinase 13 (CDK13)
17. Cysteine and glycine rich protein 3 (CSRP3)
18. Denaturing high performance liquid chromatography (DHPLC)
19. Dilated cardiomyopathy (DCM)
20. EF hand (EFh)
21. Embryonic day 15.5 (E15.5)
22. Embryonic stem cells (ESCs)
23. Engineered heart tissue (EHT)

24. Epithelial-to-mesenchymal transition (EMT)
25. Essential E8 medium (E8)
26. Ethylenediaminetetraacetic acid (EDTA)
27. Filamin C (FLNC)
28. Fluorescence assisted cell sorting (FACS)
29. Glyceraldehyde 3-phosphate dehydrogenase (GAPDH)
30. Heart failure (HF)
31. Heart failure with reduced ejection fraction (HFrEF)
32. Heart weight to body weight ratio (HW/BW)
33. Heart weight to tibia length ratio (HW/TL)
34. Heat shock protein 27 (HSP27)
35. Heat shock protein family B (small) member 7 (HSPB7)
36. Heterozygous (Het)
37. Homozygous (Hom)
38. Hypertrophic cardiomyopathy (HCM)
39. Hypoxanthine-guanine phosphoribosyl transferase (HPRT)
40. Induced pluripotent stem cell cardiomyocytes (iPSC-CMs)
41. Induced pluripotent stem cells (iPSCs)
42. Isovolumic relaxation time (IVRT)
43. IWR-1-endo (IWR-1)
44. Knock-out (KO)
45. Left ventricular hypertrophy (LVH)
46. Left ventricular non-compaction (LVNC)
47. Matrigel (Mtg)
48. Minor allele frequency (MAF)

49. Muscle LIM protein (MLP)

50. Myosin binding protein C (MYBPC3)

51. Myotilin (MYOT)

52. Natriuretic peptides A (NPPA)

53. Natriuretic peptides B (NPPB)

54. Overall survival (OS)

55. p.Met228Thr (M228T)

56. Paraformaldehyde (PFA)

57. Phosphate-buffered saline (PBS)

58. Polymerase chain reaction (PCR)

59. Primary heart field (PHF)

60. Protospacer adjacent motif (PAM)

61. Restrictive cardiomyopathy (RCM)

62. Secondary heart field (SHF)

63. Single guide RNS (sgRNA)

64. Single stranded oligonucleotide (ssODN)

65. Sodium hydroxide (NaOH)

66. Spectrin like repeat (SR)

67. Ubiquitin proteasome system (UPS)

68. Vitronectin (Vtn)

69. Wild type (WT)

70. α 1 skeletal muscle actin (ACTA1)

71. α-actinin 1 (ACTN1)

72. α-actinin 2 (ACTN2)

73. α-actinin 3 (ACTN3)

74. α-actinin 4 (ACTN4)

75. β-myosin-heavy chain (β-MHC) (MYH7)

1. Abstract

The Z-disc acts as a protein-rich structure to tether thin filament in the contractile units also known as sarcomeres, of striated muscle cells. Numerous proteins interact in the Z-disc and are integral for maintaining the architecture of the sarcomere, while facilitating force transduction and intracellular signalling in both cardiac and skeletal muscle. Pathogenic variants in Z-disc proteins can cause diseases, e.g. cardiomyopathies. These are diseases of the heart muscle, affecting its structure and function which ultimately impede the hearts ability to pump blood around the body. They can also be associated with a high risk of sudden cardiac death. This project focused on the Z-disc sarcomeric α-actinin 2 (*ACTN2*) and its link to cardiomyopathies. Pathogenic variants in the gene coding for *ACTN2* have been identified and linked to cardiomyopathies, although there is limited understanding about the mechanisms involved. *Actn2* M228T mouse and cellular models were used to test the impact of this pathogenic variant on cardiac hypertrophy and to explore underlying disease mechanisms. Morphometrics of wild type (WT) and heterozygous (Het) adult mice were used to test for hypertrophic differences between mice of different ages and sexes. Western blots were performed on adult mouse hearts to investigate protein expression of hypertrophic markers. While increased protein expression of hypertrophic markers was observed suggesting molecular changes occurred, this was not translated into pathological signs of hypertrophy such as changes in heart weight. The homozygous (Hom) variant resulted in embryonic lethality, however no developmental delay was detected by Theiler staging at embryonic day 15.5 embryos. Both gene and protein expression were explored in hearts from homozygous embryos. An increase in *Actn2* transcript expression saw a down-regulation of the corresponding Actn2 protein, suggesting degradation of the aberrant protein. Increased expression of *Actn3* was not translated at the protein level and suggests Actn3 cannot compensate for reduction of Actn2. Increased expression was seen for genes involved in the

foetal gene programme and supports enhancement of this programme in the presence of this genetic variant. Reduced colocalisation of *Actn2* and titin seen in homozygous embryos further suggests disorganisation of sarcomeres, a feature seen in some instances of hypertrophy. Preliminary results in an induced pluripotent stem cell (iPSC) line homozygous for the variant, further suggest less mature sarcomeres in the homozygous *ACTN2* M228T variant compared to the KOLFC2 parental WT. Future work should aim to phenotype this line further. Overall, these data support the pathogenic role of *ACTN2* M228T in the development of cardiomyopathy and cardiac disease.

2. Introduction

2.1 The heart

The mammalian heart is a muscular organ comprised of four morphologically distinct chambers; the left/right atria, and the left/right ventricles. These chambers are separated by the interventricular and interatrial septa. Deoxygenated blood enters the right side of the heart before being pumped to the lungs, whilst oxygenated blood enters the left side and is pumped around the rest of the body. When the ventricles fill with blood (relax) the heart is in the diastolic part of the cardiac cycle and when the ventricles eject blood (contract), the heart is in the systolic part of the cardiac cycle [1]. Ventricular-arterial and atrio-ventricular values ensure that this flow of blood is one-directional only. Modified cardiac cells called Purkinje fibres extend from the sinoatrial node to the atrioventricular node and finally to the apex of the heart where contraction is initiated from electrical signals. Three main cardiac layers form the heart muscle; the inner layer endocardium, the middle myocardium and the outer epicardium. Heart muscle is composed of 11 functionally different cell types: endothelial, mesothelial, fibroblasts, pericytes, adipocytes, smooth muscle, neuronal, atrial cardiomyocytes, ventricular cardiomyocytes, lymphoid and myeloid cells [2]. The dominating cell type by mass (not by numbers) are the cardiomyocytes. Individual cardiac muscle cells are connected by regions called intercalated discs which allow the conduction of electrical impulses between cardiac myocytes. These cell-to-cell contacts are facilitated by different junctions: the adherens junctions (fascia adherens), desmosomes (macula adherens) and gap junctions [3]. The fascia adherens act as an anchoring site for actin filaments and interconnect actin filaments of neighbouring cells, whilst desmosomes interconnect the intermediate filaments of adjacent cells [4]. Gap junctions allow the passage of ions between cells and facilitate the movement of action potentials, therefore enabling depolarisation of the heart and synchronised contraction of the cardiomyocytes. One gap junction is formed of 6

connexin proteins that form a connexon/hemichannel that docks with another connexon. Three connexin proteins have so far been identified in cardiomyocytes: connexin 40 (Cx40), connexin 43 (Cx43) and connexin 45 (Cx45), with Cx43 being the dominant type in the ventricles [5].

2.2 The sarcomere

Each cardiac myocyte is made up of myofibrils that form cylindrical bundles within striated muscle [6]. Within the myofibrils are repeating components called sarcomeres that act as the main contractile units of cardiac (and skeletal) muscle cells. These sarcomeric regions of the myofilament lie between two Z-discs and are composed of both thick and thin filaments [7]. The thick filament's key component is myosin and forms the central A-band of the sarcomere, whilst the main component of the thin filament is actin which forms the I-band. The H-band is an area in the A-band where the thick filaments are the only longitudinal elements and the M-band is the central region of the H-band where cross-links of the thick filament are present and allow a network to form [6]. In order to contract, thin filaments are brought towards the M-line by the attachment/detachment of myosin heads from appropriate actin binding sites. Several other proteins have been identified to facilitate the interaction of the thick and thin filaments and therefore assist in the contraction of cardiomyocytes. These include proteins such as tropomyosin, troponins, tropomodulin and α-actinin (on the thin filament) as well as myomesin and myosin binding protein C (on the thick filament) [8]. It has been found that pathogenic variants of these proteins can affect the ability of striated muscles to contract and may therefore cause skeletal muscle diseases and/or cardiomyopathies [9, 10].

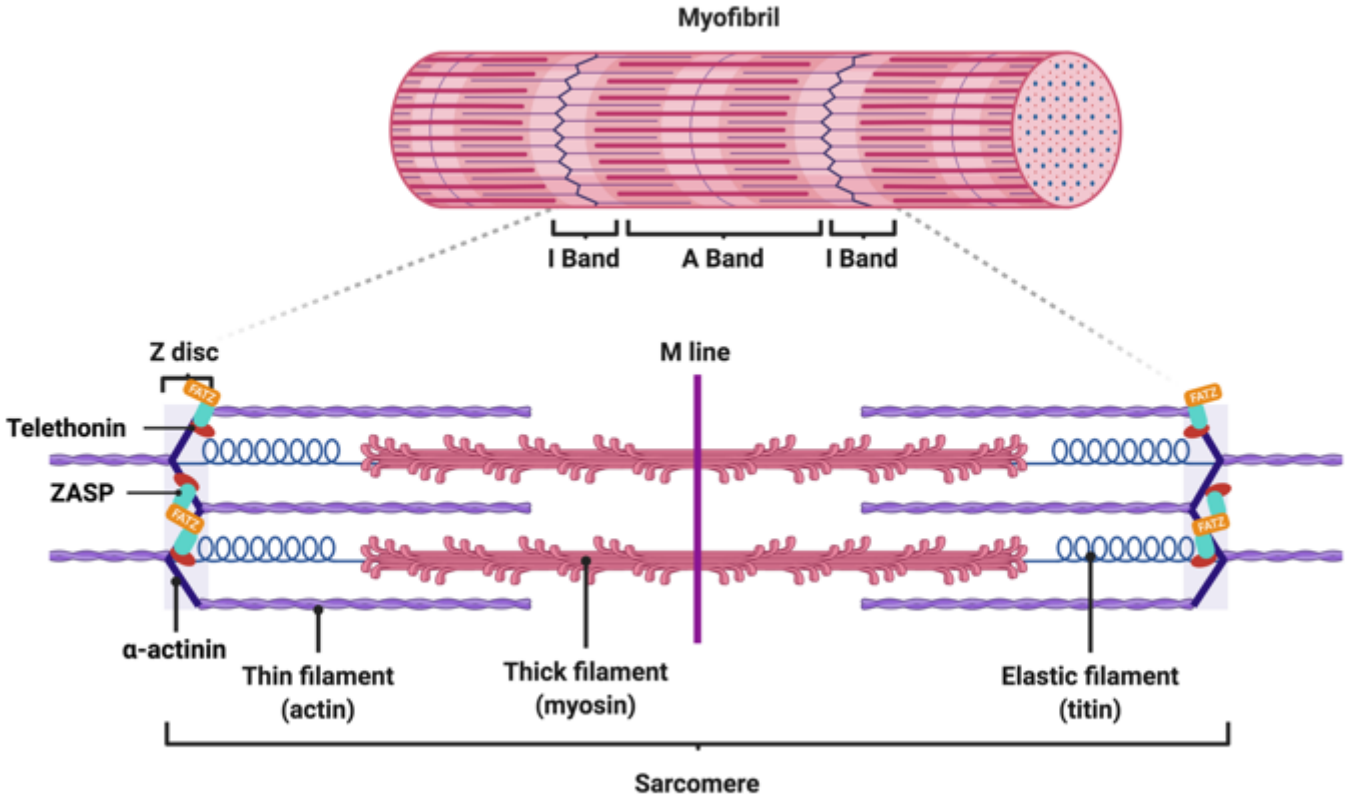

Figure 1. Schematic of the structure of the sarcomere within the myofibril, showing the location of α-actinin and some of its binding partners within the Z-disc. Created with BioRender.com.

2.3 Cardiovascular disease

Cardiovascular disease (CVD) is a group of heterogeneous diseases which affect both the heart and circulatory systems [11] (blood vessels). CVDs are chronic and gradually evolving diseases that are still one of the leading causes for premature mortality across the world. The pathogenesis of nearly all CVDs originates and progresses from atherosclerosis [12] (the build-up of plaque in artery walls). This then leads to the development of diseases such as coronary artery disease and peripheral vascular disease, which in turn may cause myocardial infarction and cardiac arrhythmias. Cardiomyopathies, a particular group of heart muscle

diseases, are an important cause of heart failure (HF) [13]. Risk factors of CVD include those of an aetiological onset such as hypertension, hyperlipidaemia, obesity, diabetes and smoking. Prevention of these risk factors helps in the reduction of this global epidemic. Where lifestyle changes are not enough, other treatments of CVD will include drugs, interventional and device treatment. Drugs prescribed may be ACE-I (angiotensin-converting enzyme inhibitor), an anticoagulant or beta blocker [14], to name only a few. If drug intervention is not sufficient and the patient's heart failure is advanced, device implantation of a left ventricular assist device may occur. If this is not enough to help patient survival, heart transplantation may be the only viable option.

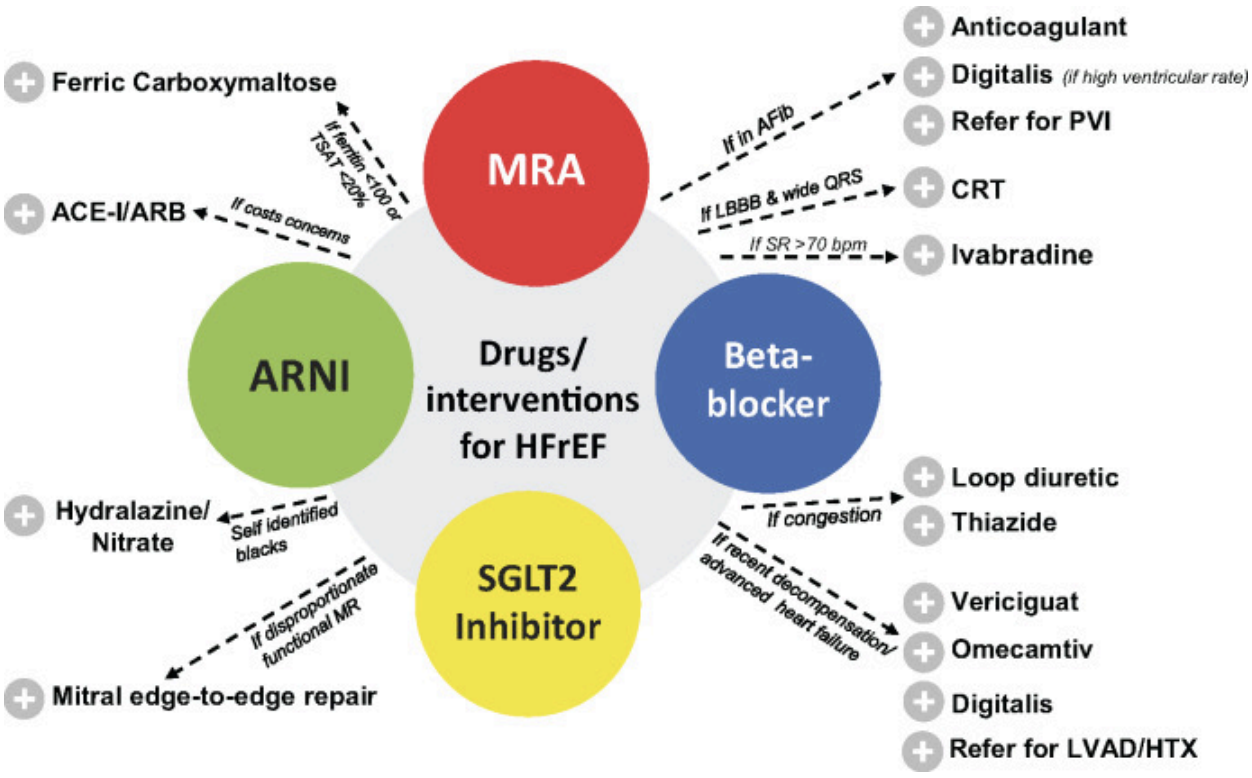

Figure 2. Figure taken from [14]. Drug, interventional, and device treatment for heart failure with reduced ejection fraction (HFrEF). Systolic HF (HFrEF) is the form of HF that is relevant for most cardiomyopathies [15] [13]. ACE-I, angiotensin-converting enzyme inhibitor; Afib, atrial fibrillation; ARB, angiotensin receptor blocker; ARNI, angiotensin

receptor/neprilysin inhibitor; CRT, cardiac resynchronization therapy; HTX, heart transplantation; LBBB, left bundle branch block; LVAD, left ventricular assist device; MR, mitral regurgitation; MRA, mineralocorticoid receptor antagonist; PVI, pulmonary vein isolation; SGLT2, sodium–glucose co-transporter 2; SR, sinus rhythm; TSAT, transferrin saturation.

2.4 Cardiomyopathies

One type of cardiovascular disease are cardiomyopathies. Cardiomyopathies (CMs) are a group of heterogeneous heart muscle diseases that can be classified as being either genetic, mixed or acquired [16]. This project aimed to focus on cardiomyopathies that have a genetic cause and are therefore a familial and inherited disease. Different types of cardiomyopathies can also be classified according to their function and which structures and systems are affected by these morphological features [9]. The majority of CMs are inherited as an autosomal dominant trait, meaning there is a 50% risk for first degree relatives of those with the disease. These are predominantly due to pathogenic missense variants (apart from myosin binding protein C, *MYBPC3*, which is characterised by loss of function changes) where only a single amino acid is changed. This can ultimately lead to progressive heart failure, arrhythmias and sudden cardiac death.

Hypertrophic cardiomyopathy

Hypertrophic cardiomyopathy (HCM) is the most common form of CM and is reported to have a prevalence of 1:500 people based on the CARDIA (Coronary Artery Risk Development in Young Adults) cohort study [17]. 50% of patients with HCM show a familial/genetic cause of the disease. HCM is characterised by an abnormally thick and stiff myocardium and as a result, filling of the ventricles might be impaired (diastolic dysfunction). The main pathogenic variants are found in gene proteins encoding both the

thick and thin contractile myofilaments in the sarcomere. These pathogenic variants have been found in the cardiac myosin binding protein C and the beta-myosin heavy chain in the thick filament, as well as mutations in the troponin complex and cardiac actin that are found in the thin filaments [18]. Two main mechanisms of HCM have been identified that result from the underlying mutations and contribute to the phenotypic nature of the disease. Firstly, there are changes in the handling of Ca^{2+} during the contractile cycle in the heart [19, 20]. An alternative mechanism results from inefficient use of ATP during contractions of the heart, which leads to an impaired force production [9]. Both of these mechanisms cause diastolic dysfunction, meaning that the ventricles cannot fill properly due to impaired relaxation. Key features of HCM include fibrosis, myocardial disarray and sudden cardiac death (through ventricular arrhythmias) [21].

Dilated cardiomyopathy

Dilated cardiomyopathy (DCM) has been found to have a genetic cause in 35% of patients and results in the heart muscle becoming extremely thin and weak. It has a prevalence of approximately 1:2500 in the general population [18]. Enlargement of the left ventricle is commonly seen, and the pump function of the heart is impaired (systolic dysfunction). In approximately 25% of patients with familial DCM, the sarcomeric protein titin has been truncated and the reading frame has been disrupted, leading to the pathogenic variant seen in the disease [22]. Other cytoskeletal genes involved in force transduction may also be affected, including those such as dystrophin and vinculin [23, 24].

Restrictive cardiomyopathy

Restrictive cardiomyopathy (RCM) can have a familial cause if there is a pathogenic variant found in the gene encoding for Filamin C (*FLNC*). A pathogenic variant in this sarcomeric protein will result in the stiffening of the heart and diastolic dysfunction, similar to that described for HCM [25].

Arrhythmogenic right ventricular cardiomyopathy

Arrhythmogenic right ventricular cardiomyopathy (ARVC) has a prevalence of 1:2000 [18] and its common disease genes code for proteins of the desmosome. Desmosomal proteins provide physical strength between neighbouring cells, they are a sub-structure within the intercalated discs; if these desmosomes are weakened through pathogenic variants then the gap junctions between cells are affected and both cell adhesion and intracellular communication become impaired. ARVC can affect either the left or right ventricle or both. It leads to cell detachment and death. This in turn results in scarring of the heart and a build-up of fibrous tissue and fatty deposits. When the ventricle walls become too thin and stretched, this causes abnormal heart rhythms/arrhythmias. Altered signalling of the Wnt/beta-catenin pathway downstream of plakoglobin, a key desmosomal component, has been suggested as the underlying mechanism of ARVC [9].

Left ventricular non-compaction

Left ventricular non-compaction (LVNC) is described as a rare form of CM with a cause that is not yet fully understood [26]. It is thought that the compaction of loose myocardial cells is halted during development, meaning the myocardium is 'spongy' and the left ventricle is susceptible to systolic dysfunction. This results in impaired contractions of the heart.

2.5 α-actinin

[The following text (2.5) is my own work and has already been published in Wadmore and Azad *et al.* IJMS 2021 [27]].

α-actinin is a protein found in the Z-disc of muscles and is involved in the cross-linking of anti-parallel actin filaments. It also interacts with titin and acts as a protein scaffold for large protein complexes [28]. The protein has four different isogenes (*ACTN1-4*), that are all closely related and perform similar functions, but display different expression profiles across

tissues. The binding of non-muscle α-actinin (*ACTN1* and *ACTN4*) to actin is regulated by the binding of calcium, whilst in muscle isoforms (*ACTN2* and *ACTN3*) binding to actin is calcium insensitive [29]. Instead, muscle α-actinin is regulated by the binding of phospholipids such as phosphatidylinositol bisphosphate [30]. *ACTN2* (located at chromosome position 1q42-43) is highly expressed in heart and skeletal muscle, while *ACTN3* (located at chromosome position 11q13.2) is exclusively expressed in skeletal muscle.

2.5.1 Structure, function and binding partners of α-actinin

α-actinin forms antiparallel homodimers [30]. It is comprised of an actin binding domain (ABD), a central rod domain with 4 spectrin repeats, and an EF hand domain (*Figure 3*). Through its binding to a variety of other signaling molecules, it has an important role in organisation of the cytoskeleton and muscle contraction [28].

A loss of function study of *ACTN2* in zebrafish embryos using antisense morpholino technology highlighted the importance of α-actinin 2 in Z-disc lateral alignment in zebrafish cardiogenesis [31]. Depletion of *ACTN2* led to a reduced end-diastolic diameter and overall reduced cardiac function. The loss of function mutants also had reduced cardiomyocyte size and number, leading to reduced ventricular chamber size. This underlines the crucial role of α-actinin for integrity in the developing heart.

2.5.2 α-actinin in disease

2.5.2.1 α-actinin in cardiomyopathies

Several studies report links between variants (*ACTN2*) and HCM. The first description was by Theis *et al.* [32]. As part of a genetics candidate gene approach, they interrogated 5 genes

coding for Z-disc-proteins, including *ACTN2*, in 239 unrelated patients with HCM by polymerase chain reaction (PCR), denaturing high performance liquid chromatography (DHPLC) and direct Sanger DNA sequencing. They identified two pathogenic variants in *ACTN2* (p.Gly111Val and p.Arg759Thr), and also reported *ACTN2* p.Thr495Met. This variant (*ACTN2* p.Thr495Met), was initially thought to be pathogenic, but now appears is too common [33] in normal populations to support a pathogenic role (*Table 1*).

Echocardiography suggested that pathogenic variants in *ACTN2* (as well as other HCM associated Z-disc genes) resulted in sigmoid septal morphology of cardiac hypertrophy.

A separate study looked at 23 individuals from a 3-generation Australian family that clinically presented with heterogeneous HCM [34]. A genome-wide linkage analysis, combined with candidate gene screening, identified *ACTN2* p. Ala119Thr. The variant was found in all 7 affected members of the HCM family. To further support the link between HCM and pathogenic variants in *ACTN2*, 297 additional probands were screened for variants in *ACTN2*. High-resolution melt analysis of four HCM families identified an additional two *ACTN2* variants (p.Glu583Ala, and p.Glu628Gly).

The *ACTN2* variant p.Met228Thr was identified in an Italian family with atypical HCM and early onset atrial fibrillation (AF) by next generation sequencing [35]. It co-segregated with disease in 11 affected family members.

ACTN2 p.Thr247Met, another variant located in the actin-binding domain, was identified in a patient who presented with familial HCM [36]. A human-induced pluripotent stem cell (hiPSC)-derived cardiomyocyte model for the variant supported its pathogenicity and suggested that the observed prolongation of QT interval in the family could be explained by the reduced interaction of the *ACTN2* p.Thr247Met variant with the L-type calcium channel. This observation lead to the successful treatment of affected family members with L-type calcium channel blocker diltiazem.

In summary, most *ACTN2* identified in HCM patients are located in the actin-binding domain (see *Table 1*). The crystal structures of two HCM-associated *ACTN2* variants (p.Ala119Thr and p.Gly111Val) located in the actin-binding domain, showed small, yet distinctive changes [37] . The p.Gly111Val variant reduced thermal stability and impacted tertiary structure of the protein, whilst the p.Ala119Thr had a more pronounced negative effect on actin binding. The variants showed weaker integration into the Z-discs than wild-type α-actinin and formed aggregates outside the Z-discs. They further showed reduced ability to leave the Z-disc with reduced fluorescent decay after photoactivation, suggesting that exchange of the protein at Z-discs is reduced in the presence of the pathogenic variants.

Associations of *ACTN2* variants with other types of cardiomyopathies are less strong: *ACTN2* p.Gln9Arg variant was identified in the DCM patient [38]. Despite demonstrating altered binding properties to Muscle LIM Protein *in vitro* and being absent in 200 control individuals, the variant would not pass current criteria of pathogenicity (based on its frequency in normal cohorts, *Table 1*).

More recently, *ACTN2* p.Leu320Arg was identified by whole-exome sequencing in a Chinese family, who presented with DCM and ventricular tachycardia [39]. 12 family members were followed up and four of them were affected by disease. All four carried had the *ACTN2* p.Leu320Arg variant that cosegregated with disease and was absent in the healthy family members.

A further study associated the *ACTN2* p.Ala119Thr with disease in an Australian family who showed cardiac phenotypic heterogeneity (LVNC or DCM) [40]. Using exome sequencing in two probands, the variant *ACTN2* p.Ala119Thr was ranked the most highly expressed in cardiac tissue according to data derived from RNAseq and found to co-segregate with disease of the four affected family members. Of note, the same change had previously been identified

in HCM patients (see above) and it is not understood why it can cause different types of cardiac disease in different individuals.

2.5.2.2 α-actinin in skeletal muscle disease

So far, only one report performing high-throughput sequencing has linked missense variants in *ACTN2* with autosomal dominant distal myopathy [10]. *ACTN2* p.Cys487Arg was identified in three families and *ACTN2* p.Leu131Pro in a further one. The missense variants in *ACTN2* co-segregated with the disease in affected family members. Clinically, they showed adult onset asymmetric distal muscle weakness, e.g. atrophy of the tibialis anterior muscle, which later progressed to proximal limb muscles.

ACTN3 p.Arg577X is a common nonsense variant (minor allele frequency, MAF, ~20 %) previously described to cause α-actinin-3 deficiency when individuals are homozygous for the X allele [41]. Hogarth *et al.* found this genotype to be a modifier of the clinical phenotype of Duchenne muscular dystrophy patients [42]. A double knock-out mouse model, lacking both dystrophin and alpha-actinin 3, showed reduced muscular strength but was protected from stretch-induced damage with age by an increase in oxidative muscle metabolism.

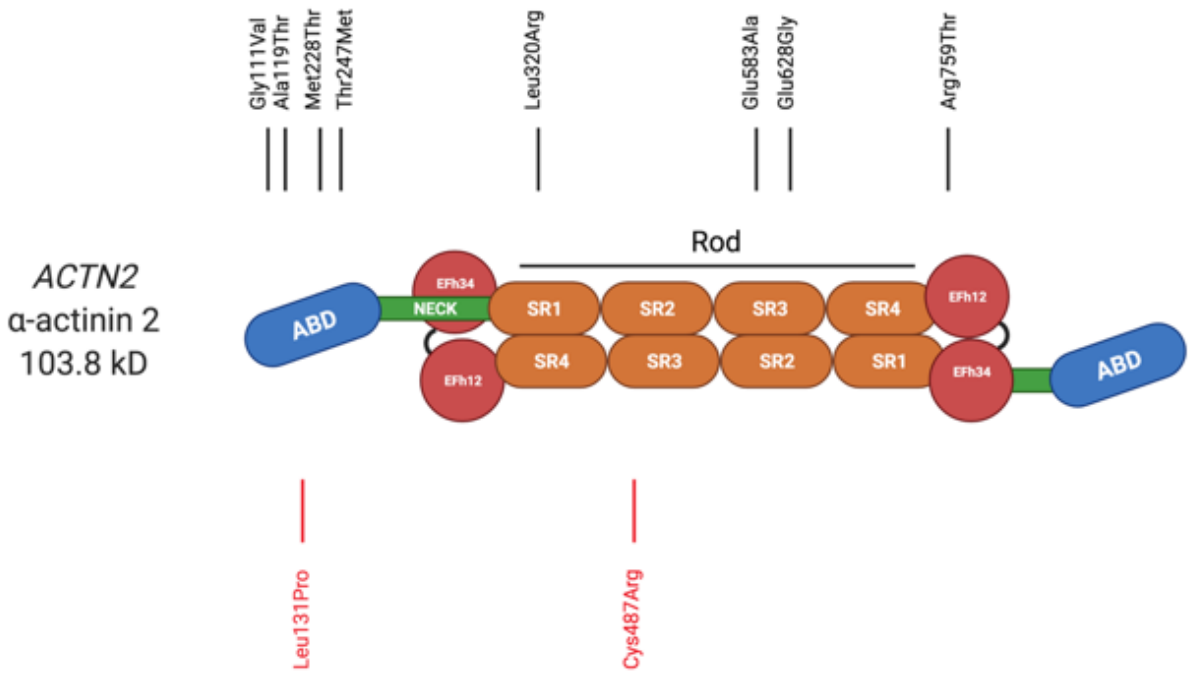

Figure 3. Schematic representation of α-actinin shown as a dimer with variants in the *ACTN2* gene that have been previously reported in individuals with a muscular (red) or cardiac (black) myopathy. Solid lines represent missense variants and dashed lines are truncations. ABD - actin binding domain, EFh – EF hand, SR – spectrin like repeat. Created with BioRender.com. Adapted from [30].

2.5.2.3 Summary

Pathogenic variants in *ACTN2* are rare and do not significantly contribute to cardiomyopathies in numbers. *ACTN2*'s association with HCM is best documented. Until now, there is only one report linking *ACTN2* to skeletal muscle disease. In light of α-actinin2's conservation and documented requirement for cardiac integrity [31], it is likely that most missense variants in *ACTN2* are detrimental to its crucial functions and hence not compatible with life. Nevertheless, the few identified ones are of mechanistic interest.

Table 1. Variants in the *ACTN2* gene that have been previously reported in individuals with a muscular or cardiac myopathy.

Name Gene	Variant	Het or Homo	Type of disease	Cardiac or Muscular	*MAF on GnomAD	Location	Ref
α-actinin *ACTN2*	p.Gln9Arg	Het	DCM	Cardiac	7.22E-04	ABD	[38]
	p.Gly111Val	**Het**	HCM	Cardiac	Absent	**ABD**	[32]
	p.Ala119Thr	**Het**	HCM, LVNC, DCM	Cardiac	Absent	**ABD**	[34] [40]
	p.Leu131Pro	Het	DM	Muscular	Absent	**ABD**	[10]
	p.Met228Thr	**Het**	HCM (with AF)	Cardiac	Absent	**ABD**	[35]
	p.Thr247Met	**Het**	HCM	Cardiac	Absent	**ABD**	[36]
	p.Leu320Arg	**Het**	DCM (with VT)	Cardiac	7.95E-06	**SR1**	[39]
	p.Cys487Arg	**Het**	DM	Muscular	Absent	**SR2**	[10]
	p.Thr495Met	Het	HCM	Cardiac	2.76E-04	SR2	[32]
	p.Glu583Ala	**Het**	HCM	Cardiac	Absent	**SR3**	[34]
	p.Glu628Gly	**Het**	HCM	Cardiac	Absent	**SR3**	[34]
	p.Arg759Thr	**Het**	HCM	Cardiac	Absent	**EF1**	[32]

Abbreviations: ABD, actin-binding domain; AF, atrial fibrillation; DCM, dilated cardiomyopathy; DM, distal myopathy; HCM, hypertrophic cardiomyopathy; Het, heterozygous; Homo, homozygous; LVNC, left ventricular noncompaction; VT ventricular tachychardia. * MAF on GnomAD: The Minor Allele Frequency (MAF) was found on The Genome Aggregation Database (gnomAD) version 3.1. All variants with MAF < 10−4 are highlighted in bold.

2.5.3 HCM-related *ACTN2* M228T variant

This project focused on the *ACTN2* variant p.Met228Thr located in the actin binding domain of the gene. As previously mentioned, this variant was first identified in an Italian family with atypical HCM and early onset atrial fibrillation (AF) by next generation sequencing [35] and the change was predicted to be deleterious. The variant co-segregated with disease in 11 affected family members and was absent in 570 control alleles from healthy individuals. Clinical features seen in the family were left ventricular hypertrophy (LVH), arrhythmias and

LVNC. The pedigree of the family can be seen in *Figure 4*. As the variant had an absent MAF value on GnomAD, this variant was predicted to be pathogenic as it was absent in the general population (*Table 1*). Understanding the impaired functions of this pathogenic variant and how it leads to HCM, will provide a greater understanding of how α-actinin functions also in the healthy myocardium; it is expected that affected activities of the protein are related to signalling functions. As Girolami *et al.* also identified AF in the patient cohort, investigating this variant was important to understand whether there is electrical signalling impairment in patients with α-actinin variants.

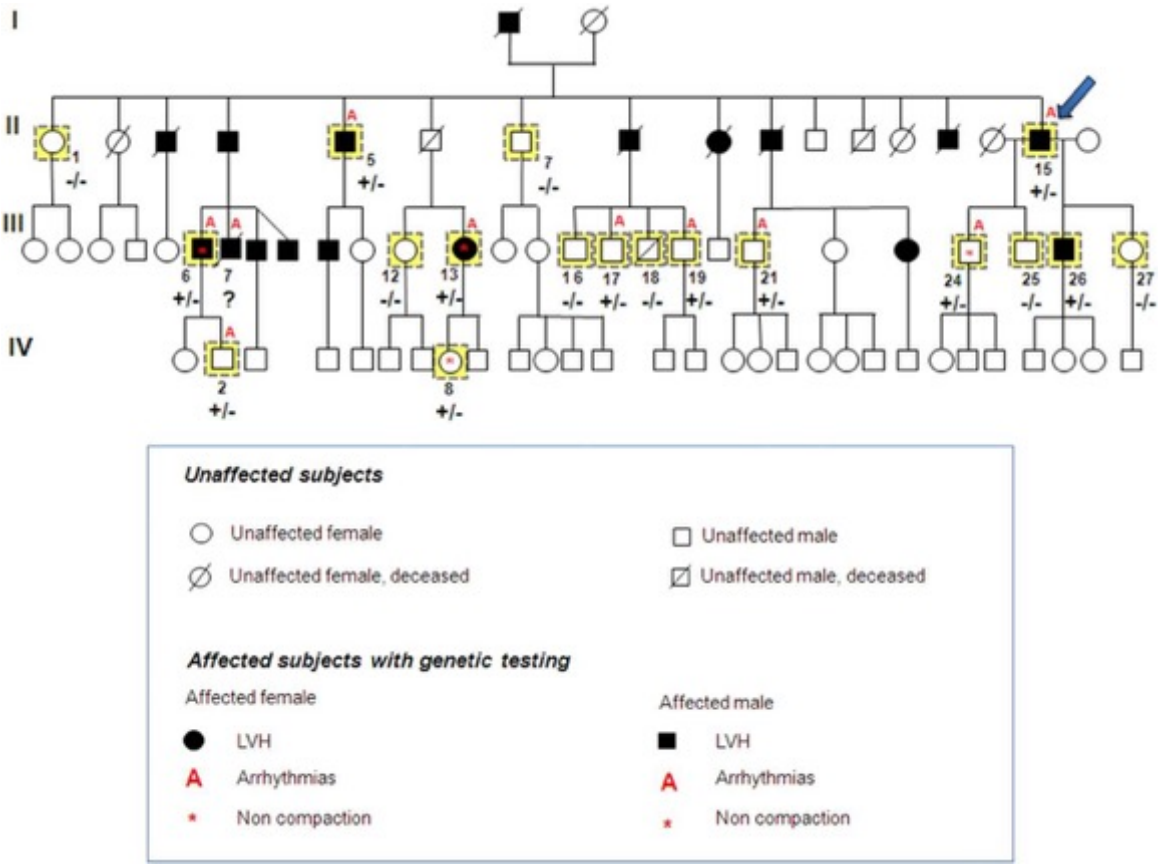

Figure 4. Pedigrees of *ACTN2* variant family. Pedigree including the results of *ACTN2* c.683T>C (p.Met228Thr) cosegregation in 18 family members. Arrow: proband; +/−, presence of the heterozygous c.683T>C (p.Met228Thr); −/−, absence of the heterozygous

c.683T>C (p.Met228Thr); ?, unknown genotype. Individuals clinically assessed and genotyped are labelled in yellow. Figure taken from [35].

2.6 Modelling cardiac disease

2.6.1 Animal models

It is not ethically possible to model cardiac disease directly on humans and human cardiac tissue is often not readily available. Animals can act as *in vivo, in vitro* and molecular models to gain understanding into the mechanisms behind the disease [43]. Small rodents such as mice and rats have provided an extensive insight into cardiac physiology and disease in humans by allowing specific parameters to be measured using techniques such as echocardiography [44], electrocardiography [45] and cardiovascular magnetic resonance imaging (CMRI) [46]. There are both advantages and disadvantages to using these murine models. The main advantages are their ease of handling/housing, relatively cheap maintenance costs, short gestation time and the ability to genetically manipulate them [47]. However, the most significant disadvantage is the difference in physiological properties and characteristics between human and rodent hearts. Differences in heart rates, kinetics, stimulation frequencies, cardiac protein expression and cardiac response to stress/exercise [43] (to name a few), need to be taken into careful consideration when extrapolating the results from animals to humans.

One animal model for *Actn2* was reported by Gupta *et al* 2012 [48]. They demonstrated both skeletal and cardiac defects in Zebrafish that had been knocked down for *Actn2* using morpholino oligonucleotide injections. Lornage *et al* 2020 [49] used both Zebrafish and mice to model Multiple Structured Core disease by expressing mutant *Actn2*. They found sarcomeric disorganisation as well as abnormal muscle structure and function, which recapitulated that seen in clinical patients.

2.6.2 Mouse embryonic heart development

Due to only small differences in developmental sequences and morphology of the atria and venous [50], mice are seen as an effective model for human development. Mouse cardiac development begins at around embryonic day 6 (E6), when cardiac progenitor cell specification occurs; these cells then start to migrate and form primary heart field (PHF) cells at around E7.5 where the cardiac crescent and secondary heart field (SHF) are formed. From E8-E8.5, the linear heart tube is formed, and sarcomere formation also allows a heartbeat to begin. From here until E9.5, cardiac looping occurs and causes left-right symmetry of the heart to be acquired. Epithelial-to-mesenchymal transition (EMT) of cells also occurs here. Between E10-E12.5, chamber differentiation takes place and the heart tube is divided into four separate chambers. From E13.5 onwards, maturation of valves and development of vessels allows a conduction system to form so that blood can flow unidirectionally (*Figure 5*) [51, 52]. Once it has reached E15.5, the mouse heart has achieved its definitive external prenatal configuration. The atrioventricular valve leaflets and coronary artery continue developing until the birth of the mouse at E20 [53]. Cardiomyocytes continue to proliferate in the mouse embryonic heart until birth [54]. This maintained proliferative action results in the expansion of the ventricular walls of the embryonic heart, which primarily takes place between E11.5-E14.5 [55]. It requires the coordinated disassembly and reassembly of sarcomeric structures within the cardiomyocytes for each division.

During embryonic development, the pathways that enable cell-survival in the heart are activated by the foetal gene programme. However, cardiomyocytes can also respond to postnatal neurohormonal or biomechanical changes in the heart that may lead to the development of hypertrophy [56]. These changes result from variations in the adult gene programme, to a programme that more resembles that of the foetal gene programme [57]. ANP and BNP are small atrial natriuretic peptide hormones, the precursor prohormones of

which are encoded by genes that are regulated by the foetal gene programme (*Nppa* and *Nppb*) [57]. The gene encoding for β-myosin-heavy chain (β-MHC) (*Myh*7), is also promoted in the foetal gene programme [58], as well as the gene encoding α 1 skeletal muscle actin (*Acta1*) [59].

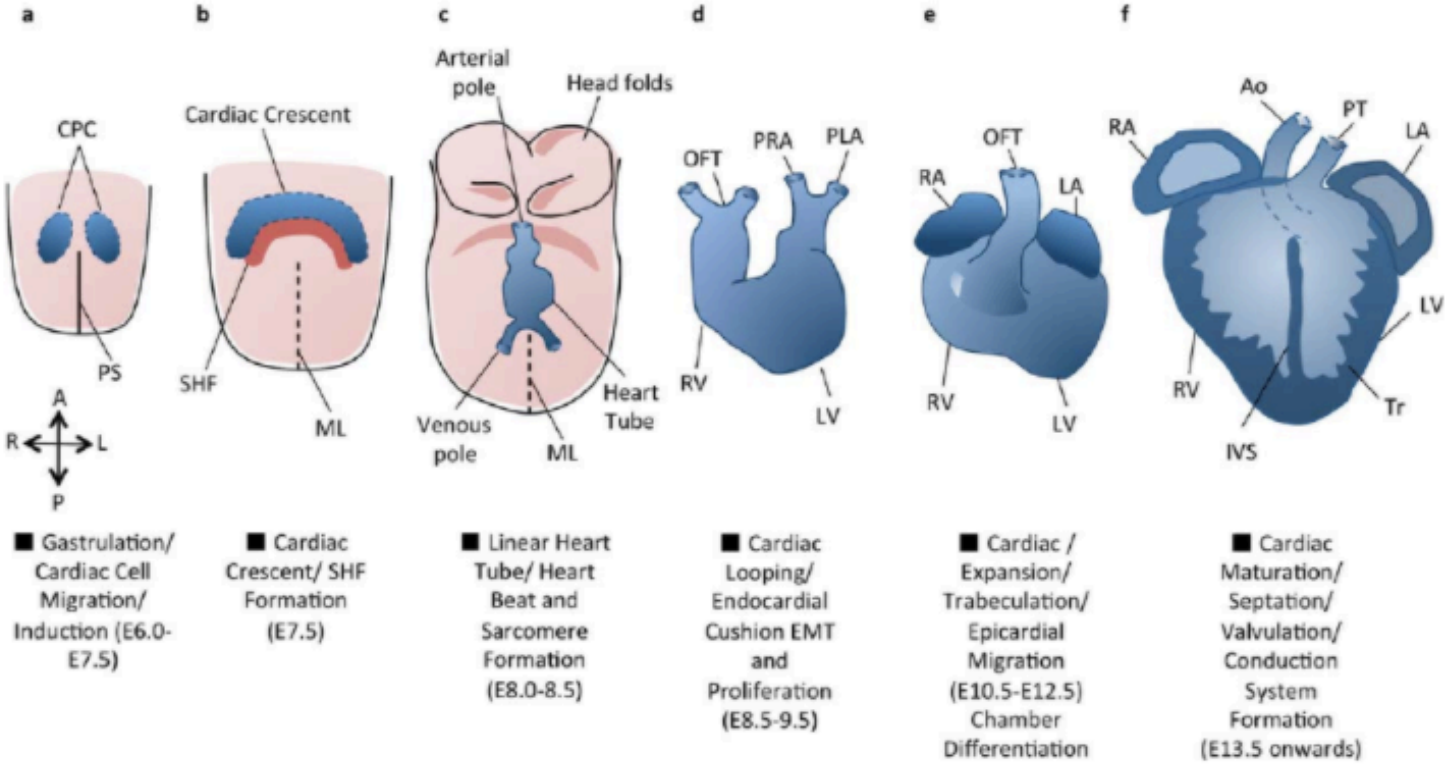

Figure 5. Figure taken from [51]. An overview of mouse embryonic cardiac development. Cardiac development progresses from the specification of cardiac progenitor cells (a) to the migration of these cells towards the midline to form the cardiac crescent (b). The developing heart then forms a linear tube (c), which under-goes dextral looping to acquire the appropriate left–right asymmetry (d). The heart tube is further subdivided into the four chambers (e), and the maturation of the endocardial cushions into the valves and development of the great vessels provides for unidirectional blood flowthrough the chambers (f). Adapted from (Buckingham et al., 2005). A = Anterior, Ao = Aorta, CPC = Cardiac Precursor Cells, IVS = Interventricular septum, L = Left, LA = Left Atrium, LV = Left Ventricle, ML = Midline,

OFT = Outflow Tract, P = Posterior, PHF = Primary Heart Field, PLA = Primitive Left Atrium, PRA = Primitive Right Atrium, PS = Primitive Streak, PT = Pulmonary Trunk, R = Right, RA = Right Atrium, RV = Right Ventricle, SHF = Secondary Heart Field, Tr = Trabeculae.

Transgenic technologies have allowed mice to become an important animal model for ineffective cardiovascular development [53]. However, as a result of abnormally developed hearts, these genetically modified mice often die in utero. *Actn2* M228T Hom mice have been found to die past embryonic day 15.5 (E15.5), hence this is the latest that these embryos can be harvested and studied.

2.6.3 Induced pluripotent stem cells (iPSCs)

To try and overcome the difficulties faced when using animal models, research is trying to move in the direction of engineered cardiac tissue. Pluripotent stem cells derived from embryonic sources (embryonic stem cells, ESCs), have been used to differentiate into cardiomyocytes [60, 61]. This technology has developed further through the use of human iPSCs with patient specific iPSC cardiomyocytes (iPSC-CMs) providing a new *in vitro* method of modelling cardiac disease [62]. iPSC-CMs have been found to share key properties with human primary cardiomyocytes, including mechanical, molecular, metabolic and electrophysiological features [62]. The main disadvantage to this technology is that iPSCs are phenotypically immature and represent foetal human cardiomyocytes [63]. If looking at cardiac diseases in adults, these immature models may not best model the electrophysiology and morphology seen in adult cardiomyocytes.

In order to reprogram somatic cells into iPSCs, Wnt signalling activation by the Gsk3β inhibitor CHIR [64], is used for mesoderm specification [65]. Deactivation of this signalling with an inhibitor such as IWR1 [66], is used for cardiomyocyte differentiation.

2.7 Aims and hypothesis

To investigate the link between the c.683T>C (p.Met228Thr) (M228T) pathogenic variant in α-actinin and its role in cardiomyopathies, this research project consists of three main chapters:

Chapter 1 (adult mouse model) looks at whether there is overt cardiac hypertrophy of Het mice and if so, if it is dependent on age and/or sex. The main hypothesis for this chapter is that *Actn2* M228T:Het hearts will have increased markers of hypertrophy compared to the WT mice; the extent might depend on sex and age of the mice (older mice and male mice are postulated to have more severe hypertrophy). Heart weights and body weight of WT and *Actn2* M228T:Het mice have been recorded at the time of harvest and are provided for this project. To normalise these values for the size of the animal, tibia length is to be determined. Heart weight to tibia length (HW/TL) ratios are calculated; increased values are an indicator of cardiac hypertrophy. In addition, heart weight to body weight (HW/BW) ratios and body weight to tibia length (BW/TL) ratios are calculated. This will help to identify the sex and age group with the highest degree of cardiac hypertrophy (if any). This is followed up by molecular investigations (e.g. Western Blotting for hypertrophic markers such as beta-myosin heavy chain, and thin filament proteins such as myotilin and cardiac troponin T). Quantitative analysis of these results will help determine if this variant has an impact on level of protein expression in the mice.

Chapter 2 (embryonic mouse model) will explore abnormalities leading to embryonic death of homozygous (Hom) embryos. Previous work has indicated that E15.5 is the last day *Actn2* M228T:Hom embryos are still consistently alive and hence embryos will be investigated at this time point (more information on mouse embryonic heart development can be found in 2.6.2). It is hypothesized that *Actn2* M228T:Hom mice display developmental delay. This will be tested experimentally by using Theiler staging to categorize fixed hands of the embryos. Genotyping of the mice will be performed and the Theiler stage distributions correlated with genotype (WT, Het or Hom). In a different set of experiments, the incorporation of α-actinin into sarcomeric structures will be assessed. Whole mounts of embryos are stained for α-actinin 2 and the sarcomeric marker titin by a collaborator. Images will be quantified for co-localisation of α-actinin with titin in these images using ImageJ. In a third set of experiments, markers of cardiac hypertrophy will be assessed in E15.5 embryos using qPCR and Western blotting. In addition, the embryonic hearts will be probed for upregulation of other actinins (*Actn1, Actn3, Actn4*) and cardiac markers (*Nppa, Nppb, Acta1, Myh7* and hypoxanthine-guanine phosphoribosyl transferase, *Hprt*), by qPCR and Western blotting (where applicable).

Chapter 3 (iPSC model) will use iPSC-CMs with the homozygous *ACTN2* M228T variant to model the contractility deficiency. This approach is used to assess sarcomere formation and integrity in a human cellular model. This variant leads to embryonic lethality, which is a challenge because many embryos need to be generated to obtain small amounts of homozygous tissue. To overcome this, an iPSC-CM model is used. This reduces the number of mice used and provides a human model system. FACS will be used to confirm the pluripotency of the iPSCs carrying the *ACTN2* M228T variant. Both parental and *ACTN2* M228T Hom cells harvested at day 16, will be used to look at sarcomere formation and

structure by immunofluorescence staining for Actn2 and titin (T12). It is hypothesized that the *ACTN2* M228T Hom cell line have dysregulation and a less defined structure of its sarcomeres compared to the parental line.

3. Materials and methods

3.1 Animal lines

Clustered regularly interspaced short palindromic repeats (CRISPR)/Cas9 nuclease technology was used to generate the mouse model harbouring the M228T variant within the *Actn2* gene. This is equivalent to the M228T *ACTN2* variant identified in humans. This was carried out at the Wellcome Centre for Human Genetics at the University of Oxford (Dr Ben Davies) and transferred to BMSU by embryo transfer. Animal studies were performed in accordance with the ethical standards laid down in the 1964 Declaration of Helsinki and its later amendments. Experimental procedures were performed in accordance with the Directive 2010/63/EU and UK Home office guidelines (project licences P572C7345 and PDCE16CB0) and approved by the respective institutional ethical review boards. Animal procedures were carried out by fully trained Personal Licence Holders. Animals were housed in specific pathogen free conditions, with the only reported positives on health screening over the entire time course of these studies being for *Tritrichomonas sp.* and *Entamoeba spp.* All animals were housed in social groups (apart from single housing with enrichment for chronic adrenergic stimulation experiments), provided with food and water *ad libitum* and, maintained on a 12h light:12h dark cycle (150–200 lux cool white LED light, measured at the cage floor).

3.2 Tibia length determination

5 mL of 0.8 M sodium hydroxide (NaOH) was added to each vial to cover the legs of the mice. 0.8 M of NaOH was made up using 16 g of NaOH pellets (Scientific Laboratory Supplies, CHE3416) added to 50 mL of water. This was then added to 450 mL water to make the final 0.8 M solution. The legs were left overnight at room temperature. The following day, the legs in NaOH were put into a 37 °C incubator for 1 hour for further digestion. The

legs were then rinsed under tap water. Patella's were removed from the tibias along with any tendons/muscles that were still attached. Tibia lengths were measured using 150-inch digital callipers (SH20) and the lengths were recorded. Lengths were documented in an Excel file and the heart weight to tibia length ratio (HW/TL) was determined. Body weight to heart weight (BW/HW) and heart weight to tibia length (HW/TL) ratios were also calculated for all the mice and mice were grouped according to age and sex. Heart weight and body weight measurements were provided by He Jiang, University of Oxford.

3.3 Coomassie

2X SDS buffer (*Table 2*) was added to each sample (volume of buffer was 4X tissue in mg), and samples were heated at 65 °C for 15 mins. Samples were lysed using a sonicator probe (CV188 3870). Samples were centrifuged for 3 mins at 300 G (Fisher Scientific, accuSpin Micro 17R) and the pellets were removed. Samples were diluted 1:10 (20 µl neat sample with 180µl 1.5X SDS buffer (*Table 2*) and were aliquoted into separate tubes. 3 µl of each sample was loaded into a Mini-PROTEAN TGX Precast Gel (4-15%) for use with Tris/Glycine buffers (BIO-RAD, #456-1086) along with 2 µl of Precision Plus Protein™ Dual Color Standards protein ladder (BIO-RAD, #1610374). Samples were run in a Mini-PROTEAN Tetra System (BIO-RAD) with 10X diluted running buffer (GENEFLOW, B9-0032) until the bands had run sufficiently. The resulting gel was stained with Coomassie dye (BIO-RAD, #161-0400) and subsequently with de-stain (50% H_2O, 20% acetic acid and 30% methanol) to reveal protein bands. The gel was imaged on a Konica Minolta multifunctional device (MFD) scanner and Gapdh for WT females was used to normalise loading of the samples using ImageJ (more information in 3.10 statistical analysis).

3.4 Western blots

Samples were loaded into a Mini-PROTEAN TGX Precast Gel for use with Tris/Glycine buffers along with 2 µl of Precision Plus Protein™ Dual Color Standards protein ladder. Samples were run in a Mini Trans-Blot cell using a Mini-PROTEAN Tetra System with 10X diluted running buffer (*Table 2*) until the bands had run sufficiently. Amount loaded was based on normalised quantities to Gapdh, which was calculated from the Coomassie staining. The resulting gel was transferred onto a membrane using an iBlot 2 transfer machine (Invitrogen by Thermo Fisher Scientific) and iBlot 2 NC Mini Stack (Invitrogen by Thermo Fisher Scientific, 2NM130121-01). After transfer, the membrane was stained with Ponceau S solution (0.1% (w/v) in 5% acetic acid) (SIGMA, P7170-1L) and imaged on a scanner to check for the presence of proteins. The membrane was then washed in water and blocked in 5% milk TBST (0.1% TWEEN 20) for 1 hour to prevent non-specific binding. Primary antibodies (*Table 3*) were added (5% milk TBS) and the membranes were left in the cold-room overnight. The following day, membranes were washed for 5X 5 minutes in TBST (0.1% TWEEN 20). Secondary antibodies (*Table 4*) were then added (1% milk) and left for a minimum of one hour. Membranes were rinsed in TBS (0.1% TWEEN 20) (*Table 2*) before 3X 20-minute washes in TBS (0.5% TWEEN 20) (*Table 2*). Membranes were then imaged on the Odyssey Fc Imaging system (LI-COR).

Western blots on embryonic hearts were performed following the same procedure as outlined above. Embryonic hearts from WT, Het and Hom mice for the *Actn2* M228T variant were harvested at E15.5. The heart tissue was homogenized with a BioPulverizer (Thistle Scientific) and collected using 1.5X SDS buffer before being loaded and ran on a Mini-PROTEAN TGX Precast Gel for use with Tris/Glycine buffers.

Table 2. Buffers

Buffer	Composition/compounds	Final concentration
Tris/Glycine buffer (runnincg buffer)	Tris	0.025 M
	Glycine	0.192 M
	SDS	0.1 %
TBS (0.1% TWEEN)	Tris/Tris HCl	25 mM
	NaCl	0.13 M
	KCL	0.0027 M
	TWEEN 20	0.1 %
TBS (0.5% TWEEN)	Tris/Tris HCl	25 mM
	NaCl	0.13 M
	KCL	0.0027 M
	TWEEN 20	0.5 %
1.5X SDS-SB	Tris-Cl (pH 6.8)	75 mM
	Sodium dodecyl sulfate	3 % w/v
	Bromophenol blue	0.15 % w/v
	Dithiothreitol (DTT)	150 mM
	Glycerol	15 % w/v
2X SDS-SB	Tris-Cl (pH 6.8)	100 mM
	Sodium dodecyl sulfate	4 % w/v
	Bromophenol blue	0.2 % w/v
	Dithiothreitol (DTT)	200 mM
	Glycerol	20 % v/v

Table 3. Primary antibodies

Antigen	Host	Company	Catalogue number	Dilution
MYH7	Rabbit	Proteintech	22280-1-AP	1:1500
ACTN2	Rabbit	Abcam	EP2529Y	1:2000
MYOT	Rabbit	Proteintech	10731-1-AP	1:1500
CTNT	Mouse	ThermoFisher Scientific	MAS-12960	1:2000
GAPDH	Rabbit	EMD Millipore Corp	ABS16	1:5000
HSP27	Rabbit	Cell Signalling Technology	2442S	1:500
HSPB7	Rabbit	Proteintech	15700-1-AP	1:500
FLNC (R1899)	Sheep	University of Dundee	MRCPPU	1:1000
ACTN3	Rabbit	AbCam	GR97028-8	1:1000

Table 4. Secondary antibodies

Antigen	Coupled to	Host	Company	Catalogue Number	Dilution
Anti-Rabbit IgG	IRDye 800CW	Goat	LI-COR	925-68071	1:5000
Anti-Mouse IgG	IRDye 800CW	Goat	LI-COR	926-32210	1:5000

3.5 Hand development of mice embryos

A Leica Microsystem (Tl3000 Ergo stereoscope) was used to investigate the level of hand development in mice embryos at E15.5. The hands were documented blind (genotype unknown) and were grouped according to the level of hand development seen by Theiler staging [67].

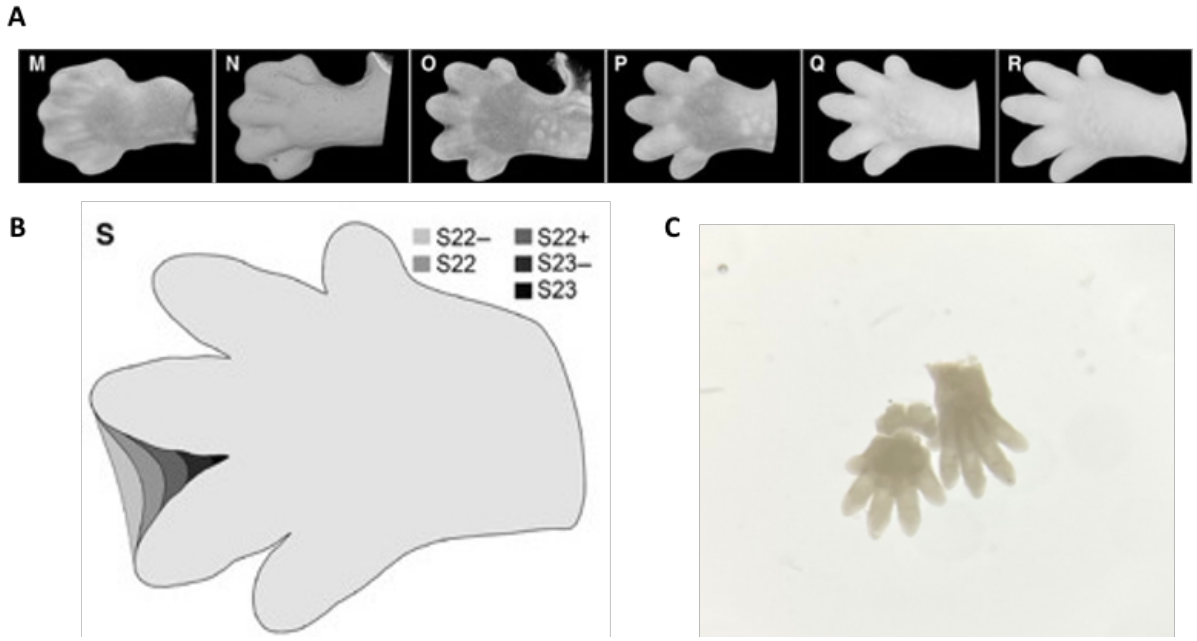

Figure 6. A: Volume-rendered 3D model of embryo hands, stages are as follows: M=S21, N=S22-, O=S22, P=S22+, Q=S23-, R=S23 [67]. **B:** Scheme representing the development of the integral space between the 3rd and 4th digit from stages S22-S23 [67]. **C:** Image taken on Leica Microsystem of embryonic hands at E15.5. Hands were classified as stage S23 according to Theiler staging.

3.5.1 Genotyping

i) DNA Extraction:

REDExtract-N-Amp Tissue PCR Kit (SIGMA-ALDRICH, XNAT-100RXN) was used for DNA extraction and PCR. To each tail sample, 100 µl extraction solution (SIGMA, E7526-

24ML) and 25 µl tissue preparation solution (SIGMA, T3073-3ML) was added. These were gently vortexed and the sample was then briefly centrifuged (AccuSpin Micro 17, Fisher Scientific) and incubated at room temperature for 10 minutes. They were then incubated at 95 °C for 3 minutes. 100 µl neutralisation solution B (SIGMA, N3910-24ML) was added to each sample and these were gently vortexed then centrifuged at 300 G for 1 minute. Samples were stored at 4 °C.

ii) PCR:

Master mixes were made up for the number of samples to be run, including positive and negative controls:

Table 5. Reagents required for 20 µl PCR reaction

	Per 20 µl reaction:
REDExtract-N-Amp PCR reaction mix (SIGMA, R4775-1.2ML)	10 µl
DNase-free water	4 µl
Primer reverse (SIGMA, HA14313396-001) 5'-CTGCATGGGTCCTGTGTTTC-3'	1 µl
Primer forward (SIGMA, HA14313395-001) 5'-CACTCGTGTGTTAAGGGGCA-3'	1 µl

16 µl master mix and 4 µl of the DNA extract was pipetted in. The tubes were sealed with lids to avoid evaporation of samples. The tubes were then centrifuged and the PCR was run at

63 °C annealing temperature on a Labcycler Basic (011-103) machine (SensoQuest) (3 min at 94 ºC, 1 min at 94 ºC, 1 min at 63 ºC, 30 sec at 72 ºC, cycle to 2nd step 35 times, 10 min at 72 ºC, keep at 10 ºC forever). The thermocycler program for primers was used. “Save and run” was pressed and the block containing the PCR plate was selected. At the end of the cycles the program was stopped, and the thermocycler was switched off. The PCR products were stored at -20 °C.

iii) Confirmation of successful amplification by PCR

To confirm successful amplification by PCR, 1 µl of each PCR product was added to 9 µl H_2O and 2 µl Gel Loading Dye purple (6X), no SDS (New England Biolabs, B7025S). Samples were then run on 2% agarose gel (Geneflow agarose powder, A4-0746, 1X TBE from 10X stock, Invitrogen, 15581-044, PAGE GelRed Nucleic Acid Gel Stain 50,000X in water, Biotium, 41008-500µl) to check that bands were present. 2 µl 1 kb Plus DNA Ladder (New England Biolabs, N3200S) was used as a marker.

iv) Purifying the PCR

QIAquick PCR and Gel Cleanup Kit (100) (QIAGEN, 28506) was used to purify the remaining PCR product (~19 µl), following the instructions provided. 5X volume buffer PB binding buffer was added to 1 volume PCR (100 µl PB) in a 2mL collection tube. Samples were centrifuged for 1 minute to bind the DNA and the flow-through was discarded. 750 µl PE wash buffer was added to the column and samples were centrifuged for a further minute. Flow-through was discarded and the column was placed back in the same tube. Tubes were centrifuged for another minute to remove any residual wash buffer. The columns were placed in a clean 1.5 mL microcentrifuge tube and 50 µl buffer EB was added to elute the DNA. The tubes were then centrifuged for another minute. Samples were stored at -20 °C until needed.

v) Digestion of purified PCR product

3 µl of CutSmart buffer (New England Biolabs, B7204S) and 0.5 µl of the restriction enzyme HgaI (New England Biolabs, R0154S) were added to 27 µl of the purified PCR mixture. Samples were incubated at 37 °C for 2 hours. They were then heat inactivated for a further 2 hours at 65 °C. 6 µl of 6X loading dye was added to each sample.

vi) Agarose gel and imaging

A total of 35 µl of each sample was run on 2% agarose gel until the bands had run sufficiently. Gels were then imaged on a Gene Genius Bio Imaging-System (Syngene). Bands present were used to determine the genotype of the samples (*Figure 7*). Due to time constraints when optimising the PCR, genotyping of the remaining samples was performed commercially by Transnetyx, using the probe "Actn2-2 MUT".

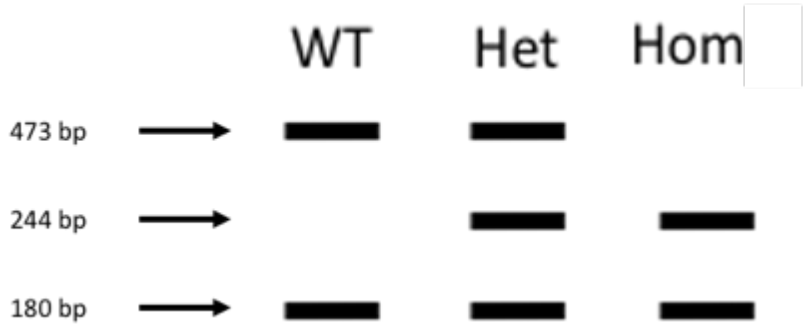

Figure 7. Positioning of bands used to determine the genotype (WT, Het or Hom) of the samples. Expected sizes of the bands are indicated with arrows.

Bands present on the agarose gels revealed genotypes of the samples, showing them to be either WT or Het (no homozygotes (Homs) were identified) (*Figure 8*). A sample previously identified as Het was used as a positive control. Blanks were also used as negative controls, but they appeared to be contaminated as bands were present. Due to technical difficulties and

time constraints, genotyping of all other samples was performed commercially by Transnetyx. *Table 6* shows all the genotypes identified from the samples analysed.

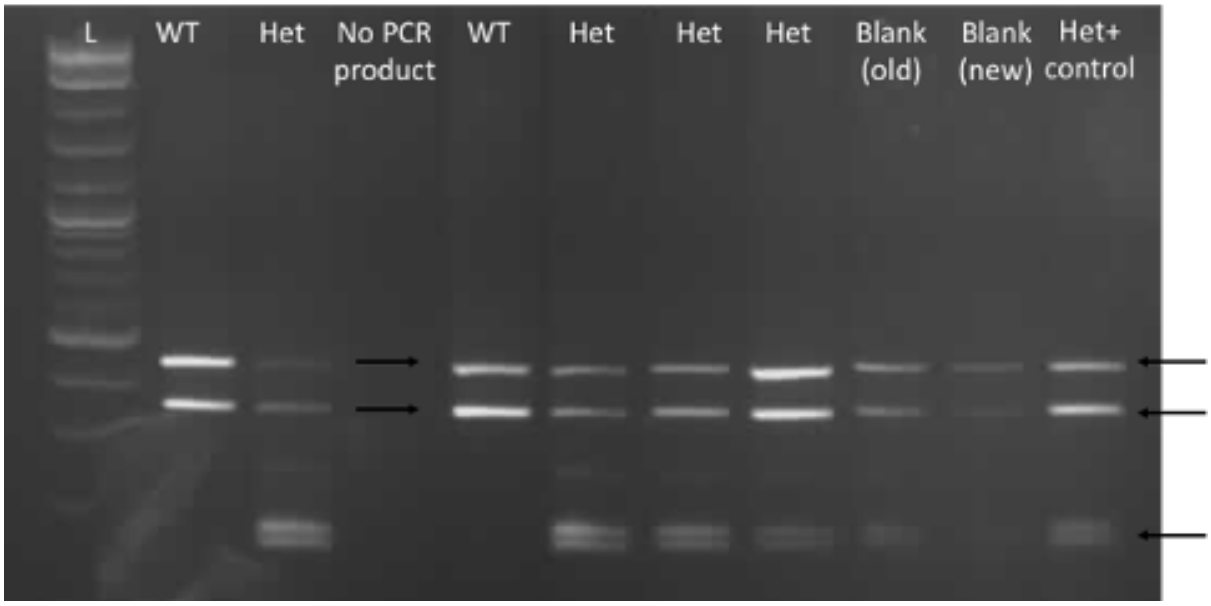

Figure 8. Genotypes of samples F3.2-8, two blanks labelled Blank (old) and Blank (new), and a Het+ control. L indicates ladder marker. WT samples can be identified with two bands, Het samples with three (indicated with arrows). Expected band sizes can be found in *Figure 7.*

Table 6. All the samples looked at and their identified genotypes. No PCR detected indicates that no bands were detected.

Sample identity	Genotype
F5.1	WT
F5.2	Het
F5.3	Het
F5.4	No PCR detected
F5.5	No PCR detected

F5.6	No PCR detected
F5.7	No PCR detected
F5.8	Het
F5.9	Het
F5.10	Het
F3.2	WT
F3.3	Het
F3.4	WT
F3.5	WT
F3.6	Het
F3.7	Het
F3.8	Het

3.6 qPCR

3.6.1 RNA extraction

RNA extraction was carried out using the Direct-zol™ RNA Microprep kit (Zymo Research, R2080).

i) Buffer preparation

10 mL of ethanol (100%) was added to 40 mL Direct-zol™ RNA PreWash. 48 mL 100% ethanol was then added to 12 mL RNA Wash Buffer concentrate. Lyophilized DNase 1 was reconstituted with 275 µl RNase-Free water.

ii) Sample preparation

Embryonic mouse hearts were homogenised in 800 µl TRI reagent (Zymo Research R2050-1-50), in a innuSPEED Lysis Tube (AJ 845-CS-1030050) and the Precellys®24 homogenizer from Bertin Technologies for 1 minute. Homogenised tissue was then transferred into a new nuclease-free tube.

iii) RNA purification

An equal volume of 100% ethanol (800 µl) was added to the lysed sample in TRI reagent and mixed thoroughly. The mixture was transferred into a Zymo-Spin™ IC Column in a collection tube and was centrifuged. During RNA purification, centrifugation occurred at 13,000 x g for 30 seconds unless stated otherwise. The column was transferred into a new collection tube and the flow-through was discarded. For DNase 1 treatment, 400 µl RNA wash buffer was added to the column and centrifuged. 5 µl DNase 1 (6 U/µl) and 35 µl DNA Digestion buffer were added to an RNase-free tube and mixed by gentle inversion. This mix was then added directly to the column matrix. This was incubated at room temperature for 15 minutes. 400 µl Direct-zol™ RNA PreWash was added to the column and centrifuged. The flow-through was discarded and the wash step was repeated. 700 µl RNA Wash Buffer was added to the column and centrifuged for 1 minute to ensure the wash buffer was completely removed. The column was then transferred into an RNase-free tube. 15 µl of RNase-Free water was then added directly to the column matrix and centrifuged in order to elute the RNA. The NanoDrop® ND-1000 UV-Vis Spectrophotometer from Thermo Scientific was used to test both the purity and concentration of the eluted RNA.

3.6.2 cDNA conversion

A cDNA conversion master mix was made up and is shown in *Table 7*. RNA samples were diluted with RNase-Free water to a concentration of 10/ng/ ul. 10 µl of the master mix was added to 10 µl of the RNA mix in domed PCR tubes (100 ng RNA per reaction) (Star Lab,

I1405-8200). Reactions were performed using a MiniAmp Plus Thermal Cycler, Applied Biosystems by Thermo Fisher Scientific. Reactions were carried out at 25 °C for 10 minutes, 37 °C for 2 hours and held at 4 °C until removed from the machine.

Table 7. cDNA conversion master mix.

Reagent	Volume per sample in µl (10 µl per sample total volume)
10X Reverse Transcriptase buffer (Applied Biosystems, 4319981)	2
25X dNTP's (Applied Biosystems, 4367381)	0.8
10X random primers (Applied Biosystems, 4319979)	2
Reverse transcriptase (Applied Biosystems, 4308228)	1
Nuclease free H_2O	4.2

3.6.3 qPCR

1 µl cDNA from each sample was mixed with 9 µl qPCR master mix (TaqMan, *Table 8*) on a qPCR plate (Applied Biosystems, 4306737), to give a final volume of 10 µl. The plate was

wrapped with MicroAmp Optical Adhesive Film (Applied Biosystems, 4311971) and briefly centrifuged before being run on the qPCR machine. The negative control consisted of 1 µl RNase-Free H_2O and 9 µl master mix.

Table 8. TaqMan master mix used for qPCR. 1 µl cDNA from each sample was mixed with 9 µl qPCR master mix for a total volume of 10 µl that was ran on a qPCR plate.

Reagent	Volume per sample (µl)
2X fast master mix (Applied Biosystems, 4444554)	5
Nuclease-free H_2O	3
FAM probe (target)	0.5
VIC probe (***Gapdh***) (Applied Biosystems, 4351309)	0.5

Table 9. Target (FAM) probes included in the qPCR. All probes were multiplexed with *Gapdh* and were from the mouse species.

Target (FAM) probe
Actn1 (Applied Biosystems, 1697689 G6)
Actn2 (Applied Biosystems, 1918550 B11)

Actn3 (Applied Biosystems, 1477458 A12)
Actn4 (Applied Biosystems, 1518501 D3)
Actc1 (Applied Biosystems, 1656011 F10)
Nppa (Applied Biosystems, 1964727 F1)
Nppb (Applied Biosystems, 1951648 F1)
Acta1 (Applied Biosystems, 1968649 D2)
Myh7 (Applied Biosystems, 1974712 F8)
Hprt (Applied Biosystems, 1974746 D11)

3.6.4 Immunofluorescence image analysis

Immunofluorescence images were stained and imaged by an external collaborator (E. Ehler, KCL) and were quantified to assess the sarcomeres. Embryos collected at 15.5 days were stained for α-actinin (green) and titin (red). Nuclei were stained blue and were excluded from the analysis. The JACoP plugin on ImageJ was used to calculate a correlation coefficient. This determined the level of α-actinin and titin correlation in WT, Het and Hom embryos. In turn, this helped analyse myofilament integrity and assess for abnormalities in the sarcomeres of the embryos. The Image J plugin Colocalisation finder was used to generate cytofluorograms that gave an image of the level of colocalisation seen.

A failed beta-catenin and alpha-actinin stain on an embryo and an adult mouse cardiomyocyte stained with alternating Z-and M band markers were used as negative controls (correlation coefficient of 0). A different adult mouse cardiomyocyte stained with alternating Z-and M band markers was used as positive control (a correlation coefficient of 1).

Further image analysis looked at the ratio of green to yellow pixels, and therefore quantified the amount of membrane/peripheral bound Actn2 in the three different genotypes. This was determined by calculating green/green+yellow pixels; coloured pixels were counted using ImageJ and Excel was used to calculate the ratio of pixels seen.

3.7 *ACTN2* M228T variant iPSCs

3.7.1 Generation of the *ACTN2* M228T variant iPSCs

Clustered regularly interspaced short palindromic repeats (CRISPR)/Cas9 nuclease technology was used to generate the homozygous M228T *ACTN2* variant in iPSCs. A single guide RNA (sgRNA) was designed to target the site-specific Cas9 nuclease to the Methionine-228 genomic sequence. The ACTN2-sgRNA1 sequence was designed using (http://crispor.tefor.net) and was chosen due to being comparatively genome unique with minimal off-site targets. The sequence chosen was 5'-CCTGGATATTCCTAAAATGT – 3' which had the Protospacer Adjacent Motif (PAM) TGG at the end of the sequence to be cleaved. The Methionine was altered to Threonine using a single stranded oligonucleotide (ssODN) repair template for homology directed repair. In order to genotype the edited clones, an EcoRV restriction site was incorporated into the ssODN, to mark the presence of the mutant allele. The sgRNA and Cas9 formed a ribonucleoprotein complex, which was electroporated into early passage KOLF2-C1 cells. Individual clones were expanded and genotyped. This allowed the identification of the clones harbouring the desired homozygous M228T variant. Sanger sequencing of the target region was then used to confirm the M228T mutation. Fluorescent assisted cell sorting (FACS) was used to confirm pluripotency of the iPSCs. This found that all of the clones expressed high levels of the pluripotency markers OCT3/4, SOX2, NANOG and SSEA4. Karyotype analysis was used as a further quality check and confirmed that more than 20 spreads (out of 25) from each clone, had the normal

number of 46 chromosomes. This was carried out at the Wellcome Centre for Human Genetics at the University of Oxford (Dr Phalguni Rath) and iPSCs were transferred to the University of Birmingham.

3.7.2 Induced Pluripotent Stem Cell Culture

All cell culture was performed using the HPSI0114i-kolf_2 induced pluripotent stem cell line, commonly known as KOLF2 ([http://www.hipsci.org/lines/#/lines/HPSI0114i-kolf_2). Induced pluripotent stem cells were culture in Essential 8™ (E8) Medium (Thermo Fisher Scientific, A1517001) or mTeSR (StemCell, 85850). Medium was changed daily. Cells were maintained in 6 well plates coated with Vitronectin (VTN-N) Recombinant Human Protein, Truncated (A14700). Coating of plates was performed as stipulated in the manufacturer's manual. All cells were incubated at 37 °C and 5 % CO_2. Cells were passaged at 80 % confluency. Dissociation of the cells was performed using 0.5 mM ethylenediaminetetraacetic acid (EDTA) (Thermo Fisher Scientific, 15575020) for 5 minutes at room temperature. Cells were plated at a density between 10,000 and 30,000 cells/cm^2 in Essential 8 Medium or mTeSR, supplemented with ROCK inhibitor Y-27632 (Selleck, S1049) to give a final concentration of 10 μM. Media was changed after 24 hours back to Essential 8 Medium or mTeSR containing no ROCK inhibitor.

3.7.3 Thawing of iPSCs

ROCK inhibitor Y27632 (Selleck S1049) was added to mTeSR or Essential 8 medium to give a final concentration of 10 uM ROCK inhibitor mTeSR or Essential 8 medium. This solution was transferred into a 15 mL falcon tube. The cryovial containing the cells was quickly defrosted in a 37 °C water bath (<30 seconds). The cells were transferred to the mTeSR or

Essential 8 ROCK inhibitor solution and then spun down (300 G for 3 mins) and resuspended in 1 mL mTeSR or Essential 8/ROCK. 1 mL of the cell mix was plated with an extra 1 mL mTeSR or Essential 8/ROCK in one well of a 6 well plate coated in matrigel or vitronectin. The plate was placed in the incubator overnight (37 °C at 5 % CO_2).

3.7.4 Freezing of iPSCs

The media from the wells was aspirated and 2 mL of EDTA was added per well. This was left for 5 minutes at room temperature before being aspirated off. 1 mL mTeSR was used to wash the cells off and was subsequently transferred into a 15 mL falcon. A further 1 mL of mTeSR was used to wash the well of any remaining cells. 10 µl of the cells were mixed with 10 µl of trypan blue 0.4% (Gibco, 15250) and vortexed before the cells were counted. The cells were spun at 300 G for 3 minutes and resuspended in mFreSR (StemCell, #05855) to give a final concentration of approximately 1 million cells per vial (per 1 mL). These were stored at -80 °C overnight before being transferred to liquid nitrogen.

3.7.5 Induced Pluripotent Stem Cell Cardiomyocyte differentiation

To optimise the differentiation of the *ACTN2* iPSCs, different protocols were tested, and variations of the protocols were used to see which was most favourable. Comparisons of the different techniques can be found in *Table 10.*

Table 10: Comparison of the CHIR/IWR1 protocol and the BMP4+AA/KY02111+XAV939 protocol. The table shows the different reagents used in the protocols on each day. *Note for the CHIR/IWR1 protocol: RPMI-Glucose (Gibco, 11879-020) +B27+Ins is used instead of

RPMI+B27+Ins (2 mL) for up to 3 days (without medium change) (typically started on d11-d12).

Day	CHIR/IWR1 (original)	BMP4+AA/KY02111+XAV939
-1 (pre-conditioning)	mTeSR 1:200 Mtg	StemPro34 SFM* 1:100 2 mM L-Glutamine 1 ng/mL BMP4 1:100 Mtg
0	RPMI+B27-MinusIns 8 μM CHIR	StemPro 1:100 L-Glutamine 10 ng/mL BMP4 8 ng/mL Activin A
1	50% CHIR dilution using RPMI+B27-MinusIns (eg. 2 mL added to each well of a 6-well plate)	-
2	Full RPMI+B27-MinusIns medium change	RPMI+B27-MinusIns 10 μM KY02111 10 μM XAV939
3	RPMI+B27-MinusIns 3 μM IWR	-
4	-	RPMI+B27+PlusIns 10 μM KY02111 10 μM XAV939
5	Medium change to plain RPMI+B27-MinusIns	-
6	-	Medium change to plain RPMI+B27+PlusIns (Medium changes continue every-other day)
7	Medium change to plain RPMI+B27+PlusIns (Medium changes continue every-other day)	-

3.7.5.1 Differentiation using CHIR/IWR1

To start with, the protocol using the small molecules CHIR/IWR [68] was used to try and differentiate the iPSCs into cardiomyocytes. iPSCs were seeded at approximately 100,000 cells per well in a 6-well plate, 3-4 days before the start of differentiation. A matrigel (Mtg) sandwich was made by adding Corning™ Matrigel™ Membrane Matrix (1:200) to mTeSR on Day -1. On day 0 (90-95% confluency), 8 μM CHIR-99021 (Stratech, A3011) was added to RPMI+B27-MinusIns (Gibco, 11875-093 with Gibco A18956-01) (1:50). 2 mL of this solution was added to each well. On day 1 (after 24 hours), 2 mL RPMI+B27-MinusIns was added to each well, to dilute the CHIR concentration by half. Day 2 involved a medium change with RPMI+B27-MinusIns (2 mL). On day 3, the cells were treated with 5 μM IWR-1-endo (Stratech, S7086-SEL) in RPMI+B27-MinusIns. On day 5, the media was changed with RPMI+B27-MinusIns. The media was subsequently changed on day 7 with RPMI+B27+Ins (Gibco, 11875-093 with Gibco 17504-044) and was subsequently changed every other day.

When the standard protocol did not work, a gradient of CHIR concentrations was used to try and differentiate the cells. See *Figure 9*. For this, cells were seeded onto a 12 well plate to minimise the amount of media needed. As the CHIR gradient still did not produce differentiating cells, both a CHIR gradient and seeding density gradient were used. The BMP4+AA/KY02111+XAV939 protocol was also tested using this seeding density gradient. This can be seen in *Figure 10*.

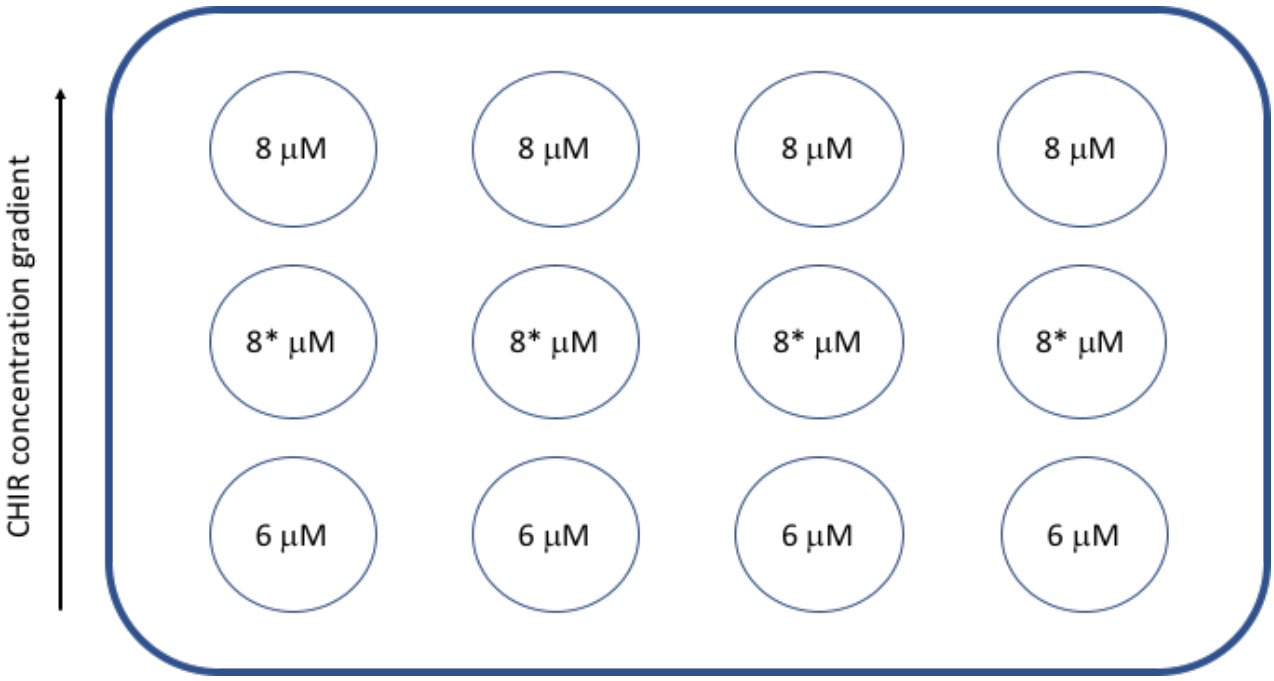

Figure 9. A 12-well plate showing the CHIR concentration gradient used during the CHIR/IWR1 protocol. 8* followed the original CHIR/IWR1 protocol, except on day 1 where 0.5 mL of the media was removed and replaced with 0.5 mL of fresh RPMI+B27-MinusIns. This diluted CHIR from 8 µM to 2 µM.

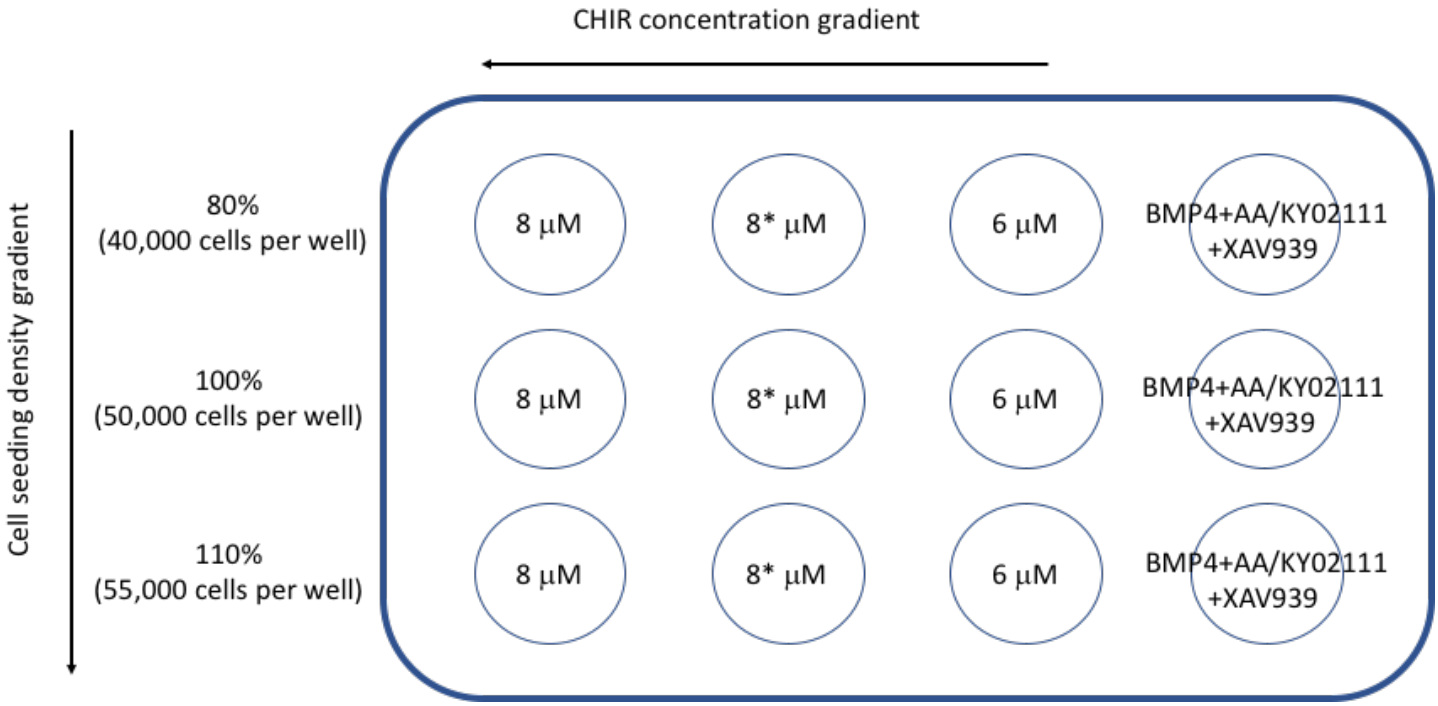

Figure 10. A 12-well plate showing the CHIR concentration and cell seeding density gradient used during the CHIR/IWR1 and BMP4+AA/KY02111+XAV939 protocol (CHIR was used in the CHIR/IWR1 protocol only). 8* followed the original CHIR/IWR1 protocol, except on day 1 where 0.5 mL of the media was removed and replaced with 0.5 mL of fresh RPMI+B27-MinusIns. This diluted CHIR from 8 μM to 2 μM. The standard BMP4+AA/KY02111+XAV939 protocol was used for the final row of wells as shown.

3.7.5.2 Differentiation using BMP4+AA/KY02111+XAV939

IPSCs were differentiated into cardiomyocytes using a currently unpublished protocol kindly provided by Chris Denning (University of Nottingham). A schematic of this protocol can be seen in *Figure 11*. Undifferentiated iPSCs were seeded onto 6 well plates coated in Corning™ Matrigel™ Membrane Matrix (Fisher Scientific, 11573620) (1:100) as stipulated according to the manufacturer's manual. On Day -1 when the cells were approximately 60 % confluent, E8 medium was changed to StemPro™-34 SFM (Thermo Fisher Scientific, 10639011) supplemented with Recombinant Human BMP-4 Protein (BMP-4) (1ng/mL) (R&D Systems, 314-BP-010/CF), L-Glutamine 2 mM (Thermo Fisher Scientific, 25030024) and Mtg (1:100). After 10 hours (Day 0), the medium was changed to StemPro™-34 SFM that was supplemented with L-Glutamine (2 mM final concentration), BMP-4 (10 ng/mL final concentration) and Human Activin A Recombinant Protein (Activin A) (Thermo Fisher Scientific, PHC9564) (8 ng/mL final concentration). On Day 2 medium was changed into RPMI+B27-MinusIns, supplemented using KY02111 (TOCRIS, 4731) with XAV 939 (TOCRIS, 3748) (both at 10 μM final concentration). On Day 4 (48 hours later), medium was changed to RPMI+B27+PlusIns with KY02111 and XAV 939 (both at 10 μM final concentration). On Day 6 (48 hours later), medium was changed to RPMI+B27+PlusIns and was subsequently changed every other day until the cells were plated for staining on D16.

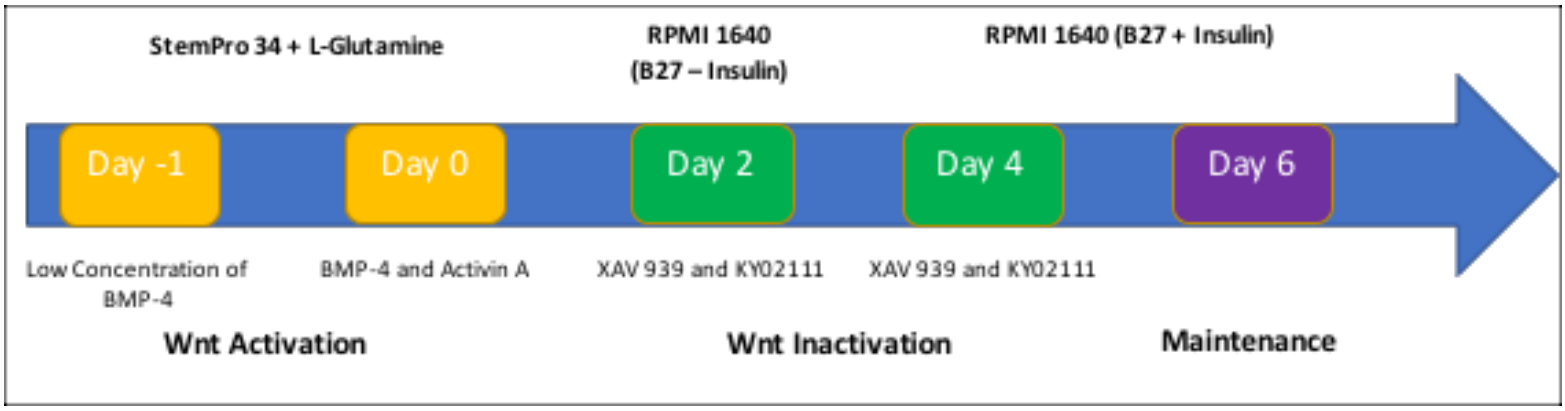

Figure 11. Kindly provided by PhD student Max Cumberland (University of Birmingham). Schematic representation of the unpublished cardiac differentiation (Chris Denning, University of Nottingham). Wnt signalling pathway activation enables mesodermal specification. This is achieved using the recombinant proteins BMP-4 and Activin A. Inactivation of Wnt signalling is achieved using the small molecules KY02111 and XAV 939.

3.8 Fixing and staining of cardiomyocytes

3.8.1 Splitting Cardiomyocytes

Both *ACTN2* and parental cardiomyocytes were split into 24 wells of a 96 well plate that had been coated with Mtg. The media was aspirated from the cells and they were washed with 1 mL of phosphate buffered saline (PBS) (Gibco, 10010023) before being incubated in TryplE Express (Gibco, 12605-010) for 6 minutes in the incubator. The cells were washed off the plate with 2 mL of RPMI+B27(+Ins) with 10 % Knock out replacement serum (Gibco, 10828028) and 2 μM Thiazovivin (Selleck, S1459). The cells were spun at 300 G for 3 mins and the pellet was resuspended in this plating media. The cells were seeded into the wells of the 96 well plate at varying densities and incubated at 37 °C 5 % CO_2 for 3 days prior to fixation and staining.

3.8.2 Fixation and Staining

To fix the cells the media was removed, and the cells were washed twice with PBS. Samples were fixed in 4% paraformaldehyde (PFA) for 15 minutes at room temperature. The PFA was removed and the samples were washed twice with PBS. The samples were blocked and permeabilized in blocking buffer solution (500 mL 1X PBS, 25 mL Foetal Bovine Serum (FBS) (Sigma-Aldrich, MFCD00132239), 5 g Bovine Serum Albumin (BSA) (Sigma, A3311), 2.5 mL Triton X-100 (Sigma, T8787)), for 30 minutes. Subsequently, they were incubated with the primary antibodies (Actn2 1:500 or T12 1:15) (Abcam, Ab68167 and Made in-house by Elizabeth Ehler KCL London,) for 60 mins at room temperature. The samples were then washed in blocking buffer without Triton X-100 and incubated with secondary antibodies (Anti-rabbit 1:500 (Invitrogen, 2256822) for *Actn2* and Anti-mouse 1:500 (Life Tech, 1745855) for T12) and Sytox Orange dye 1:10,000 (Invitrogen, 2189174) for 60 mins in the dark at room temperature. Samples were washed twice in PBS and then imaged. Plates were imaged using the Olympus inverted fluorescence microscope camera (XM-10).

3.9 FACS

3.9.1 Sample preparation

Cells were detached from the wells using 1 mL of TriplE per well for 2 minutes in the incubator. They were then washed with PBS and the cell mix was collected and total number of cells were counted. 1 million cells were put into each 1.5 mL eppendorf tube which were spun for 3 mins at 300 G and the supernatant was removed, leaving the cell pellet. There were 16 samples in total, 8 WT and 8 *ACTN2* Hom. 4 of each genotype would be unstained, whilst the other 4 would be stained with OCT4+Fluorescein and SOX2+APC.

3.9.2 Staining the cells

The cell pellet was resuspended in 1 mL FACS buffer (Invitrogen, 00-4222-26) and incubated with 1 µl LIVE/DEAD™ Fixable Violet Dead Cell Stain Kit for 405 nm excitation (Invitrogen, L34955) for 30 mins on ice. The samples were washed by centrifuging for 5 mins at 500 G, removing the supernatant and resuspending the pellet in 500 µl of FACS buffer. After two washes, the pellets were resuspended in 400 µl Fixation Buffer (Invitrogen, 88-8824-00) and incubated on ice covered from light for 30 mins. Samples were then washed by centrifuging for 5 mins at 500 G, removing the supernatant and resuspending the pellet in 500 µl Permeabilization Buffer 1X working solution with 1-part 10X concentrate with 9 parts distilled water (Invitrogen, 88-8824-00). This was repeated a second time. The pellets were resuspended in another 500 µl Permeabilization Buffer with the conjugated primary antibodies (see *Table 11*). Samples were incubated in the cold room overnight. The following day, samples were washed twice in 500 µl Permeabilization buffer before the pellets were resuspended in 1 mL FACS buffer and analysed by flow cytometry.

Table 11. Primary antibodies with their appropriate conjugates used in the FACS protocol.

Primary antibody	Conjugate
Human/Mouse Oct-3/4 Fluorescein-conjugated Antibody (R&D systems, IC1759F-100)	Rat IgG_{2B} Fluorescein-conjugated Antibody (R&D systems, IC013F)
Human/Mouse SOX2 APC-conjugated Antibody	Mouse IgG2A APC-conjugated Antibody

(R&D systems, IC2018A)	(R&D systems, IC003A)

3.10 Statistical analysis

Graph Pad Prism version 9.0.0 (86) for Mac OS X (GraphPad Software, San Diego, California USA, www.graphpad.com) was used to test for normality before producing graphs and testing for significance. Two-way ANOVA, One-way ANOVA, unpaired T-tests and Chi-squared tests were used where appropriate. Sidak's multiple comparison tests were performed to compare the groups being looked at when two-way ANOVA was performed, and Tukey's multiple comparison was used for one-way ANOVA. A critical significance value of 0.05 was chosen for all proceeding statistical tests. Going forward, values of significance are as follows: **** (P = <0.0001) *** (P = 0.0001 to 0.001) ** (P = 0.001 to 0.01) * (P = 0.01 to 0.05). No * or ns (P = ≥0.05). Western blots were quantified using Image J [69]. Proteins investigated in Western blots were normalised against WT females for the housekeeping protein glyceraldehyde 3-phosphate dehydrogenase (Gapdh). FACS data was analysed and gating strategies were computed by Dr Jasmeet Reyat using FlowJo.

4. Results

4.1.1 Presence of the homozygous pathogenic variant in *Actn2* (M228T) does not affect heart weight

To determine the impact of M228T pathogenic variant in the *Actn2* gene on heart size, hearts were removed and weighed (HW) before being normalised to body weight (BW). When comparing HW to BW, no significant differences were found in this ratio to be related to genotype. Sex differences were only seen for male vs female Heterozygotes (Hets) in the 37-38 weeks age group (P=0.039, *Figure 12C).*

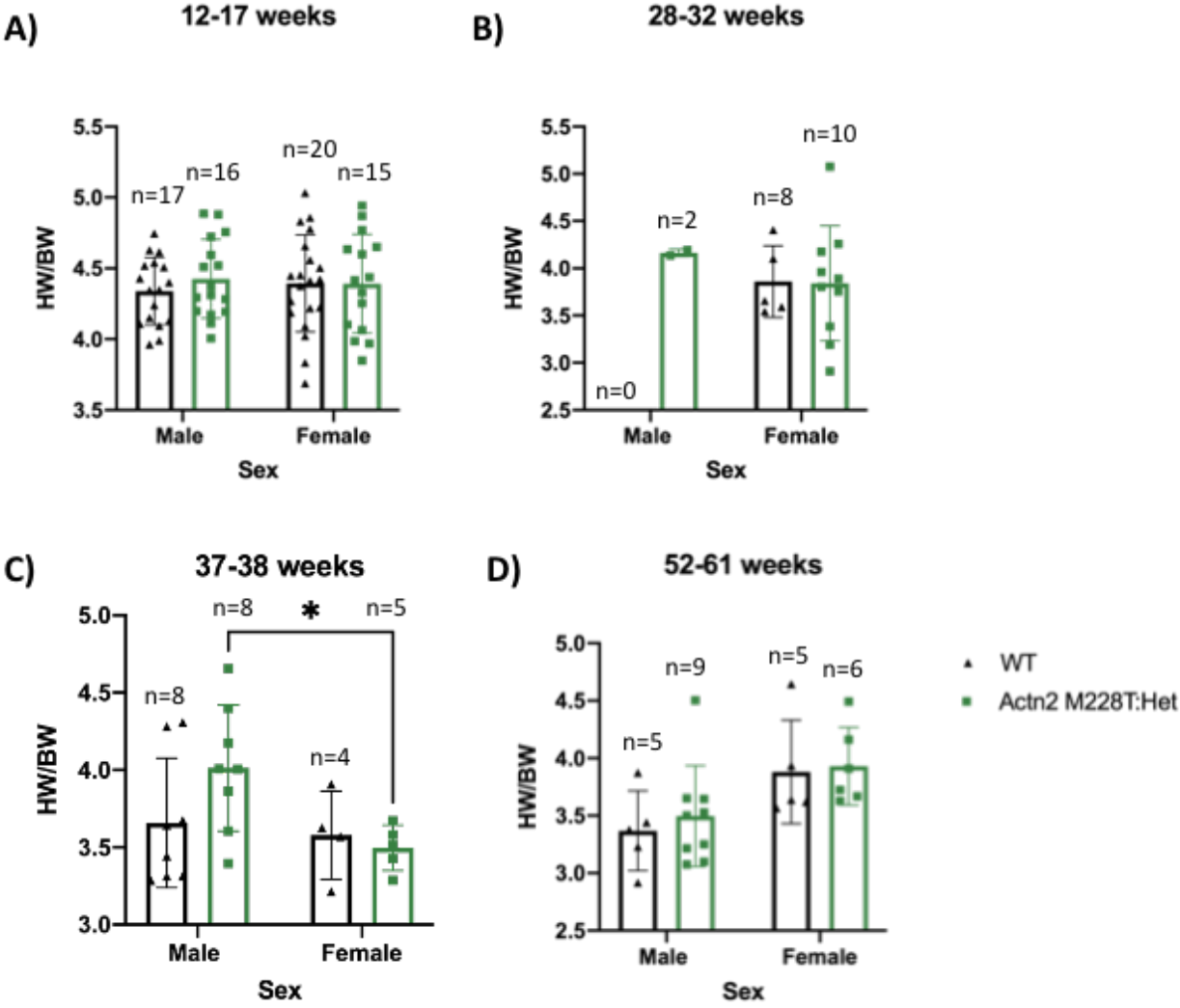

Figure 12. Heart weight to body weight ratio (HW/BW) of male and female mice of different genotypes (WT and *Actn2* M228T:Het). Individual data points are shown and n numbers represent the number of mice in each group**. A:** 12-17 weeks. **B:**28-32 weeks. **C**: 37-38 weeks. **D**: 52-61 weeks. Data presented as mean ± SD. A 2-way ANOVA was performed.

Tibia length (TL) is a more standard and widely used measure of heart weight, due to fluctuations that occur in BW. Once the mouse reaches adulthood, the tibia length is stable and means that TL is a better tool for normalisation compared to BW. This explains why clearer differences were found when heart weights were normalised for TL instead of BW. As expected, there was a significant difference ($P<0.0001$) between males and females, independent of genotype, for mice in age groups 12-17 weeks and 52-61 weeks (*Figure 13A, 13D*). No significance was found between the different genotypes or between males/females of any other age groups.

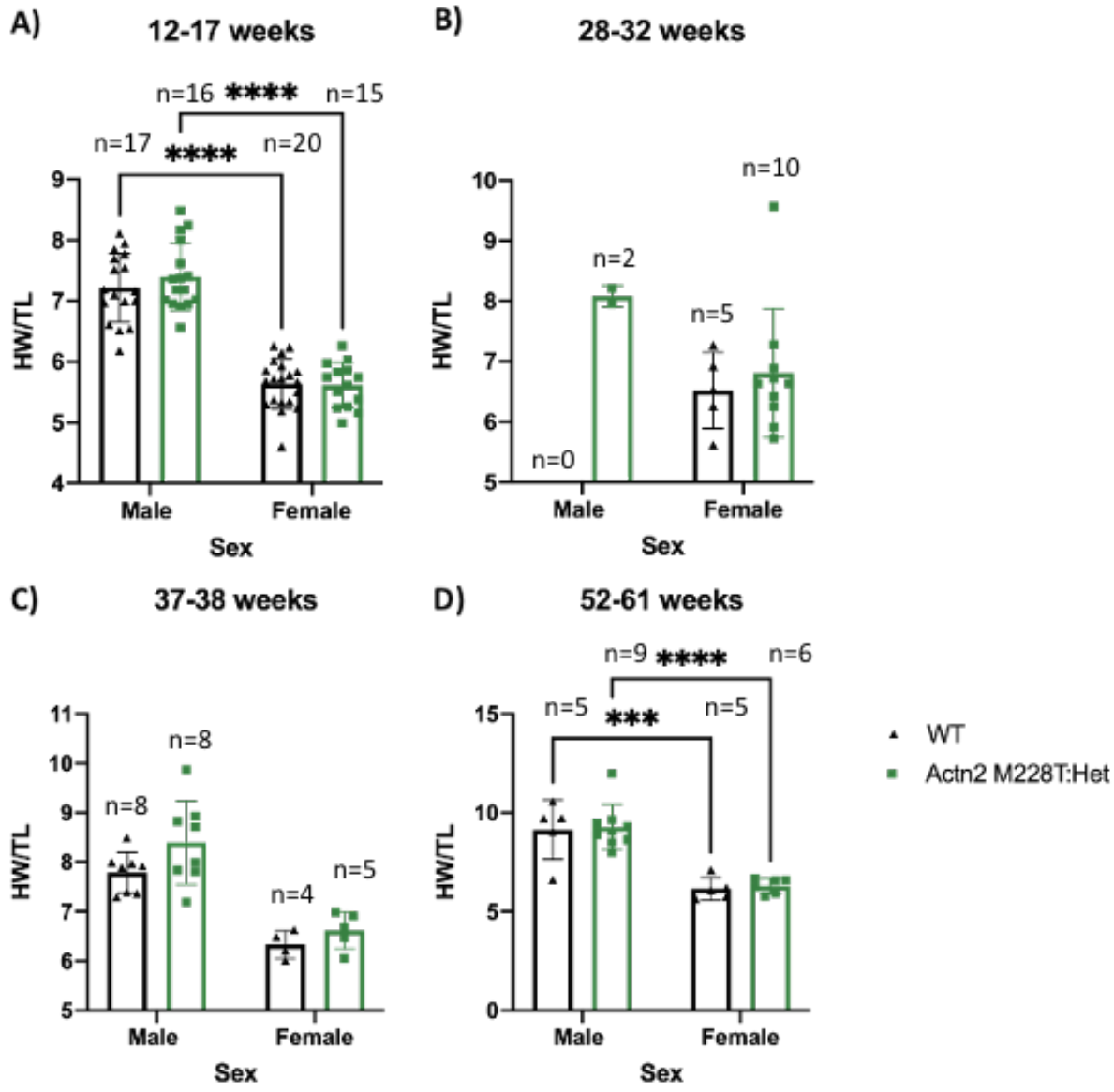

Figure 13. Heart weight to tibia length ratio (HW/TL) of male and female mice of different genotypes (WT and *Actn2* M228T:Het). Individual data points are shown and n numbers represent the number of mice in each group**. A:** 12-17 weeks. **B:**28-32 weeks. **C**: 37-38 weeks. **D**: 52-61 weeks. Data presented as mean ± SD. A 2-way ANOVA was performed.

4.1.2 Presence of the pathogenic variant in *Actn2* (M228T) does not affect body weight/tibia length ratio in adult mice

To quantify any differences in BW between WT and Het mice, BW was recorded at the relevant ages and normalised to TL to account for any differences in body length. As expected, statistical analysis revealed males to be significantly heavier compared to age-match females at 12- 17 weeks, $P<0.0001$ (*Figure 14A*) and 52-61 weeks (*Figure 14D*). No significant differences were found within age-groups between WT and Het animals, therefore the presence of the pathogenic variant in *Actn2* (M228T) did not affect the weight of these adult mice.

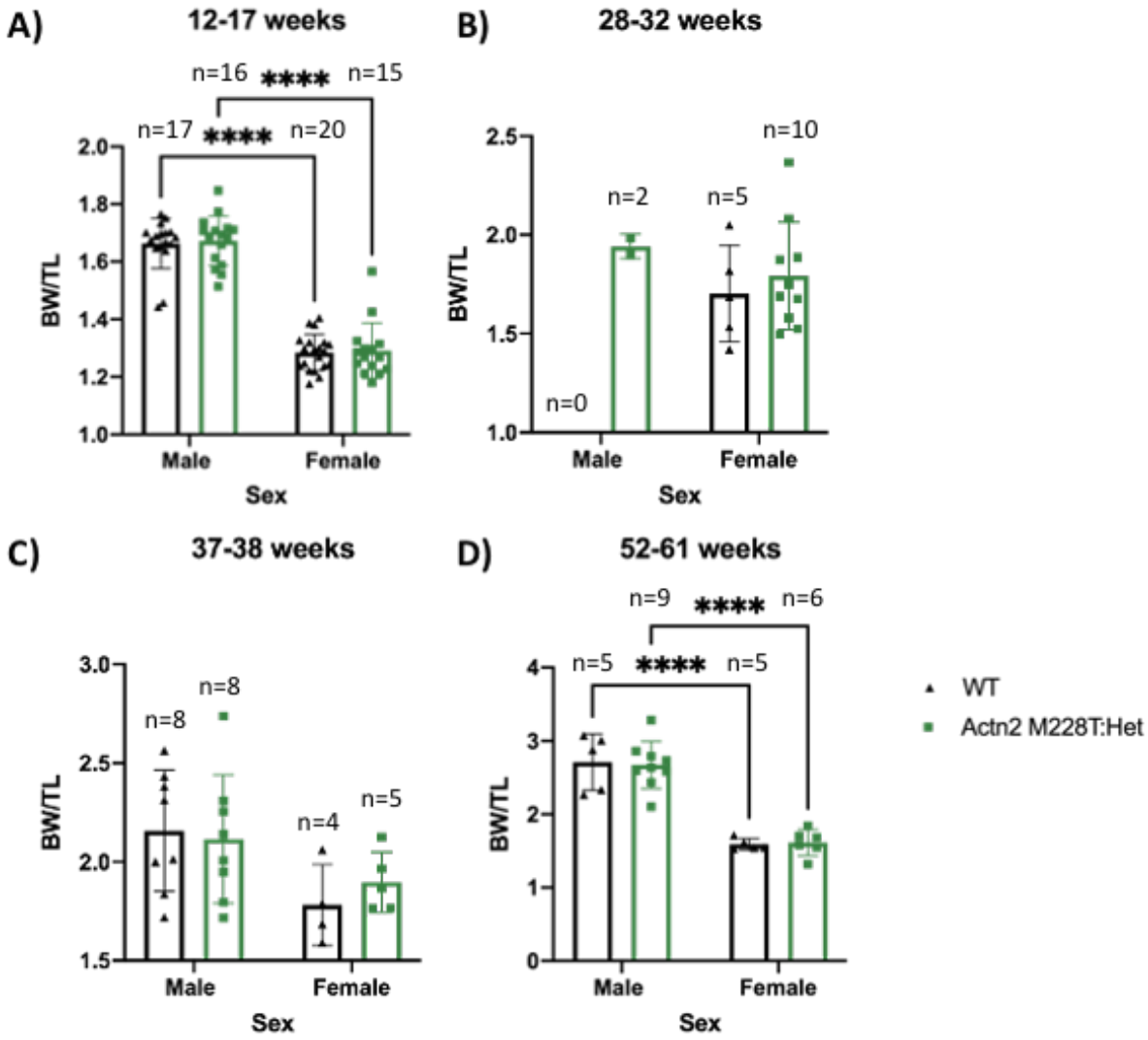

Figure 14. Body weight to tibia length ratio (BW/TL) of male and female mice of different genotypes (WT and *Actn2* M228T:Het). Individual data points are shown and n numbers represent the number of mice in each group**. A:** 12-17 weeks. **B:**28-32 weeks. **C**: 37-38 weeks. **D**: 52-61 weeks. Data presented as mean ± SD. A 2-way ANOVA was performed.

4.1.3 Myotilin and heat shock protein 27 levels are increased in *Actn2* M228T mouse hearts

To determine whether mice heterozygous for the M228T pathogenic variant in *Actn2* had altered α-actinin 2 (Actn2) protein expression, Western blotting was used to evaluate levels

of protein expression in 38-week-old male and female WT and Het mice. Across both genotypes the levels of expressed Actn2 was consistent (*Figure 15A*). However, the levels of Actn2 expression were significantly reduced in females when compared to males (*Figure 15Bi*; P = 0.03).

To investigate any occurrence of hypertrophy at a molecular level as a consequence of the M228T *Actn2* pathogenic variant, protein markers were evaluated by Western blot. Expression of beta-myosin heavy chain (Myh7) was reduced in females heterozygous for the M228T pathogenic variant when compared to Het males (*Fig 15Bii*, P = 0.02). Although there is a trend between male WT and Hets, this is not conclusive due to low n numbers. Myotilin (Myot) appeared to have higher expression in Het males compared to Het females (*Figure 15Biii*). More importantly, there was a statistically significant difference between WT and Het animals (between males; P <0.0001, between females; P = 0.0355). Cardiac troponin T (cTnT) appeared to be consistently expressed across both genotypes and sexes (*Figure 15Biv*). Heat shock protein 27 (Hsp27) appeared to have higher expression in Hets compared to WTs, however this was not statistically significant (*Fig 15Bv*). Interestingly, Het males had increased expression of Hsp27 when compared to Het females (P = 0.013). Heat shock protein family B (small) member 7 (HspB7) showed higher expression levels in male Hets compared to WTs (P = 0.002, *Figure 15Bvi*). A significant increase in HspB7 expression was also seen in Het males compared to Het females (P = 0.001).

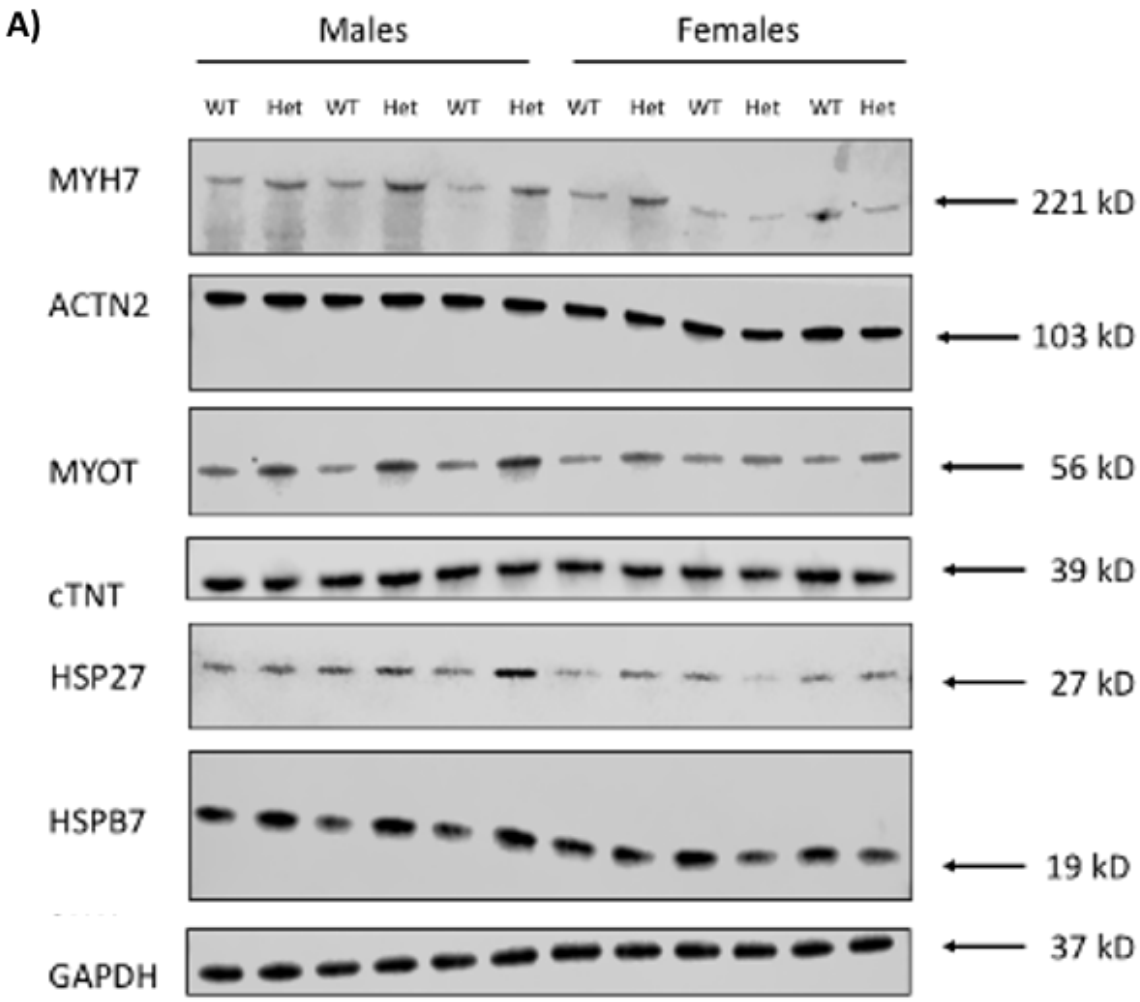
A)
Males
Females
WT
Het
WT
Het
WT
Het
WT
Het
WT
Het
WT
Het
MYH7
221 kD
ACTN2
103 kD
MYOT
56 kD
cTNT
39 kD
HSP27
27 kD
HSPB7
19 kD
GAPDH
37 kD

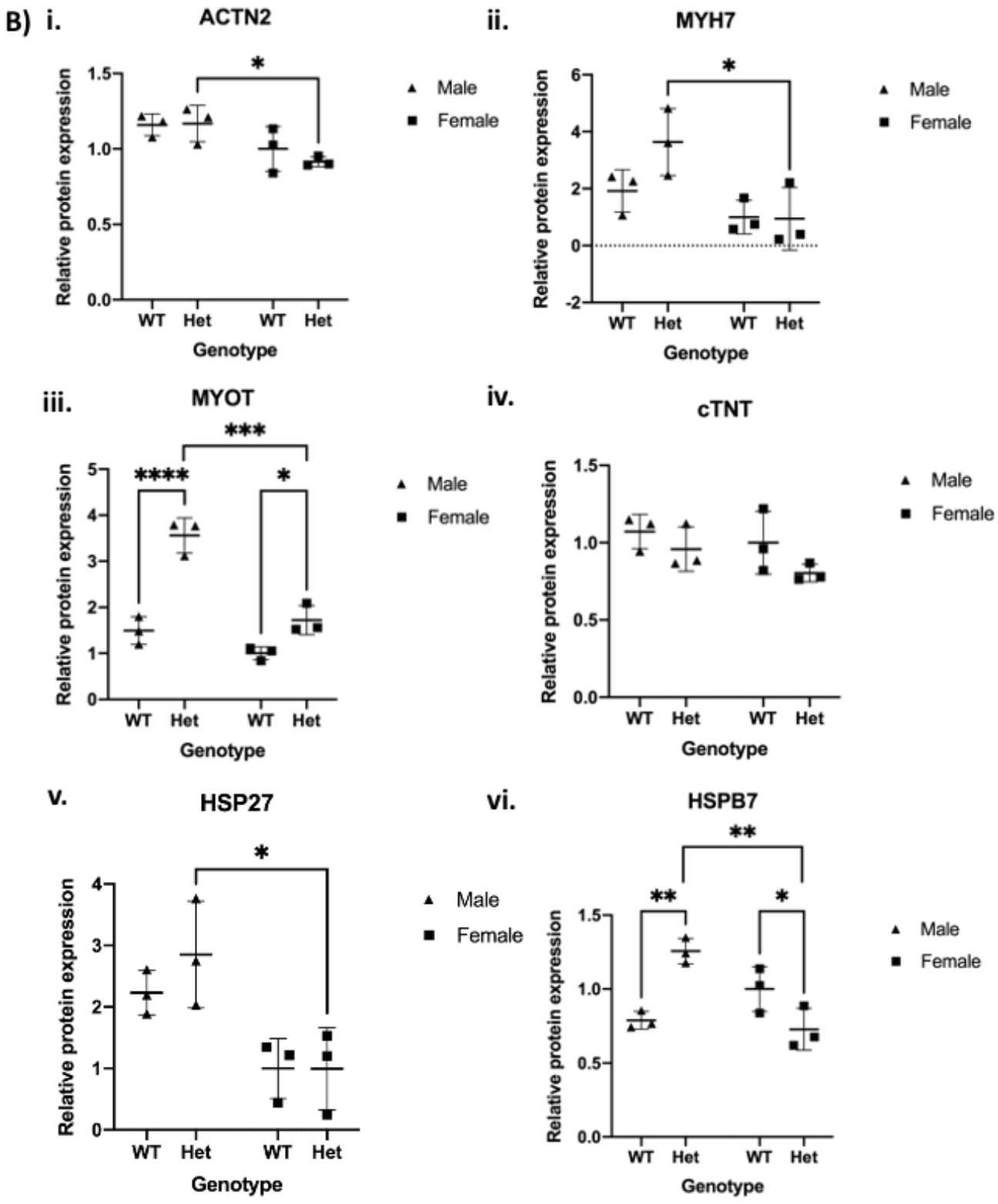

Figure 15. A: Western blot analysis of protein expression levels for male and female mice that are either WT or Het for the *Actn2* M228T variant. Proteins are shown from the highest molecular weight to the lowest. Arrows with corresponding numbers represent molecular

weight. Proteins were chosen due to being markers of hypertrophy or due to being upregulated in other models of cardiomyopathy [70] and GAPDH was used to normalise the other proteins. **B:** Relative protein expression of male and female mice samples that are either WT or Het for the Actn2 M228T variant. Specific proteins are looked at in each graph: **i**: MYH7, **ii**: ACTN2, **iii**: MYOT, **iv**: cTNT, **v**: HSP27, **vi**: HSPB7. GAPDH of the control group WT females (to an average of 1) (not shown), was used to normalise all the samples. Data are presented as mean ± SD (n=3). A 2-way ANOVA was performed.

Overall the adult mouse model for *Actn2* M228T Het, appeared to show no difference in the parameters for HW/TL, HW/BW or BW/TL when compared to the WT. However, at a molecular level, the presence of the pathogenic variant increased levels of Myot and HspB7 compared to the WT, with more striking differences in the males.

4.2 Embryonic mouse model

The M228T pathogenic variant in *Actn2* is embryonic lethal when homozygous (Jiang and Gehmlich, unpublished data), however it is known that homozygous (Hom) mice do survive until E15.*5, in utero*. Therefore, to investigate the impact of being Hom for this pathogenic variant in mice development and survival, Het females were time mated with Het males. The presence of a vaginal plug was designated E0.5. Resultant embryos were collected at E15.5, hearts were removed and front limbs were fixed in formalin. Tail snips were also taken for subsequent genotyping.

4.2.1 Genotype does not affect embryonic development indicated by Theiler stage

To assess the developmental stage of embryos from each genotype, front limbs were observed while still being blinded to genotype and compared to Theiler stage criteria [67]. A

Chi-squared test on absolute numbers of embroys showed no significance (P = 0.3690) between genotype and Theiler stage of the mice (*Figure 16*).

Figure 17 represents the weight distribution of embryos collected at E15.5 across genotypes. There was a larger variation in the weights of Het and Hom embryos when compared to WT embryos across all collections at E15.5, however the means were similar between genotypes (WT; 0.40, Het; 0.37, Hom; 0.38). The dotted line represents the 10th percentile, a common clinical marker of small for gestational age. Overall, 26.4%, 37.8% and 36.1% of WT, Het and Hom embryos fall below the 10th percentile respectively. Statistical testing revealed non-significance (chi-squared test). This further supports the Theiler staging results that genotype has no significant difference on embryonic development.

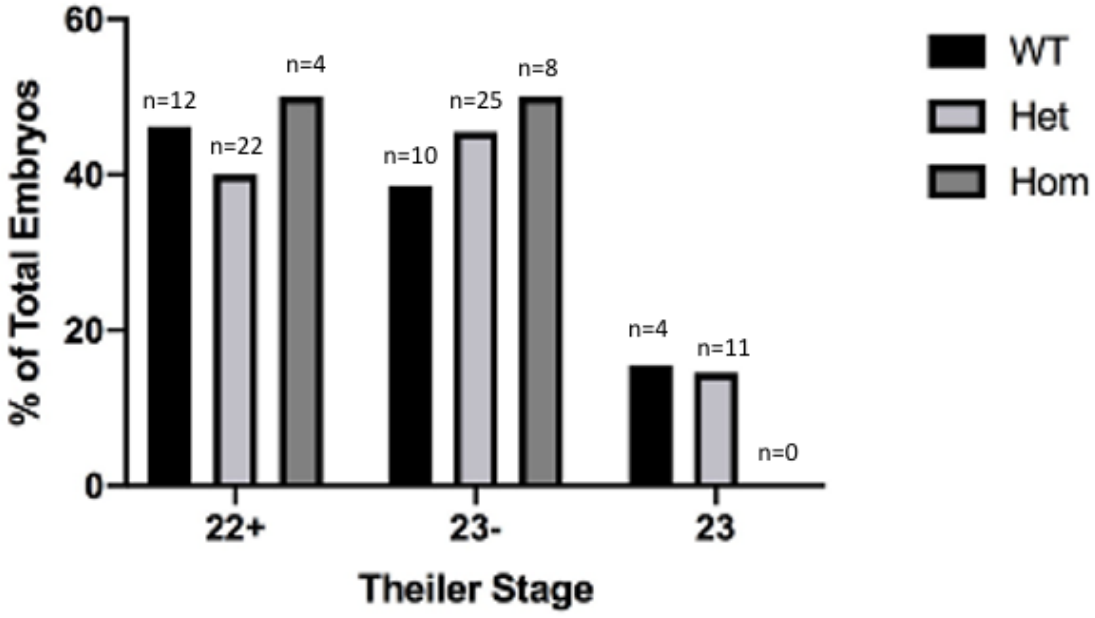

Figure 16. % of total embryos that have been grouped according to genotype (WT, Het or Hom), that are either stage 22+, 23- or 23 according to Theiler stage for identifying phenotype of the mice embryos collected at E15.5. Each genotype is set to 100%. A total of 96 embryos were assessed. n numbers are indicated with n.

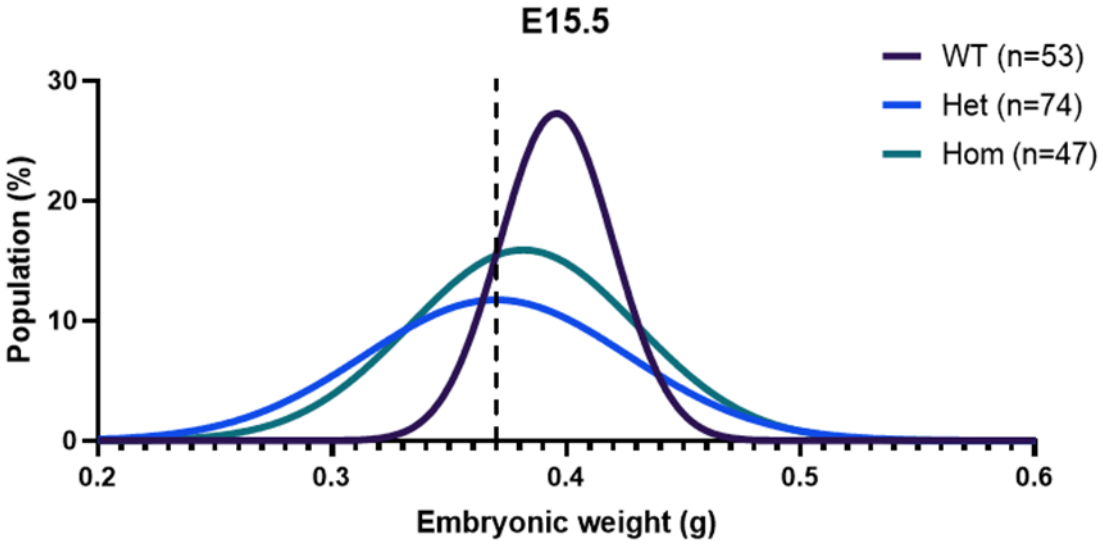

Figure 17. Provided by Dr Sophie Broadway-Stringer (University of Birmingham). A distribution curve for embryonic weight at E15.5 for all three genotypes (WT, Het and Hom). Dotted line represents the 10th percentile.

4.2.2 Homozygous embryos have increased gene expression of *Actn2* and *Actn3*

qPCRs were used to explore the impact of the *Actn2* M228T variant on expression of the actinins (*Figures 18*). No significant difference was seen for gene expression of *Actn1, Actn4* or *Actc1* (*Figure 18*) between the WTs and Homs. *Actn2* and *Actn3* expression was increased in Homs (*Figure 18B* and *C* respectively) (P = 0.0067 and P = 0.0072 respectively).

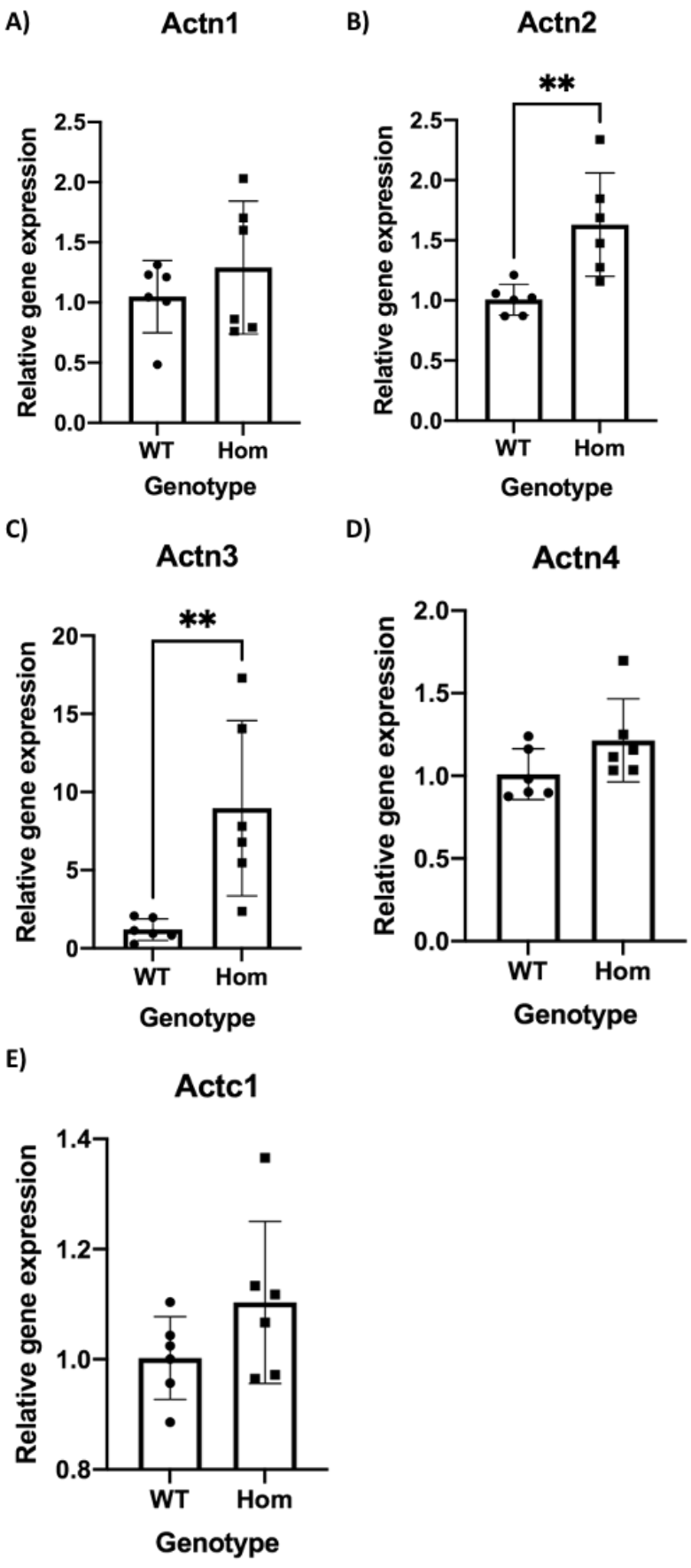
A)
Actn1
Relative gene expression
2.5
2.0
1.5
1.0
0.5
0.0
WT
Hom
Genotype
B)
Actn2
**
Relative gene expression
2.5
2.0
1.5
1.0
0.5
0.0
WT
Hom
Genotype
C)
Actn3
**
Relative gene expression
20
15
10
5
0
WT
Hom
Genotype
D)
Actn4
Relative gene expression
2.0
1.5
1.0
0.5
0.0
WT
Hom
Genotype
E)
Actc1
Relative gene expression
1.4
1.2
1.0
0.8
WT
Hom
Genotype

Figure 18. Relative gene expression of embryonic mice (E15.5) samples that are either WT or Hom for the *Actn2* M228T variant. Specific genes are looked at in each graph: **A:** *Actn1* **B:** *Actn2* **C:** *Actn3* **D:** *Actn4* **E:** *Actc1*. *Gapdh* (not shown) was used to normalise all the samples. Individual points are shown. Error bars represent standard deviation from the mean (mean +/- SD). Statistical tests performed were unpaired T-tests.

Further qPCRs were performed to investigate expression of genes involved in the foetal gene programme (*Nppa, Nppb, Acta1* and *Myh7*). The housekeeping gene (*Hprt*) was also investigated. Statistical significance was found between WTs and Homs for all genes except *Hprt* (*Figure 19E*). *Nppa* showed a significant difference of P = 0.0009 (*Figure 19A*) and *Nppb* found P = 0.0026 (*Figure 19B*). *Acta1* found significance of P = 0.0459 (*Figure 19C*), whilst *Myh7* had a difference of P = 0.0365 (*Figure 19D*). Genes involved in the foetal gene programme (*Nppa, Nppb* and *Myh7*) showed upregulation in the Hom setting.

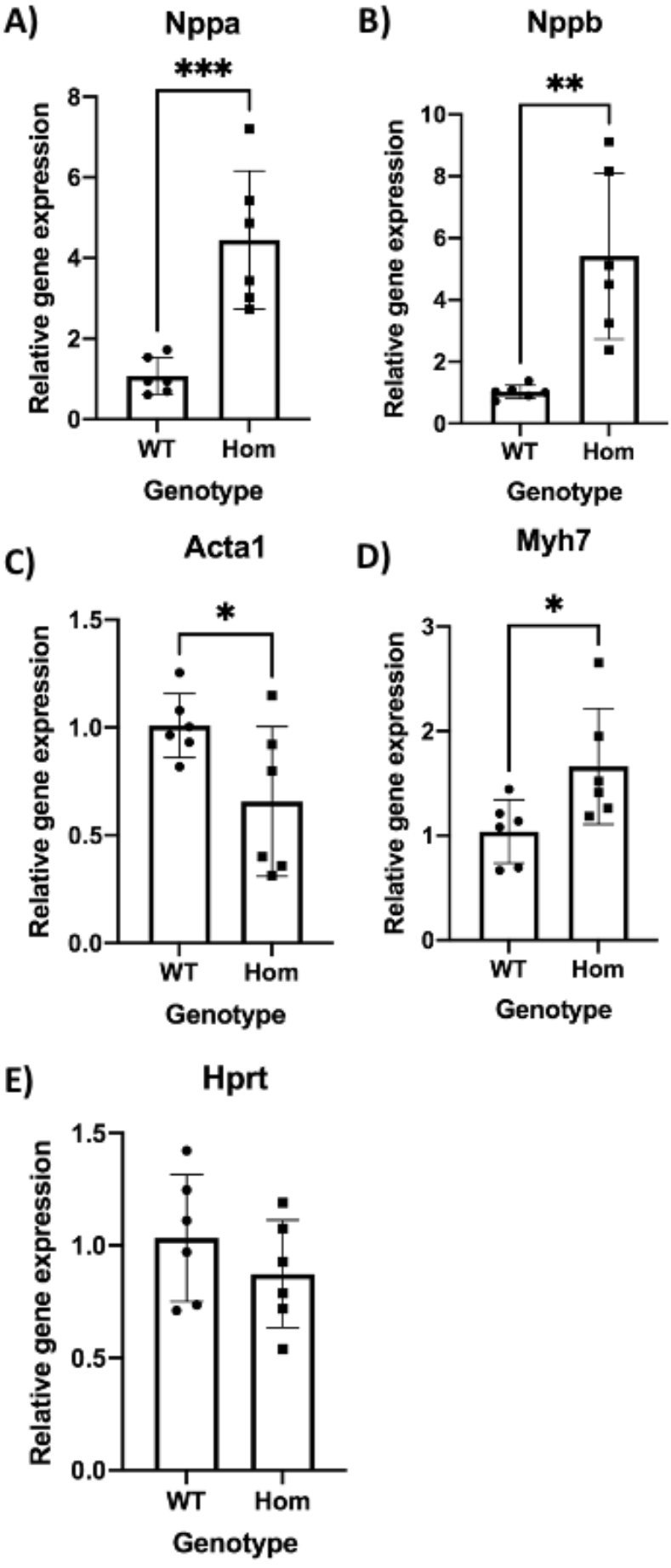
A)
Nppa
***
Relative gene expression
8
6
4
2
0
WT
Hom
Genotype
B)
Nppb
**
Relative gene expression
10
8
6
4
2
0
WT
Hom
Genotype
C)
Acta1
*
Relative gene expression
1.5
1.0
0.5
0.0
WT
Hom
Genotype
D)
Myh7
*
Relative gene expression
3
2
1
0
WT
Hom
Genotype
E)
Hprt
Relative gene expression
1.5
1.0
0.5
0.0
WT
Hom
Genotype

Figure 19. Relative gene expression of embryonic mice (E15.5) samples that are either WT or Hom for the *Actn2* M228T variant. Specific genes are looked at in each graph: **A:** *Nppa* **B:** *Nppb* **C:** *Acta1* **D:** *Myh7* **E:** *Hprt*. *Gapdh* (not shown) was used to normalise all the samples. Individual points are shown. Error bars represent standard deviation from the mean (mean +/- SD). Statistical tests performed were unpaired T-tests.

4.2.3 Homozygous embryos have reduced Actn2 protein expression

Markers of hypertrophy in adult Het mice were indicative of changes at a molecular/protein level (*chapter 4.1.3*), therefore, to assess the previously effected proteins in a homozygous model of this pathogenic variant, Western blotting was used. Het embryos were also included in this analysis. There appeared to be a visibly lower amount of Actn2 in the homozygous embryos (*Figure 20A*). Experiment for Actn2 was done in triplicate and in combination there is statistical significance between WT and Het ($P = 0.0003$) and WT and Hom ($P < 0.0001$) groups (*Figure 20B*).

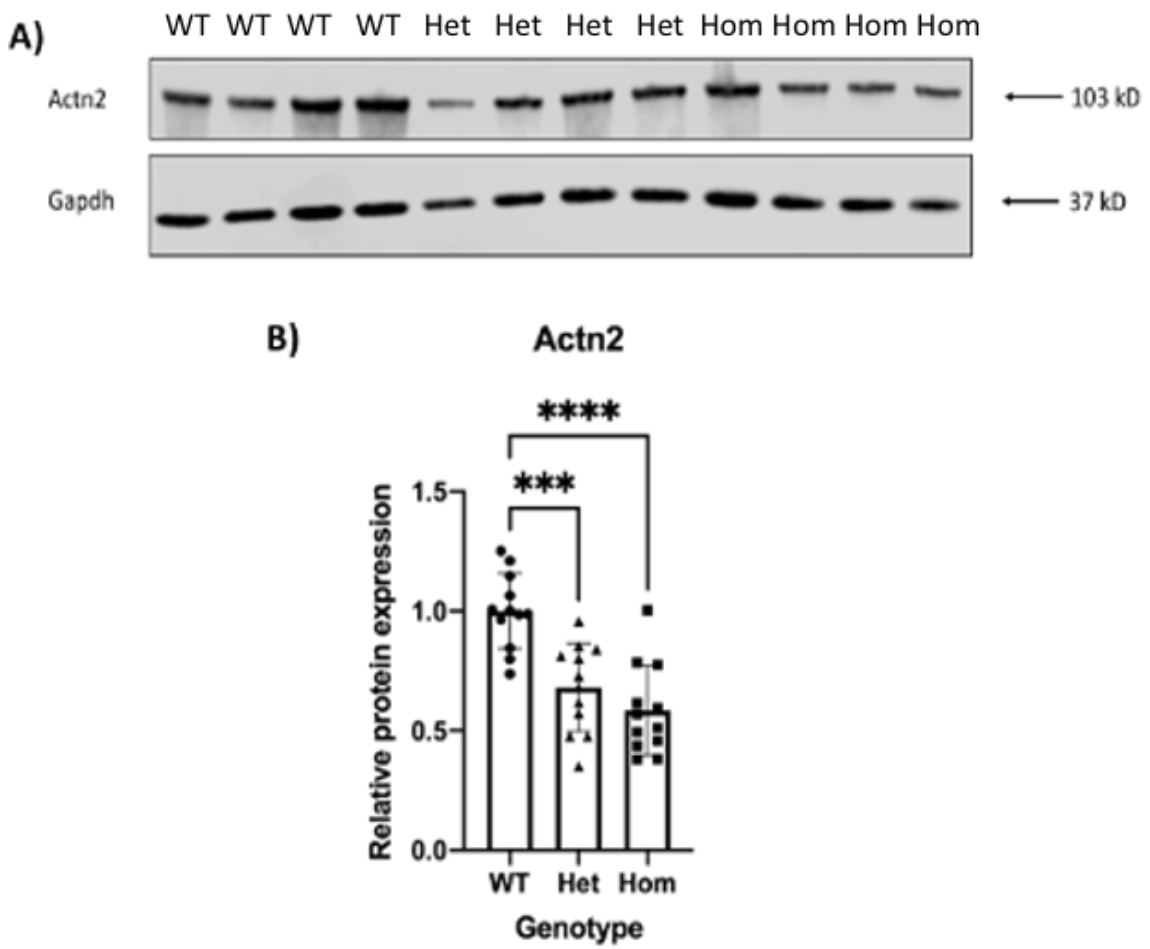

Figure 20. A: Western blot analysis of Actn2 and Gapdh protein expression levels for embryonic (E15.5) mice that are either WT, Het or Hom for the *Actn2* M228 variant. Proteins are shown from the highest molecular weight to the lowest. Arrows with corresponding numbers represent molecular weights of the appropriate proteins and therefore where the proteins run on the gel. A molecular weight marker (not shown) was used as a standard. **B:** Relative protein expression of Actn2 in embryonic mice (E15.5) samples that are either WT, Het or Hom for the *Actn2* M228T variant. Experiment was done in triplicate, with 4 biological replicates. Gapdh (not shown) was used to normalise all the samples. Individual points are shown. Error bars represent standard deviation from the mean (mean +/- SD). Statistical tests performed were one-way ANOVA and Tukey's mutiple comparison post hoc.

No significant difference was seen or found for Actn3 between the different genotypes (*Figures 21A and B*). Actn3 was looked at to investigate further the elevated gene expression seen in qPCR in Hom compared to WT embryo samples (*Figure 18C*). Actn3 is normally only highly expressed in skeletal muscle but was used here to check whether it compensated for the down-regulation of Actn2, which it did not.

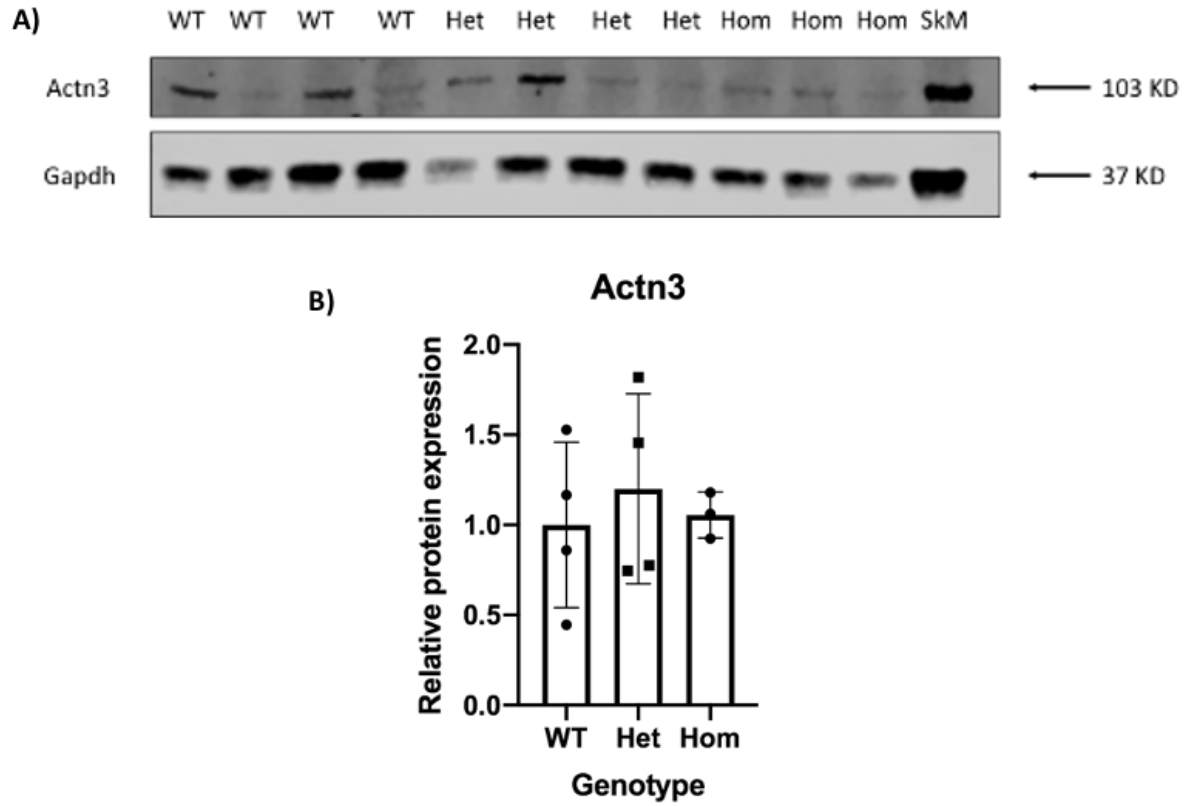

Figure 21. A: Western blot analysis of Actn3 and Gapdh protein expression levels for embryonic (E15.5) mice that are either WT, Het or Hom for the *Actn2* M228 variant. Proteins are shown from the highest molecular weight to the lowest. Arrows with corresponding numbers represent molecular weights of the appropriate proteins and therefore where the proteins run on the gel. A molecular weight marker (not shown) was used as a standard. Actn3 was chosen due to being a marker of hypertrophy and Gapdh was used to normalise. **B.** Relative Actn3 protein expression of embryonic mice (E15.5) samples that are either WT,

Het or Hom for the Actn2 M228T variant. Gapdh (not shown) was used to normalise all the samples. Individual points are shown. Error bars represent standard deviation from the mean (mean +/- SD). Statistical tests performed were one-way ANOVA and Tukey's mutiple comparisons.

Further proteins that are linked to hypertrophy and other cardiomyopathies were also investigated. No visible difference could be seen for Myh7 between genotypes (*Figure 22A*), which was confirmed with no significance being found in the multiple comparison tests (*Figure 22Bi*). No significant difference was seen or found for HspB7 (*Figures 22A and 22Bii*). A significant difference of P = 0.0135 was seen between WT and Het embryos for Hsp27 (*Figure 22Biii*).

Filamin C (Flnc) is a an important protein for the organisation and stabilisation of the actin cytoskeleton, it is also crucial for embryonic heart development and formation of sarcomeric architecture [71]. Due to the suspected impact of the pathogenic variant of *Actn2* (M228T) on embryonic heart development, protein expression of Flnc was investigated, with no significant differences seen across all genotypes (*Figure 22Biv*).

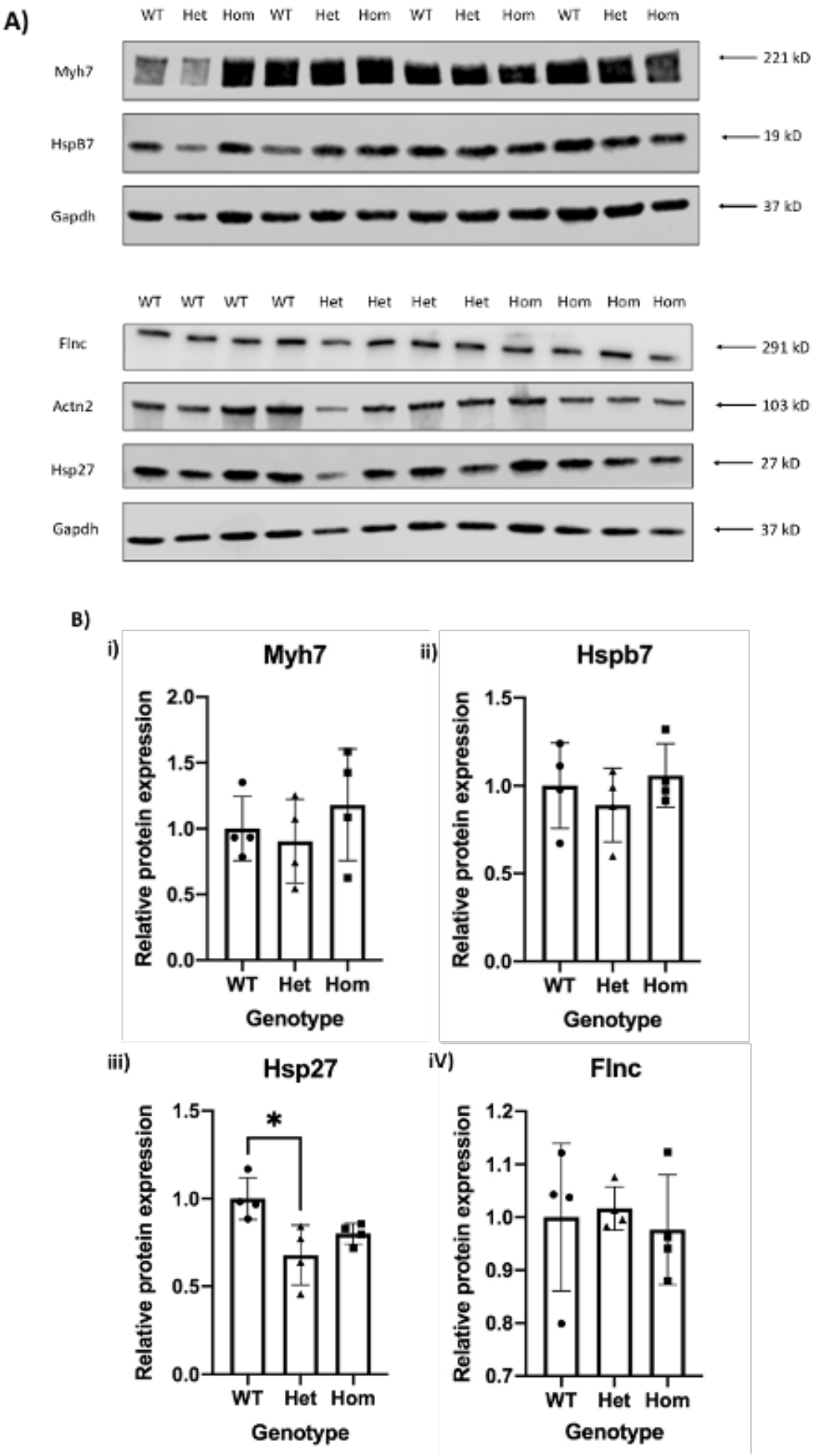
A)
WT Het Hom WT Het Hom WT Het Hom WT Het Hom
Myh7
HspB7
Gapdh
221 kD
19 kD
37 kD
WT WT WT WT Het Het Het Het Hom Hom Hom Hom
Flnc
Actn2
Hsp27
Gapdh
291 kD
103 kD
27 kD
37 kD
B)
i)
Myh7
Relative protein expression
2.0
1.5
1.0
0.5
0.0
WT Het Hom
Genotype
ii)
Hspb7
Relative protein expression
1.5
1.0
0.5
0.0
WT Het Hom
Genotype
iii)
Hsp27
*
Relative protein expression
1.5
1.0
0.5
0.0
WT Het Hom
Genotype
iV)
Flnc
Relative protein expression
1.2
1.1
1.0
0.9
0.8
0.7
WT Het Hom
Genotype

Figure 22. A: Western blot analysis of protein expression levels for embryonic (E15.5) mice that are either WT, Het or Hom for the *Actn2* M228 variant. Proteins are shown from the highest molecular weight to the lowest. Arrows with corresponding numbers represent molecular weights of the appropriate proteins and therefore where the proteins run on the gel. A molecular weight marker (not shown) was used as a standard. Proteins were chosen due to being markers of hypertrophy and Gapdh was used to normalise the other proteins. **B:** Relative protein expression of embryonic mice (E15.5) samples that are either WT, Het or Hom for the *Actn2* M228T variant. Specific proteins are looked at in each graph: **i**: Myh7 **ii:** Hspb7 **iii:** Hsp27 **iv:** Flnc. Gapdh (not shown) was used to normalise all the samples. Individual points are shown. Error bars represent standard deviation from the mean (mean +/- SD). Statistical tests performed were one-way ANOVA and Tukey's mutiple comparisons.

4.2.4 Homozygous embryos show reduced colocalisation of Actn2 with Titin

Colocalisation of Actn2 with a titin Z-disc epitope (using the T12 antibody) was looked at using immunofluorescence images of WT, Het and Hom mouse embryos, with an aim to investigate sarcomeric structure and organisation in the pathogenic *Actn2* M228T variant. Qualitative image analysis appeared to show reduced colocalisation of Actn2 with Titin in the Hom embryos (*Figure 23, merged Hom image*). Scatter plots showing level of correlation were generated using ImageJ (*Figure 23B*), to further support the reduced correlation seen in the Hom embryos.

To test the hypothesis that reduced colocalisation was seen in the Hom embryos, image analysis for colocalisation coefficients was performed on ImageJ and quantitative colocalisation analysis was performed using one-way ANOVA. Colocalisation was looked at for the total of each image (*Figure 24*). Correlation coefficients were calculated for each image and for each animal.

Colocalisation analysis for each image (*Figure 24A*), found a significant difference in colocalisation coefficients between Het and Hom embryos ($P < 0.0001$), as well as Hom and WT embryos ($P < 0.0001$). No significant difference was found between Het and WT embryos. Correlation analysis for each animal (*Figure 24B*), also found a significant difference between Het and Hom embryos ($P < 0.0001$), and Hom and WT embryos ($P < 0.0001$). No Significant difference was found between Het and WT embryos.

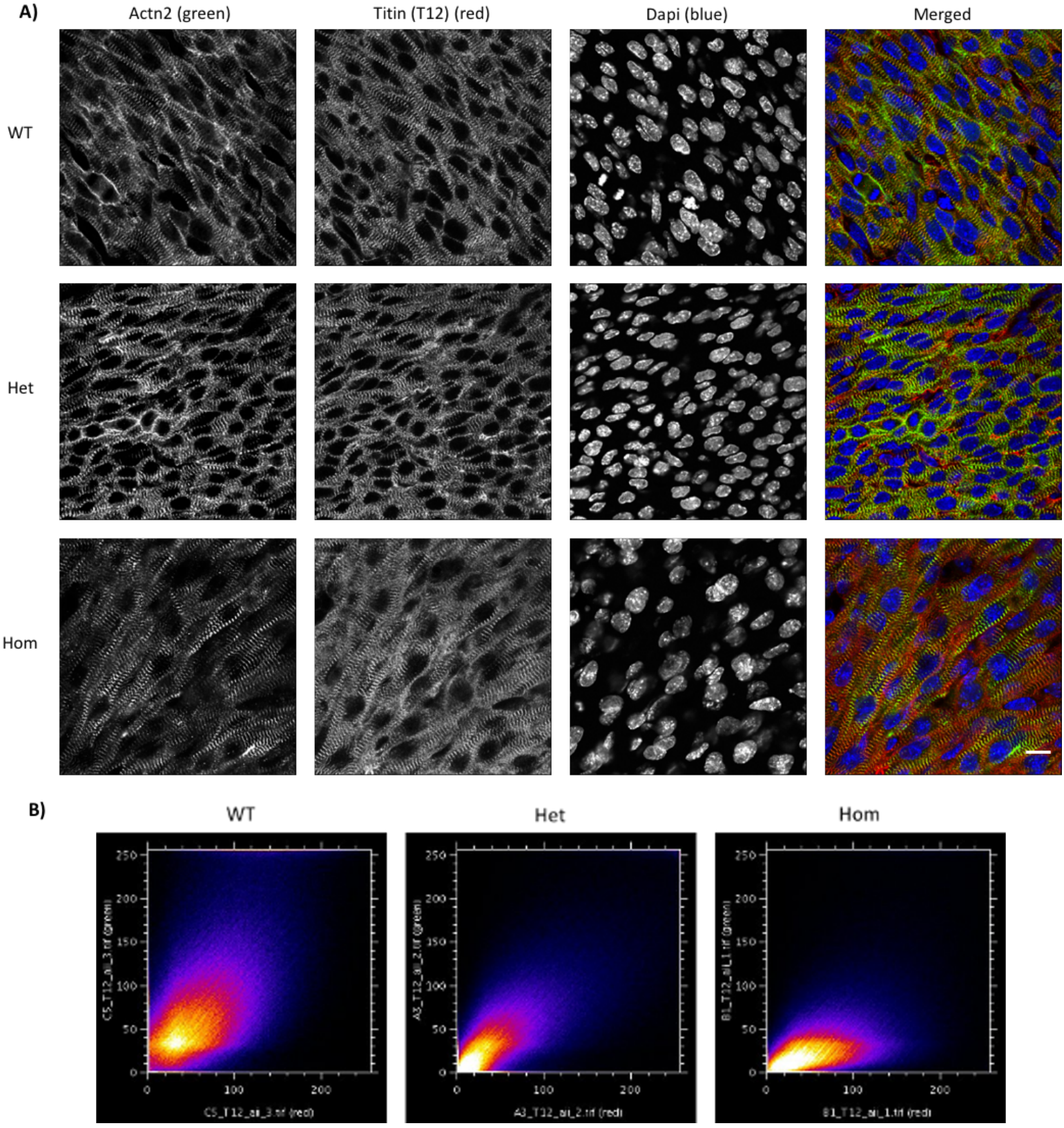

Figure 23. A: Immunofluorescence on embryonic (E15.5) mouse heart cells for all three genotypes of the *Actn2* M228T variant (WT, Het and Hom). Cells were stained for Actn2

(green) (far-left column), Titin (T12) (red) (second column from the left) and nuclei with Dapi (blue) (third column from the left). Merged images are shown in the far-right column (Actn2, T12 and Dapi). Scale bar represents 10 μm. **B:** Scatter plots generated using ImageJ for colocalisation of Actn2 with Titin in all three genotypes (WT, Het and Hom).

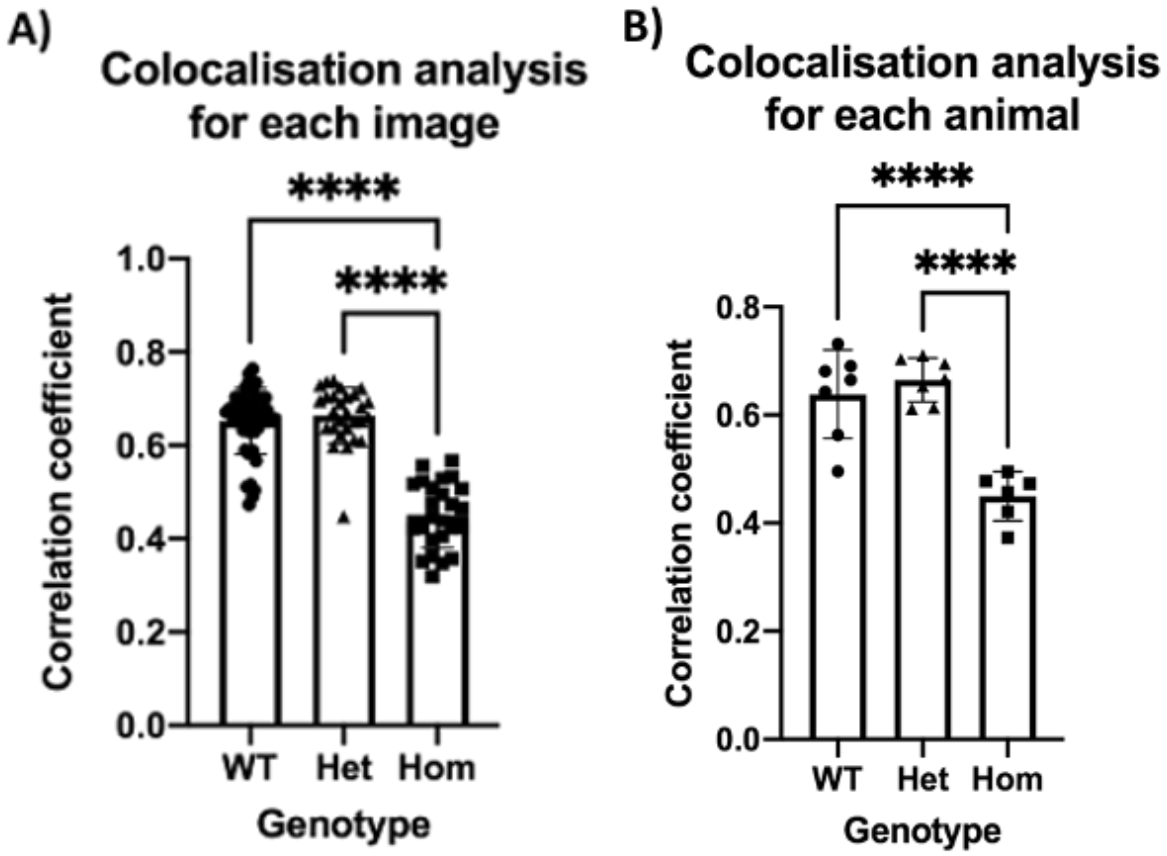

Figure 24. Colocalisation analysis looking at the correlation coefficient of embryonic sarcomeres that have been stained for α-actinin and titin. Het, Hom and WT embryos have been investigated and multiple comparisons were performed using Tukey's multiple comparison tests. Error bars represent standard deviation from the mean (mean +/- SD). **A:** one-way ANOVA looking at the correlation coefficient of each animal, with each animal having multiple images analysed. **B:** one-way ANOVA looking at the mean correlation coefficient of each animal.

A different approach to quantify Actn2 localization in embryonic hearts was to calculate for each image, how much Actn2 does not colocalise with sarcomeric titin T12 stain, using the formulae:

$$\frac{\boldsymbol{Green(Actn2\ not\ colocalising\ at\ sarcomere)}}{\boldsymbol{Green(Actn2\ not\ colocalising\ at\ sarcomere) + yellow(Actn2\ colocalising\ with\ titin)}}$$

This gives a ratio of how much Actn2 is not incorporated into the sarcomere, shown in the images (*Figure 25*). Colocalisation for non-sarcomeric Actn2 (*Figure* 25) showed a significant difference between Het vs Hom (P = 0.0091) and Hom vs WT (P = 0.0105) when looking at each image (*Figure 25A*), however, no significant differences were seen when comparing between each animal (*Figure 25B*).

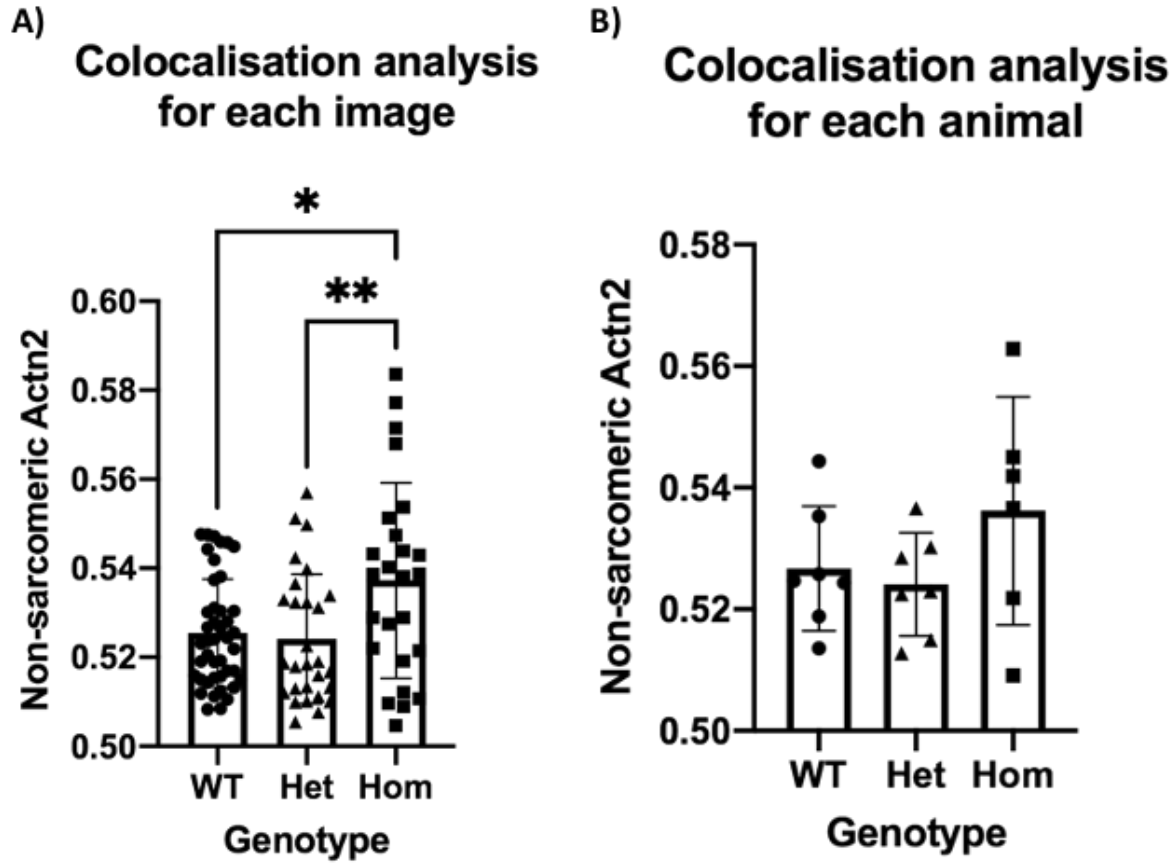

Figure 25. Colocalisation analysis looking at non-sarcomeric Actn2 in images of embryonic sarcomeres that have been stained for α-actinin and titin. Het, Hom and WT embryos have been investigated and multiple comparisons were performed using Tukey's multiple comparison tests. Error bars represent standard deviation from the mean (mean +/- SD). **A:** one-way ANOVA looking at the correlation coefficient of each animal, with each animal having multiple images analysed. **B:** one-way ANOVA looking at the mean correlation coefficient of each animal.

4.3 Generation of a homozygous *ACTN2* M228T human-induced pluripotent stem cell line to investigate cardiomyocyte function

To understand the relevance of the findings seen in the mouse model harbouring the *Actn2* M228T pathogenic variant, a more physiologically relevant model using human cells was generated. To do this, human-induced pluripotent stem cells were targeted using CRISPR/Cas9 to target ACTN2 on the 7th exon using a guide RNA containing the M228T pathogenic variant. Successful genome editing was assessed by screening iPSC clones for indels and Sanger sequencing *(data not shown).* This was carried out at the Wellcome Centre for Human Genetics at the University of Oxford (Dr Phalguni Rath) and iPSCs were transferred to the University of Birmingham. The iPSC line used was homozygous for *ACTN2* M228T.

iPSCs were assessed for their pluripotency markers using flow cytometry. Both the *ACTN2* M228T iPSC line and the parental KOLF2 WT line showed robust protein expression of the pluripotency transcriptional markers Oct3/4 and Sox2 (*Fig 26*; the gating strategy is shown in panel *A*).

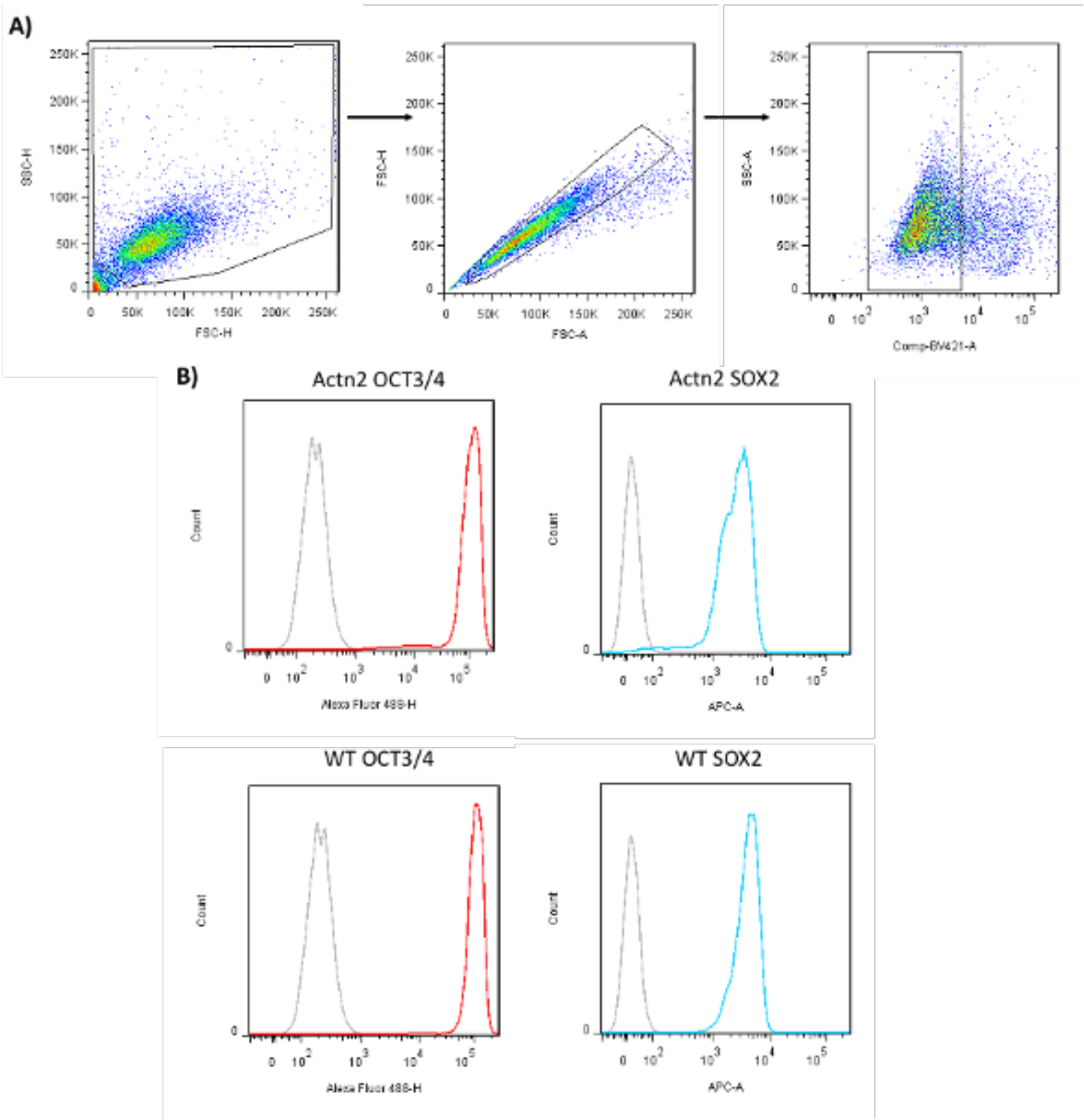

Figure 26. A: Gating strategies used for FACS analysis; arrows indicate progression from one gate to the next. **B:** FACS plots for both the parental and *ACTN2* M228T Hom line for

OCT3/4 and SOX2 with their corresponding fluorophores. Red indicates OCT3/4 and blue indicates SOX2.

To understand if the *Actn2* M228T variant causes similar sarcomeric defects observed in the murine cardiomyocytes and how this variant affects contractility, both *ACTN2* M288T iPSCs and the WT parental KLOF2 iPSCs were differentiated into cardiomyocytes (*see methods for details on the differentiation protocol*). Results of all the differentiation attempts can be seen in *Table 12*.

Table 12. A summary of all differentiation attempts for the *ACTN2* M228T Hom iPSCs. Shown are which protocol (or version of a particular protocol) were used, as well as what the cells were plated on (Mtg or Vtn, 6-well or 12-well plates), and which day the cells died at or when they started beating. Successful differentiations can be seen in red.

Differentiation attempt number	Method used to differentiate	Plated onto	Day at which cells died or started beating
1	CHIR/IWR1 (original)	Mtg (6 well plate)	Died on Day 3
2	CHIR/IWR1 (CHIR concentration gradient)	Mtg (12 well plate)	Died on Day 4
3	BMP4+AA/KY02111 +XAV939	Mtg (6 well plate)	Died on Day 1
4	CHIR/IWR1 (CHIR concentration gradient)	Mtg (6 well plate)	Died on Day 5
5	BMP4+AA/KY02111 +XAV939	Mtg (6 well plate)	Died on Day 1
6	Both (CHIR and seeding gradient)	Mtg (12 well plate)	Died on various days (one well seeded at 100% using BMP4+AA/KY02111 +XAV939 survived and started beating on day 11)
7	Both (CHIR and seeding gradient)	Mtg (12 well plate)	Died on various days (5 wells beating on day 14 across all CHIR gradients seeded at 80 and 100%)
8	CHIR/IWR1	Vtn (6 well plate)	Died on Day 6

Overall, the most successful differentiations were those seeded at 100 % using BMP4+AA/KY02111+XAV939, which started beating on Day 11.

Once iPSCs had been successfully differentiated into cardiomyocytes (iPSC-CM), they were plated for immunofluorescence analysis of sarcomere structures. iPSC-CM were stained for Actn2 in green and nuclei in red (*Figure 27*). ımages of the cells were then acquired using a fluorescent microscope with 20X and 40X objectives (*experimental details are in materials and methods*). These data show the establishment of an *ACNT2* M288T line which were differentiated successfully into cardiomyocytes.

Furthermore, preliminary results showed that the *ACTN2* M228T iPSC line is able to differentiate into beating cardiomyocytes that were beating visually as strong as the parental line (*Figure 27*). Upon closer inspection, sarcomeres (stained by Actn2) appeared less mature in the *ACTN2* M228T line (*Figure 28*). However, as staining was performed on Day 16, sarcomeric structure of both cell lines may have been immature (iPSC-CM maturity is normally defined as Day 30). Future studies will focus on phenotyping this line further (*more information can be found in discussion*).

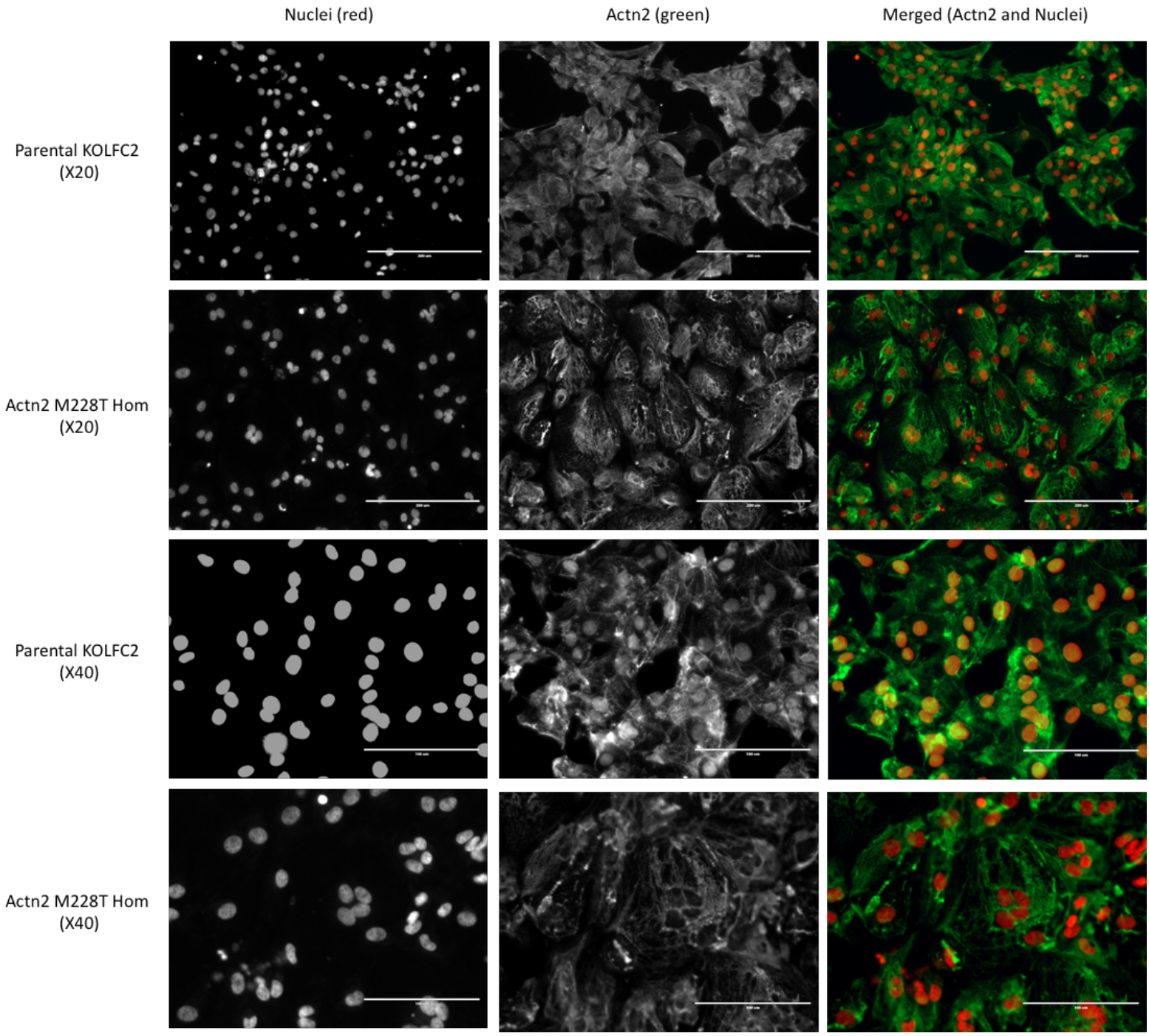

Figure 27. Images of Parental KOLFC2 and *ACTN2* M228T Hom cardiomyocytes that have been fixed on Day 16 (D16) and stained for Actn2. On merged images, green indicates Actn2 staining and red indicates nuclei staining. Scale bar indicates 200 µm at X20 magnification

and 100 μm at X40 magnification. Left panel indicates red channel (nuclei) and middle panel indicates green channel (Actn2). Right panel shows merged images (nuclei and Actn2).

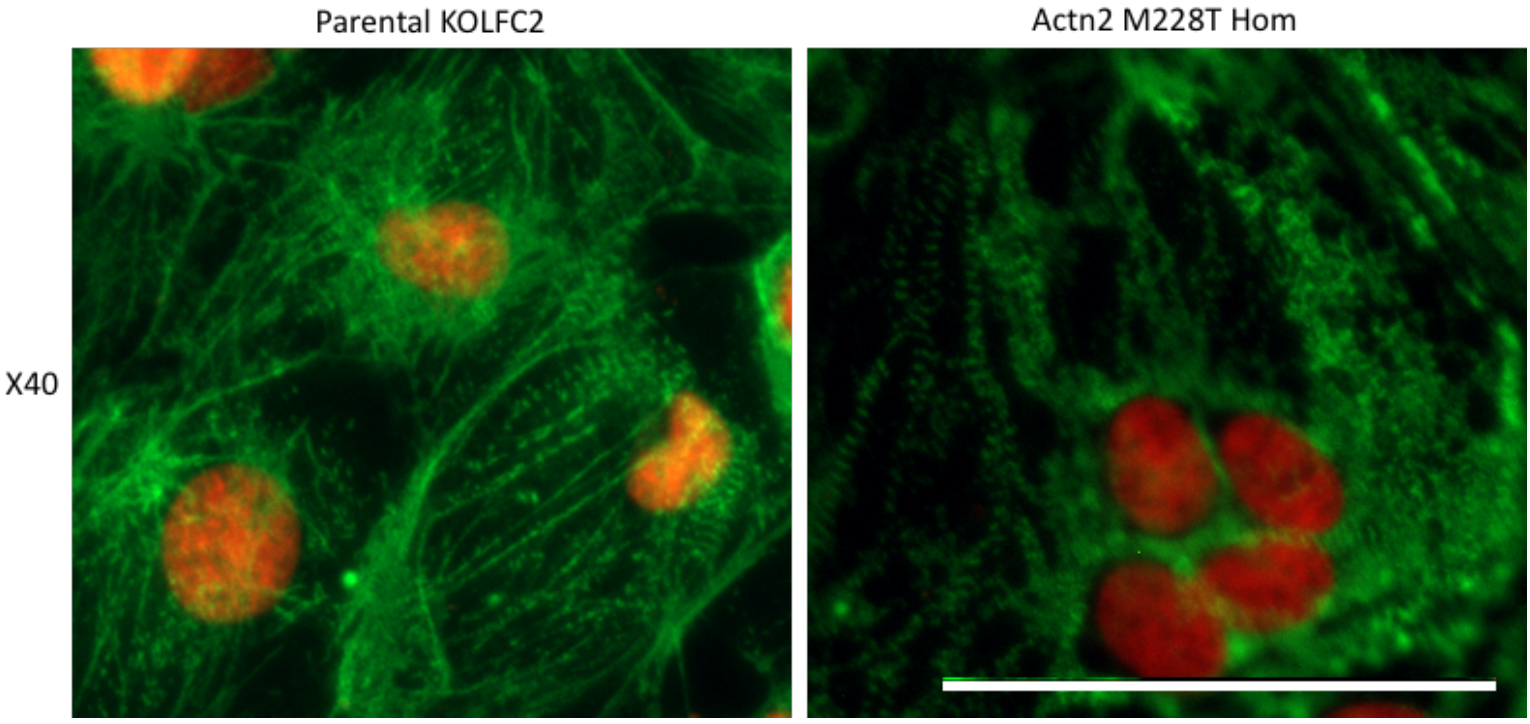

Figure 28. Zoomed in images of Parental KOLFC2 and *ACTN2* M228T Hom cardiomyocytes that have been fixed on Day 16 (D16) and stained for Actn2. Magnification is X40 and scale bar represents 100 μm.

Overall, these data show the successful generation of an *ACTN2* M228T homozygous line that can be differentiated into ventricular cardiomyocytes using established differentiation protocols.

5. Discussion

This project used three different approaches to investigate the effect of the *Actn2* M228T variant and its link to heart disease. The first model was an adult mouse that was heterozygous for the *Actn*2 M228T variant. Findings saw no difference in heart weight of the Het mice compared to the WT. However, expression of the hypertrophic marker Myot was increased in both male and female Het mice whilst the cardiomyopathy marker Hsp27, was increased in male Het mice only in comparison to male WT. The second approach looked at embryonic (E15.5) mice that were homozygous for the *Actn2* M228T variant. Results found increased gene expression of *Actn2* with reduced expression of the Actn2 protein, while the increased gene expression of *Actn3* did not have an impact on Actn3 protein levels. Transcripts of the foetal gene programme were also increased (*Nppa, Nppb* and *Myh7*) in Hom embryos at E15.5, while no difference in protein expression was seen for the hypertrophic and cardiomyopathy markers Myh7, Hspb7, Hsp27 or Flnc. Images of the embryos also found reduced colocalisation of Actn2 with titin in Hom embryos compared to the WT. The final model investigated cardiomyocyte function using the Hom *ACTN2* M228T variant in an iPSC line. The hom line was found to be pluripotent and when differentiated into cardiomyocytes, the Hom cells appeared to have less mature sarcomeres than the WT line.

5.1 Adult mouse model

5.1.1 The effect of the *Actn2* M228T pathogenic variant on heart weight

HW/BW is a parameter used to investigate levels of hypertrophy in mice. The HW/BW ratio of Het *Actn2* M228T is comparable to the WT, suggesting no changes in cardiac growth in the presence of the variant. A significant increase in HW/BW ratio was seen in Het male mice at 37-38 weeks of age in relation to age-matched Het females. This is indicative that

male mice possessing the genetic variant may be at an increased risk of developing a hypertrophic phenotype over female mice.

HW/TL is a more robust and commonly used parameter used to assess hypertrophy in mice compared to HW/BW. No significant changes were found for HW/TL between the different genotypes for any of the age groups, suggesting no difference in levels of cardiac hypertrophy between the mice. HW/BW or TL ratios are fairly insensitive morphometric markers of macroscopic hypertrophy, while transcript changes have been found to be sensitive [72]. In a homozygous titin A178D mouse model of mild DCM, researchers also found a normal HW/TL. However, molecular changes were present such as an increased foetal gene programme as well as increased hypertrophic signalling [72]. Molecular activation of hypertrophic pathways, such as the foetal gene programme, may have occurred in the *Actn2* mouse model but not yet translated into macroscopic hypertrophy. The mice were also still fairly young in comparison to the age of development in the human condition. This suggests that no significant difference in HW/TL is not indicative of the absence of hypertrophy.

It is well known that differences in body weight are representative of sexual dimorphism within mammals. More specifically, C57BL/6 male mice, a similar strain to that being studied, were found to have a greater body mass, fat mass and lean mass than females (accessed via [73]). Reynolds *et al* [74] found that male mice had a much greater body mass and fat mass compared to female mice, therefore BW/TL ratio was calculated to give an indication of the relative size of the mice in the presence of the M228T genetic variant [75]. Males were found to have a greater BW/TL ratio and therefore a greater size in the majority of age groups looked at.

This data supports that the significant increase observed between HW/TL ratios of males and respective genotype-matched females in age groups 12-17 weeks and 52-61 weeks, is a sex related phenomenon rather than genotype related. Sex differences in mice have previously been reported and may offer an explanation as to the differences seen in these parameters. For example, Haroon *et al* [76] report that male FVB/N mice, had significantly increased HW/BW and HW/TL ratios in comparison to the female mice, suggesting this may be the result of differences in sex hormones, thus supporting sex differences seen in the mice.

5.1.2 Increased levels of Myot and Hsp27 were seen in the *Actn2* M228T variant

The ACTN2 protein is expressed in both skeletal and cardiac muscle and has key roles in binding to actin and stabilising the sarcomere, which acts as the contractile unit of striated muscle [28]. ACTN2 also acts as a signalling hub in the sarcomere, based on its interactions with other signalling proteins such as titin, telethonin and ZASP [77] and ion channels, e.g. small conductance Ca^{2+} activated K^{+} channels [78] and Kv1-type potassium channels [79]. Changes in cardiac signalling and sarcomeric scaffolding may offer an explanation for the pathogenic phenotypes seen in *ACTN2* variants, although further molecular work is needed to confirm these proposals.

In this study, Western blotting was used to investigate known biomarkers of hypertrophy and other cardiac diseases [70]. Gapdh protein expression was used for normalisation of all samples, due its consistent expression in all cell types, regardless of genotype [80].

Male Het mice had significantly higher Actn2 protein expression when compared to age-matched female Het mice, suggesting a sex difference in the expression of Actn2 in the presence of the pathogenic variant.

If the heart is subjected to stress, a common response is to supress the expression of post-natal genes and to revert to a predominantly foetal gene programme [81]. The MYH7 isoform

has been found to be upregulated in the human heart when under stress (heart failure), and in the human foetal heart [82]. Other models such as Homozygous titin A178D [1] mice or cMyBP-C knock-in (KI) mice [12] have been found to show an increased expression of Myh7, supporting the fact that this protein is upregulated in respect to cardiac hypertrophy. Although no significant difference in Myh7 expression was seen between the WT and Het *Actn2* M228T mice, a significant difference for Male vs Female Het's was found. This suggests a sex related impact on the expression levels of Myh7 in the presence of the pathogenic variant, further supported at the transcript level, where qPCR analysis revealed increased Myh7 expression in M228T Het male mice in comparison to WT controls (data by Dr C Hooper, Gehmlich group, University of Oxford, unpublished).

Variants in *MYOT* have been highly reported in skeletal muscle disease (myotilinopathies), and may cause Z-disc structural abnormalities as a result of protein aggregation due to impaired degradation [83]. However, there have been no reports of isolated cardiomyopathy where *MYOT* variants have been directly linked to the cardiac phenotype [27]. A patient with the *MYOT* p.Ser60Phe variant presented with myopathy and displayed a cardiomyopathy phenotype [84] but no cases been have found for cardiomyopathy alone [27]. For Myot, significant changes were seen between WT vs Het (Males) and WT vs Het (Females), suggesting a genotypic-dependent impact on expression with higher levels being seen in Het mice compared to WT mice with the *Actn2* M228T variant. A significant difference was also seen for Male vs Female Het's in Myot, revealing increased expression of Myot in Het males compared to Het females. With little knowledge on the role of *MYOT* in the pathogenesis of cardiomyopathies, it suggests that increased MYOT expression levels could act as a novel marker for cardiac hypertrophy. This is a hypothesis currently tested in the group.

Cardiac regulatory protein, cTnT mediates the interaction of actin with myosin and is regulated by calcium [85]. Elevated levels of circulating cTnT have been associated with greater disease severity in patients with HCM [86]. In human ventricular tissue, levels of cTnT were decreased in the diseased heart compared to normal tissue [87], suggesting different expression levels of circulating and tissue cTnT in cardiac disease. The fact that the sarcomeric thin filament protein troponin T was not changed in the *Actn2* M228T variant, implies that the variant does not alter the stoichiometry of thin filament composition, at least in the samples tested.

Heat shock proteins such as HSP27 have previously been found to reduce protein aggregation induced by stress, thereby acting as a protective mechanism against damage to the myocardium [88]. Increased expression of *HSP27* has been reported in cardiac disease [89] and increased levels of HSP27 phosphorylation have been found in the hearts of patients with HCM [90], which leads to protection against apoptosis. Levels of this protein may be useful as a biomarker for hypertrophy as higher levels of expression in the heart indicate cardiac stress and the need for a protective mechanism. In our model, no changes between genotypes were seen in the samples being investigated, suggesting this protective pathway was not activated in the *Actn2* M228T Het mice. However, male Het mice did express higher levels of Hsp27 in comparison to Het females, suggesting sex-related differences in expression. Sex differences in cardiac Hsp27 expression have been reported for patients with HCM, although in this case females were found to have higher expression levels [91]. Unaltered levels seen in this adult mouse model may be a result of their still relatively young age and Hsp27 protein levels should be investigated in aged mice.

In cardiac muscle, HspB7, another member of the small heat shock protein family, has been identified as an actin filament length modulator, through its binding to monomeric actin and inhibiting its polymerisation [92]. Like Hsp27, HspB7 acts as to stabilise the sarcomere and protect cardiac cells against proteostasis derailment [93] and increased expression has been found in induced hypertrophic hearts [94]. This suggests an essential role of HspB7 in maintaining the integrity and conduction properties of adult cardiomyocytes [95]. Increases in both mRNA and protein expression have been found for Hsp27 and HspB7 [96] in a mouse model of HCM, which is homozygous for the cysteine and glycine rich protein 3 (CSRP3) C58G missense variant. Similarly, in this study, male mice heterozygous for the *Actn2* pathogenic variant had increased expression levels of HspB7, indicative of a molecular hypertrophic phenotype. However, female mice heterozygous for the variant displayed a decrease in this protein when compared to age-matched WT females. In the human population, studies have found that pre-menopausal females are better protected against hypertrophy compared to males, due to the counteracting role of estrogen in pro-hypertrophy pathways [97]. As HspB7 acts in a cardioprotective manner [98], this suggests that females may be able to compensate for the lower HspB7 levels through sex specific hormones such as estrogen.

In the majority of proteins looked at during this study, there appears to be sex-related differences in protein expression levels in the presence of pathogenic variant but not in the WT animals. Sex-related differences in cardiac function have previously been reported for both rodents and humans [99]. For example, observed effects were different for males compared to female mice with R(403)Q α-Myhc [100]. Male mice displayed cardiac chamber dilation and heart failure whilst females showed hypertrophy and preserved function. In addition, a missense cTnT (R92Q) mouse model of HCM also displayed sex differences in

their observed effects [101], with males displaying a reduced heart size compared to WT, whilst females showed no difference in heart size compared to WT.

Clinical studies have found that the severity of clinical HCM is/was greater in women compared to men [102]. Differences in protein expression that are regulated by sex hormone related transcriptional factors may be one explanation. Research has found that 46 different proteins are differentially expressed between male and female HCM samples [91], and 7 sex hormone related transcription factors were found to have binding sites to regulate these proteins. This suggests that sex hormones play a part in the transcriptional regulation of proteins that drive sex differences seen in HCM, although other mechanisms are also involved [91]. Females with HCM have been found to have a reduced exercise performance compared to males [103], which suggests that the sex differences seen may be an effect of increased physical activity and exercise performed by the male mice.

5.2 Embryonic mouse model

5.2.1 The *Actn2* M228T variant had no impact on embryonic development indicated by Theiler staging

Previous studies using a zebrafish model found that Actn2 is vital for Z-disc organisation in embryos [31], and Actn2-deficient hearts show reduced sarcomeric assembly [48]. It was therefore suspected that *Actn2* M228T Hom embyos collected at E15.5 would show developmental delay in comparison to the WT embryos. Previous studies investigating a different embryonic lethal null variant have shown that mutant embyros were developmentally delayed according to Theiler staging when collected at E14.5 [67]. According to Theiler staging, the level of webbing and therefore gaps between the finger digits, can be used to define the stage of development of the mice.

No significant differences were found when correlating Theiler stage (either 22+, 23- or 23) to genotype (WT, Het or Hom) of the embryos. This suggests that no gross developmental delay was seen in the embryos, even in the homozygous setting. This is in contrast to other mouse models which looked at similar signalling pathways and proteins, where developmental delay have previously been reported: One study found embryonic lethality before day E12.5 in a cardiac-specific *HspB7* knock-out (KO) mouse model [92]. *Figure 29* shows the developmental delay in the KO mice compared to normal development seen in the WT embryos. Another study found that cyclin-dependent kinase 13 (Cdk13), which is involved in congential heart defects, KO mice, had embryonic lethalithy at E16.5 [104]. Developmental delay was also seen with embryoic morphology, hence the embryonic death observed in the *Actn2* M228T mice cannot be attributed to a simple delay in embryonic development.

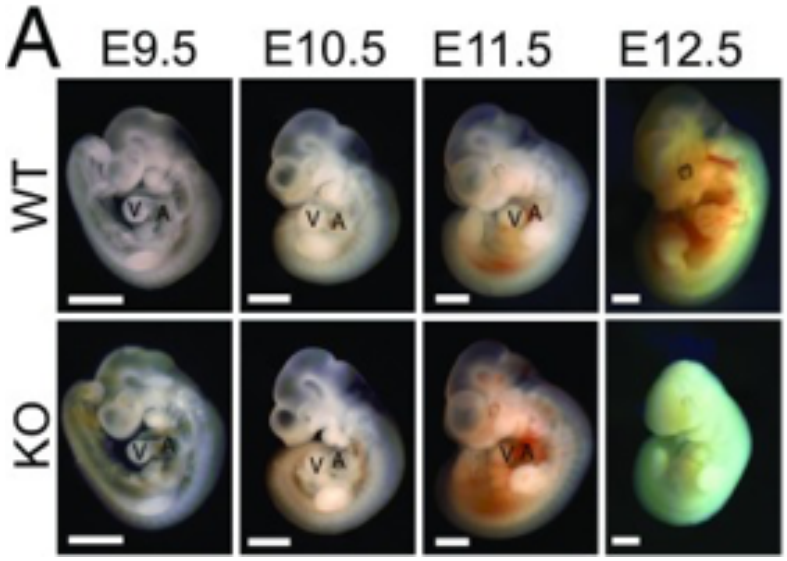

Figure 29. Images of WT and *HspB7* KO embryos from E9.5 to E12.5. A, left atria; V, left ventricle. (Scale bar: 1 mm.) Figure from [92].

5.2.2 Homozygous embryos had increased gene expression of *Actn2* and *Actn3* with reduced Actn2 protein expression

Increased gene expression of both *Actn2* and *Actn3* was seen in the *Actn2* M228T hom embryos compared to the WT. The increase in *Actn2* expression may be the cells response to the damage inflicted on the genetic code, forcing the cell to produce more transcript in attempt to produce more functional Actn2 protein. For example, Ehsan *et al* [96] saw a 2.5 fold upregulation of *Csrp3* transcript in mice that were homozygous for the *Csrp3* C58G variant, which also saw a reduction in the encoded muscle LIM protein (MLP). This supports how increased transcript levels might try to rescue reduced protein stability in the presence of a genetic variant. However, in this study Western blotting revealed that the increase in transcript was not mirrored by protein expression and resulted in a decrease in Actn2 levels in hearts from Hom embryos relative to WT embryos. One explanation for this may be that the missense variant results in a non-functional Actn2 protein which is degraded by an intracellular degradation system, e.g. the ubiquitin proteasome system (UPS) or by autophagy. Previous studies have shown that other proteins such as myotilin are degraded by the UPS [105]. The HCM causing C58G variant of *CSRP3* was investigated by Ehsan *et al* [96], who presented the role of the UPS in MLP degradation and supported protein degradation as a possible cause of HCM. Vignier *et al* [106] demonstrated the importance of the UPS in the degradation of mutant protein in a cardiac myosin binding protein C (cMyBP-C) knock-in mouse model of HCM, further supporting the degradation of mutant Actn2 protein seen in the Hom *Actn2* M228T variant. Future studies should aim to explore the reduction of Actn2 protein expression in this model further, to understand if there is increased degradation by the UPS in the hom setting compared to the WT.

Due to being expressed in both cardiac and skeletal tissue, variants in *ACTN2* are associated with both cardiomyopathy and skeletal myopathy [107] while, *ACTN3* variants are known to only be associated with skeletal myopathy. A previous study found that *Actn3*-KO mice had upregulation of Actn2 and other Z-disc associated proteins such as myotilin and ZASP [108], as a compensatory mechanism, which resulted in a milder phenotype [109].When looking at the reverse scenario in this mouse model with the decrease in Actn2 protein expression, upregulation of the *Actn3* transcript was seen, but this was not translated into changes at protein level. These results suggest that the Actn3 protein has distinctly different functions and has evolved to optimise its own role and hence cannot compensate for loss of Actn2. No significant differences in transcript levels between the genotypes were observed for the other actinins (*Actn1, Actn4*) or for *Actc1*. ACTN1 and ACTN4 proteins that are transcribed from their respective genes, are predominantly non-muscle isoforms and are sensitive to Ca^{2+} binding [110]. High expression levels of ACTN1 have been associated with both shorter event-free and overall survival (OS) of acute myeloid leukaemia patients [111], while high levels of ACTN4 have been found to promote metastasis in gastric cancer [112] and are reported to be a biomarker for OS for oral tongue cancer patients [113]. As ACTN1 and 4 are not expressed highly in cardiac tissue, it is not surprising that changes in expression did not occur between the different genotypes. These results suggest that the functions of ACTN1 and 4 are independent of ACTN2 and so they cannot compensate for the lack of ACTN2 protein seen.

Actc1 also showed no significant difference in expression levels between the genotypes. *ACTC1* encodes for cardiac α-actin and forms a complex with three troponins and tropomyosin to form the thin contractile filament of the sarcomere [114]. Variants of *ACTC1* have been linked to atrial septal defect, later leading to DCM, although the regulatory

mechanisms behind this have not been fully explored [114]. In mice that lack *Actc1*, myofibrillar disarray has been noted and these mice have been reported to have embryonic lethality [115]. As no difference was seen for *ACTC1* expression, the thin filament of the sarcomere is not affected in the *Actn2* M228T variant.

Further investigation by qPCR found that genes involved in the foetal gene programme (*Nppa, Nppb* and *Myh7*), were upregulated in the Hom setting. *Nppa* and *Nppb* genes encode for atrial natriuretic factor and brain natriuretic peptide. In clinical cardiology, these are used as important biomarkers of hypertrophy [116]. When the heart is subjected to pathological stress, the heart releases the pro-peptides and causes the expression of *Nppa* and *Nppb* to be increased in the ventricular cardiomyocytes [117]. As cardiac hypertrophy is a form of stress on the heart, reactivation of this foetal gene programme is commonly seen and is thought to act as a compensatory mechanism whilst playing a role in cardiac remodelling [118-120]. It is therefore not surprising that increased expression of *Nppa* and *Nppb* was seen in the homozygous setting. As previously explained (5.1.2), *MYH7* is also involved in the foetal gene programme and its upregulation is commonly seen in hypertrophic cardiomyopathy [121]. The increase in *Myh7* at the gene level seen in the homozygous setting, further supports the increase of the foetal gene programme and suggests the hearts of the Hom mice activate hypertrophic signalling. As part of the activation of the foetal gene programme, one would expect an increase in *Acta1* expression, however, for unexplained reasons, the transcript is down regulated in the embryonic hearts.

Myh7, HspB7 and Hsp27 were investigated at the protein level as they act as either markers of hypertrophy or are indicators of cardiomyopathies. These proteins were also implicated in the adult Het mice. Although gene expression of *Myh7* was increased, this was not translated

at the protein level where no significant difference was found between the genotypes. Previous studies have shown that mutant myosin can be ubiquitinated and degraded by the proteasomal pathway [122], so no decreased Myh7 expression may suggest that Myh7 protein is not affected by this homozygous variant and normal protein turnover is occurring. No significant difference was found for protein expression levels of HspB7 between the genotypes. HspB7 KO mice result in embryonic lethality by day 12.5 [92], showing the importance of this protein in development, specifically in the development of cardiomyocytes. However, unaffected protein expression of HspB7 in the *Actn2* M228T Hom mice indicates this heat shock protein may not be involved here. Hsp27 levels were also unaffected by genotype. Patients with HCM have been found to have elevated levels of HSP27 [123], supporting the protective role of the protein. Transgenic mice with high levels of Hsp27 have also been found to develop cardiomyopathy [124]. However, this has not been translated to mouse embryos where neither overexpression or down regulation of Hsp27 altered embryonic heart development [125]. This suggests that Hsp27 may be more relevant to adult models and less involved in the embryonic heart.

FlnC plays an important role in the organisation and stability of the actin cytoskeleton; it therefore is also involved in the development of the heart and sarcomeric formation [126]. Apart from Actn2, FlnC can cross link actin filaments in the Z-disk, albeit, in a different orientation [127]. As the *Actn2* M228T variant is suspected to result in Actn2 instability, it was hypothesized that FlnC might compensate for the loss of actin crosslinking ability. However, no impact on FlnC protein expression was seen in the Hom *Actn2* M228T variant. This suggests that stability of the actin cytoskeleton through FlnC binding remains unaffected in the *Actn2* M228T variant.

5.2.3 Colocalisation analysis of immunofluorescence images showed reduced Actn2 and Titin colocalisation in the Homozygous embryos

Actn2 has a key role in anchoring titin in the Z-disk to maintain muscle integrity by the binding of Actn2's calmodulin-like domain with titin's Z-repeats [77]. The colocalisation of Actn2 with titin can therefore give an indication as to the level of organisation and stability of the sarcomere. In the Hom M228T variant, colocalisation of Actn2 with titin was found to be reduced when compared to the WT, indicating reduced organisation in this variant. A study by Haywood *et al* [37] investigated the effect of two HCM-linked *ACTN2* variants (A119T and G111V), which reside in the calponin-homology domain. In comparison with the M228T variant used in this study, these variants also affect the actin binding domain (ABD) of the functional protein. The researchers found a slightly reduced capability of the variants to bind with actin; they also speculated that in normal circumstances, there is a mechanical strain between the actin and titin binding sites on the ACTN2 that allows the protein to be incorporated into the Z-discs. They propose that this strain may be reduced with the lower ability to bind with actin, suggesting colocalisation and binding of ACTN2 and titin (as well as actin), may be reduced in these variants. Further research found that loss of titin always resulted in the striated patterns of Z-disk ACTN2 to be disrupted [128], and suggests that colocalisation of both proteins is needed for successful Z-disk formation.

5.3 iPSC-CMs with the hom *ACTN2* M228T variant

5.3.1 Both the *ACTN2* M228T iPSC line and parental KOLF2 WT line showed robust protein expression of the pluripotency transcriptional markers

In order to test for pluripotency of the Hom *ACTN2* M228T line, expression of the pluripotency markers Oct3/4 and Sox2 was investigated using FACS. This was important to show that the cells were dividing and growing so differentiation into cardiomyocytes could

be attempted. Results showed that both the WT KOLFC2 parental line and the Hom *ACTN2* M228T line had robust expression of the pluripotency transcriptional markers. It further supports that the Hom iPSC variant is able to differentiate into all three germ layers. Oct3/4 and Sox2 binding has been found to be highly active in undifferentiated embryonic stem cells [129], supporting the idea that the iPSCs investigated were in fact pluripotent and had not yet spontaneously differentiated.

5.3.2 Sarcomeric staining qualitatively showed less mature sarcomeres in the *ACTN2* M228T cell line

Preliminary results showed that the *ACTN2* M228T Hom line could be differentiated into ventricular cardiomyocytes that visually appeared to beat just as effectively as the KOLFC2 parental WT line, using the BMP4+AA/KY02111+XAV939 differentiation method. This suggests that the contractile unit of the sarcomere is still able to assemble in the Hom line and beating can still occur. It also suggests that as in the WT line, gap junctions are able to form and allow the passage of ions between cells, in turn facilitating the movement of action potentials [130]. By enabling depolarisation, synchronised contraction of the cardiomyocytes can occur and allow the cells to beat [131].

Research from Haywood *et al* [37] found that variants affecting the ABD had small effects on structure and behaviour of ACTN2 and impacted its ability to function normally. They suggest that a reduced actin binding capability may reduce both the amount and rate of exchange of ACTN2 that occurs in the Z-disks. Staining of adult cardiomyocytes showed that although ACTN2 was able to localise to Z-disks in all genotypes, the integration of the ACTN2 variants appeared to be weaker than for the WT protein. Fluorescence decay after photobleaching was also reduced in the ACTN2 variants compared to the WT, suggesting

that although ACTN2 can be incorporated into the Z-disks in the pathogenic variants, these aberrant proteins are less able to leave the Z-disk and may form protein aggregates. These data support the staining images seen in the present study, where Z-disk formation is seen even in the Hom line, but that weaker incorporation of ACTN2 appears into the sarcomere was observed in the Hom M228T embryos.

5.4 General discussion

Several *ACTN2* variants have been identified in cardiomyopathies [27] . As previously discussed, Haywood *et al.* investigated the A119T and G111V variants also located in the ABD of ACTN2, and looked at their possible effects on the phenotype of the HCM [37]. Small, yet distinctive changes were found in the crystal structure of the resulting ABD in these variants. *ACTN2* T247M, another variant located in the ABD, was identified in a patient who presented with familial HCM [36]. An iPSC-derived cardiomyocyte model for the variant supported its pathogenicity, suggesting the observed QT interval prolongation in the patient could be explained by the reduced interaction of the *ACTN2* variant with the L-type calcium channel. Further *ACTN2* variants are discussed in 2.5.2 and can be identified in *Table 1*. As previously mentioned, α-actinin2's conservation and documented requirement for cardiac integrity [31], may be the reason that most missense variants in *ACTN2* are detrimental to its crucial functions and hence not compatible with life. The majority of identified variants are located in the ABD of ACTN2 (*Table 1*) and are hence predicted to interrupt actin binding, although molecular studies have revealed different outcomes as a result of these variants. For example, the G111V variant impacted tertiary structure of the protein, whilst the A119T had a negative effect on actin binding. Both variants formed aggregates outside the Z-discs and showed reduced ability to leave the Z-disc with reduced fluorescent decay after photoactivation. This suggests that having these pathogenic variants

present reduces exchange of the protein at Z-discs. On the other hand, the pathogenicity seen in the T247M variant was explained by reduced interaction with the L-type calcium channel, suggesting the role of ion channels and currents in the pathogenicity of this variant. This diverse range of effects seen as a result of *ACTN2* variants supports the need for further studies into the mechanisms behind their pathogenicity. Future work should therefore explore in more detail the dynamics of ACTN2 and its effect on processes such as calcium handling, and how these impact cardiomyopathies.

5.5 Future considerations

Molecular work should further investigate Actn2 turnover, as a current theory is that the dis- and re-assembly of sarcomeres in dividing embryonic cardiomyocytes is impaired.
Other aspects could be a potential activation or even overload of the UPS by increased Acn2 degradation as well as structural and biophysical studies of the impact of the M228T change on protein structure and biding to actin. Atrogin-1 mRNA has been found as a biomarker for proteolysis as increased expression correlates with increased protein breakdown [132]. This biomarker could offer further insight into possible protein degradation seen with this variant.
Dr F. Mohammed (University of Birmingham) modelled the structure of the ABD in the *ACTN2* M228T variant (unpublished data) (*Figure 30*) and found a smaller polar side chain protruding from the CH2 domain that normally contributes to interactions between CH1 and CH2. This reduces the number of contacts at the interface and adversely affect the folding of the ABD.

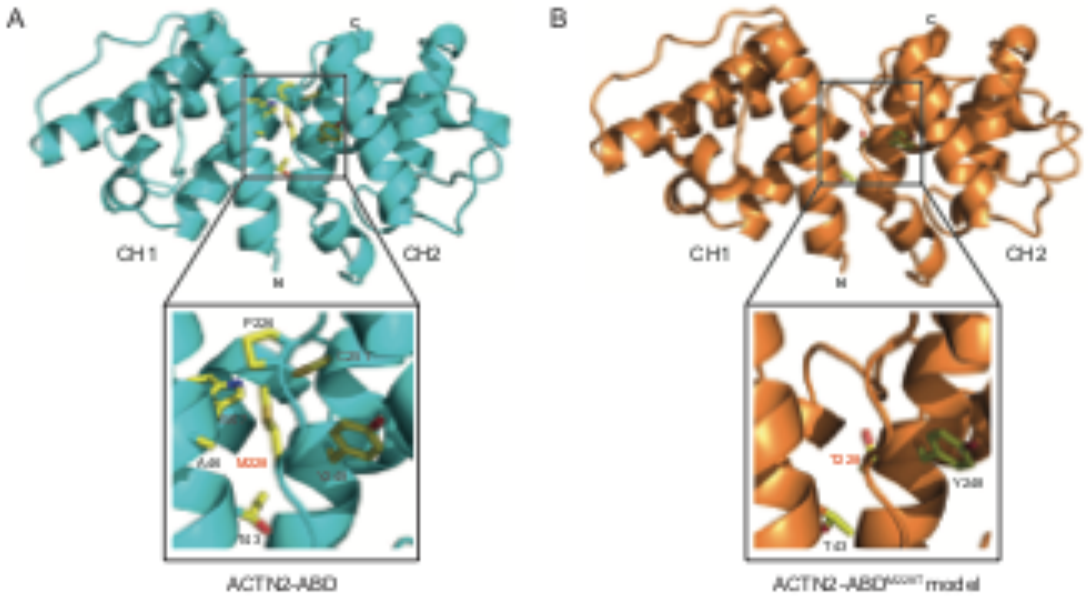

Figure 30. Structural model of ACTN2 Actin Binding Domain (ABD). Zoomed in areas show the interface between the two calponin homology domains (CH1 and CH2). **A:** Model of WT ACTN2. **B:** Model of ACTN2 M228T. Unpublished data from Dr F. Mohammed (University of Birmingham).

This molecular change offers a possible explanation for disease pathogenesis driven by the M228T variant. In comparison, Haywood *et al* [37] found that the G111V variant had a larger impact on tertiary structure and thermal stability, whilst the A119T variant had a greater effect on the actin binding. These data suggest location of the variant will impact the structure of the protein and may lead to different modes of pathogenicity.

Future studies should further investigate the impact of this variant on the electric coupling of the cell; methods such as low-throughput patch clamping and microelectrode techniques can be used to measure cell currents on an isolated cell level, whilst optical mapping has been used to simultaneously and noninvasively measure the action potential morphology of a larger number of cells [133]. Investigating the electric changes would e.g. offer insight into why atrial fibrillation is a striking feature in patients with the *ACTN2* M228T variant [35].

To investigate the iPSC model further, cardiomyocytes should be matured until Day30 and beyond. This is when the cardiomyocytes are said to have sufficiently developed to more resemble adult cells *in vivo* in both their structure and function [134]. However, Day30 is not the endpoint, but a compromise between time and maturity. The engineered heart tissue (EHT) approach may offer greater cardiomyocyte maturity and so be a more mature model for cardiac pathology [135]. Staining sufficiently mature cells and imaging on a confocal microscope would give a better indication as to the sarcomeric structure and integrity, enabling better assessment of the *ACTN2* M228T line compared to the WT. Further staining for other sarcomeric markers such as titin, would help to understand how sarcomere structures are affected.

Morris *et al* (2020) [136] used MATLAB to create an automated method of quantitatively characterising Z-disc architecture; using such a technique would give further insight into the impact of the *ACTN2* M228T variant on Z-disc structure and would allow for a more robust comparison of sarcomeric structure against the WT line.

The methods used in this research are not definitive and other approaches may be more effective in measuring hypertrophy. Patch clamping is used to measure membrane capacitance [137], which is directly proportional to cell surface area and this can be used to measure level of hypertrophy of whole cells [138, 139]. Alternatively, pulsed-wave Doppler can take snapshots of the heart either during contraction or relaxation, which can then be used to measure wall thickness and therefore hypertrophy [140]. This method can be used to assess cardiac diastolic function, including isovolumic relaxation time (IVRT) [141]; an increased IVRT reflects impaired diastolic function and suggests increased hypertrophy [142]. This could be performed on adult mice to investigate any similarities or differences.

These future experiments will help to expand the insights into pathogenic mechanisms of the *ACTN2* M228T variant. Such insights into disease mechanisms are a prerequisite for developing tailored therapies to benefit affected patients.

6. References

1. Fukuta, H. and W.C. Little, *The cardiac cycle and the physiologic basis of left ventricular contraction, ejection, relaxation, and filling.* Heart Fail Clin, 2008. **4**(1): p. 1-11.
2. Litviňuková, M., et al., *Cells of the adult human heart.* Nature, 2020. **588**(7838): p. 466-472.
3. Gutstein, D.E., et al., *The organization of adherens junctions and desmosomes at the cardiac intercalated disc is independent of gap junctions.* J Cell Sci, 2003. **116**(Pt 5): p. 875-85.
4. Kleber, A.G. and J.E. Saffitz, *Role of the intercalated disc in cardiac propagation and arrhythmogenesis.* Front Physiol, 2014. **5**: p. 404.
5. Jongsma, H.J. and R. Wilders, *Gap junctions in cardiovascular disease.* Circ Res, 2000. **86**(12): p. 1193-7.
6. Sweeney, H.L. and D.W. Hammers, *Muscle Contraction.* Cold Spring Harb Perspect Biol, 2018. **10**(2).
7. Luther, P.K., *The vertebrate muscle Z-disc: sarcomere anchor for structure and signalling.* J Muscle Res Cell Motil, 2009. **30**(5-6): p. 171-85.
8. Henderson, C.A., et al., *Overview of the Muscle Cytoskeleton.* Compr Physiol, 2017. **7**(3): p. 891-944.
9. Watkins, H., H. Ashrafian, and C. Redwood, *Inherited cardiomyopathies.* N Engl J Med, 2011. **364**(17): p. 1643-56.
10. Savarese, M., et al., *Actininopathy: A new muscular dystrophy caused by ACTN2 dominant mutations.* Ann Neurol, 2019. **85**(6): p. 899-906.
11. Francula-Zaninovic, S. and I.A. Nola, *Management of Measurable Variable Cardiovascular Disease' Risk Factors.* Curr Cardiol Rev, 2018. **14**(3): p. 153-163.
12. Flora, G.D. and M.K. Nayak, *A Brief Review of Cardiovascular Diseases, Associated Risk Factors and Current Treatment Regimes.* Curr Pharm Des, 2019. **25**(38): p. 4063-4084.
13. Seferović, P.M., et al., *Heart failure in cardiomyopathies: a position paper from the Heart Failure Association of the European Society of Cardiology.* Eur J Heart Fail, 2019. **21**(5): p. 553-576.
14. Bauersachs, J., *Heart failure drug treatment: the fantastic four.* Eur Heart J, 2021. **42**(6): p. 681-683.
15. Seferović, P.M., M.M. Polovina, and A.J.S. Coats, *Heart failure in dilated non-ischaemic cardiomyopathy.* Eur Heart J Suppl, 2019. **21**(Suppl M): p. M40-M43.
16. McKenna, W.J., B.J. Maron, and G. Thiene, *Classification, Epidemiology, and Global Burden of Cardiomyopathies.* Circ Res, 2017. **121**(7): p. 722-730.
17. Husser, D., et al., *Prevalence of clinically apparent hypertrophic cardiomyopathy in Germany-An analysis of over 5 million patients.* PLoS One, 2018. **13**(5): p. e0196612.
18. Maron, B.J., et al., *Contemporary definitions and classification of the cardiomyopathies: an American Heart Association Scientific Statement from the Council on Clinical Cardiology, Heart Failure and Transplantation Committee; Quality of Care and Outcomes Research and Functional Genomics and Translational Biology Interdisciplinary Working Groups; and Council on Epidemiology and Prevention.* Circulation, 2006. **113**(14): p. 1807-16.

19. Robinson, P., et al., *Hypertrophic cardiomyopathy mutations increase myofilament Ca.* J Biol Chem, 2018. **293**(27): p. 10487-10499.
20. Sparrow, A.J., et al., *Measurement of Myofilament-Localized Calcium Dynamics in Adult Cardiomyocytes and the Effect of Hypertrophic Cardiomyopathy Mutations.* Circ Res, 2019. **124**(8): p. 1228-1239.
21. O'Mahony, C., P. Elliott, and W. McKenna, *Sudden cardiac death in hypertrophic cardiomyopathy.* Circ Arrhythm Electrophysiol, 2013. **6**(2): p. 443-51.
22. Herman, D.S., et al., *Truncations of titin causing dilated cardiomyopathy.* N Engl J Med, 2012. **366**(7): p. 619-28.
23. Duan, D., *Challenges and opportunities in dystrophin-deficient cardiomyopathy gene therapy.* Hum Mol Genet, 2006. **15 Spec No 2**: p. R253-61.
24. Olson, T.M., et al., *Metavinculin mutations alter actin interaction in dilated cardiomyopathy.* Circulation, 2002. **105**(4): p. 431-7.
25. Tucker, N.R., et al., *Novel Mutation in.* Circ Cardiovasc Genet, 2017. **10**(6).
26. *StatPearls*. 2021.
27. Wadmore, K., A.J. Azad, and K. Gehmlich, *The Role of Z-disc Proteins in Myopathy and Cardiomyopathy.* Int J Mol Sci, 2021. **22**(6).
28. Sjöblom, B., A. Salmazo, and K. Djinović-Carugo, *Alpha-actinin structure and regulation.* Cell Mol Life Sci, 2008. **65**(17): p. 2688-701.
29. Persechini, A., N.D. Moncrief, and R.H. Kretsinger, *The EF-hand family of calcium-modulated proteins.* Trends Neurosci, 1989. **12**(11): p. 462-7.
30. Ribeiro, E.e.A., et al., *The structure and regulation of human muscle α-actinin.* Cell, 2014. **159**(6): p. 1447-60.
31. Yang, J. and X. Xu, *α-Actinin2 is required for the lateral alignment of Z discs and ventricular chamber enlargement during zebrafish cardiogenesis.* FASEB J, 2012. **26**(10): p. 4230-42.
32. Theis, J.L., et al., *Echocardiographic-determined septal morphology in Z-disc hypertrophic cardiomyopathy.* Biochem Biophys Res Commun, 2006. **351**(4): p. 896-902.
33. Walsh, R., et al., *Reassessment of Mendelian gene pathogenicity using 7,855 cardiomyopathy cases and 60,706 reference samples.* Genet Med, 2017. **19**(2): p. 192-203.
34. Chiu, C., et al., *Mutations in alpha-actinin-2 cause hypertrophic cardiomyopathy: a genome-wide analysis.* J Am Coll Cardiol, 2010. **55**(11): p. 1127-35.
35. Girolami, F., et al., *Novel α-actinin 2 variant associated with familial hypertrophic cardiomyopathy and juvenile atrial arrhythmias: a massively parallel sequencing study.* Circ Cardiovasc Genet, 2014. **7**(6): p. 741-50.
36. Prondzynski, M., et al., *Disease modeling of a mutation in α-actinin 2 guides clinical therapy in hypertrophic cardiomyopathy.* EMBO Mol Med, 2019. **11**(12): p. e11115.
37. Haywood, N.J., et al., *Hypertrophic cardiomyopathy mutations in the calponin-homology domain of ACTN2 affect actin binding and cardiomyocyte Z-disc incorporation.* Biochem J, 2016. **473**(16): p. 2485-93.
38. Mohapatra, B., et al., *Mutations in the muscle LIM protein and alpha-actinin-2 genes in dilated cardiomyopathy and endocardial fibroelastosis.* Mol Genet Metab, 2003. **80**(1-2): p. 207-15.

39. Fan, L.L., et al., *Whole-Exome Sequencing Identifies a Novel Mutation (p.L320R) of Alpha-Actinin 2 in a Chinese Family with Dilated Cardiomyopathy and Ventricular Tachycardia.* Cytogenet Genome Res, 2019. **157**(3): p. 148-152.
40. Bagnall, R.D., et al., *Exome sequencing identifies a mutation in the ACTN2 gene in a family with idiopathic ventricular fibrillation, left ventricular noncompaction, and sudden death.* BMC Med Genet, 2014. **15**: p. 99.
41. North, K.N., et al., *A common nonsense mutation results in alpha-actinin-3 deficiency in the general population.* Nat Genet, 1999. **21**(4): p. 353-4.
42. Hogarth, M.W., et al., *Analysis of the ACTN3 heterozygous genotype suggests that α-actinin-3 controls sarcomeric composition and muscle function in a dose-dependent fashion.* Hum Mol Genet, 2016. **25**(5): p. 866-77.
43. Milani-Nejad, N. and P.M. Janssen, *Small and large animal models in cardiac contraction research: advantages and disadvantages.* Pharmacol Ther, 2014. **141**(3): p. 235-49.
44. Elnakish, M.T., H.H. Hassanain, and P.M. Janssen, *Vascular remodeling-associated hypertension leads to left ventricular hypertrophy and contractile dysfunction in profilin-1 transgenic mice.* J Cardiovasc Pharmacol, 2012. **60**(6): p. 544-52.
45. Fischer, R., et al., *Angiotensin II-induced sudden arrhythmic death and electrical remodeling.* Am J Physiol Heart Circ Physiol, 2007. **293**(2): p. H1242-53.
46. Moon, H., et al., *Noninvasive assessment of myocardial inflammation by cardiovascular magnetic resonance in a rat model of experimental autoimmune myocarditis.* Circulation, 2012. **125**(21): p. 2603-12.
47. Savoji, H., et al., *Cardiovascular disease models: A game changing paradigm in drug discovery and screening.* Biomaterials, 2019. **198**: p. 3-26.
48. Gupta, V., et al., *α-Actinin-2 deficiency results in sarcomeric defects in zebrafish that cannot be rescued by α-actinin-3 revealing functional differences between sarcomeric isoforms.* FASEB J, 2012. **26**(5): p. 1892-908.
49. Lornage, X., et al., *ACTN2 mutations cause "Multiple structured Core Disease" (MsCD).* Acta Neuropathol, 2019. **137**(3): p. 501-519.
50. Krishnan, A., et al., *A detailed comparison of mouse and human cardiac development.* Pediatr Res, 2014. **76**(6): p. 500-7.
51. Clowes, C., et al., *The functional diversity of essential genes required for mammalian cardiac development.* Genesis, 2014. **52**(8): p. 713-37.
52. van den Berg, G., *Growth of the developing heart*. 2011, University of Amsterdam: UvA-DARE (Digital Academic Repository). p. 149-170.
53. Savolainen, S.M., J.F. Foley, and S.A. Elmore, *Histology atlas of the developing mouse heart with emphasis on E11.5 to E18.5.* Toxicol Pathol, 2009. **37**(4): p. 395-414.
54. Soonpaa, M.H., et al., *Cardiomyocyte DNA synthesis and binucleation during murine development.* Am J Physiol, 1996. **271**(5 Pt 2): p. H2183-9.
55. Stuckmann, I., S. Evans, and A.B. Lassar, *Erythropoietin and retinoic acid, secreted from the epicardium, are required for cardiac myocyte proliferation.* Dev Biol, 2003. **255**(2): p. 334-49.
56. Dirkx, E., P.A. da Costa Martins, and L.J. De Windt, *Regulation of fetal gene expression in heart failure.* Biochim Biophys Acta, 2013. **1832**(12): p. 2414-24.
57. Cox, E.J. and S.A. Marsh, *A systematic review of fetal genes as biomarkers of cardiac hypertrophy in rodent models of diabetes.* PLoS One, 2014. **9**(3): p. e92903.

58. Angrisano, T., et al., *Epigenetic switch at atp2a2 and myh7 gene promoters in pressure overload-induced heart failure.* PLoS One, 2014. **9**(9): p. e106024.
59. Gerçek, M., et al., *Cardiomyocyte Hypertrophy in Arrhythmogenic Cardiomyopathy.* Am J Pathol, 2017. **187**(4): p. 752-766.
60. Wobus, A.M., G. Wallukat, and J. Hescheler, *Pluripotent mouse embryonic stem cells are able to differentiate into cardiomyocytes expressing chronotropic responses to adrenergic and cholinergic agents and Ca2+ channel blockers.* Differentiation, 1991. **48**(3): p. 173-82.
61. Nir, S.G., et al., *Human embryonic stem cells for cardiovascular repair.* Cardiovasc Res, 2003. **58**(2): p. 313-23.
62. Karakikes, I., et al., *Human induced pluripotent stem cell-derived cardiomyocytes: insights into molecular, cellular, and functional phenotypes.* Circ Res, 2015. **117**(1): p. 80-8.
63. Sharma, A., J.C. Wu, and S.M. Wu, *Induced pluripotent stem cell-derived cardiomyocytes for cardiovascular disease modeling and drug screening.* Stem Cell Res Ther, 2013. **4**(6): p. 150.
64. Zhao, M., et al., *Deciphering Role of Wnt Signalling in Cardiac Mesoderm and Cardiomyocyte Differentiation from Human iPSCs: Four-dimensional control of Wnt pathway for hiPSC-CMs differentiation.* Sci Rep, 2019. **9**(1): p. 19389.
65. Kreuser, U., et al., *Initial WNT/β-Catenin Activation Enhanced Mesoderm Commitment, Extracellular Matrix Expression, Cell Aggregation and Cartilage Tissue Yield From Induced Pluripotent Stem Cells.* Front Cell Dev Biol, 2020. **8**: p. 581331.
66. Denning, C., et al., *Cardiomyocytes from human pluripotent stem cells: From laboratory curiosity to industrial biomedical platform.* Biochim Biophys Acta, 2016. **1863**(7 Pt B): p. 1728-48.
67. Geyer, S.H., et al., *A staging system for correct phenotype interpretation of mouse embryos harvested on embryonic day 14 (E14.5).* J Anat, 2017. **230**(5): p. 710-719.
68. Bhattacharya, S., et al., *High efficiency differentiation of human pluripotent stem cells to cardiomyocytes and characterization by flow cytometry.* J Vis Exp, 2014(91): p. 52010.
69. Schneider, C.A., W.S. Rasband, and K.W. Eliceiri, *NIH Image to ImageJ: 25 years of image analysis.* Nat Methods, 2012. **9**(7): p. 671-5.
70. Latchman, D.S., *Heat shock proteins and cardiac protection.* Cardiovasc Res, 2001. **51**(4): p. 637-46.
71. Schuld, J., et al., *Homozygous expression of the myofibrillar myopathy-associated p.W2710X filamin C variant reveals major pathomechanisms of sarcomeric lesion formation.* Acta Neuropathol Commun, 2020. **8**(1): p. 154.
72. Jiang, H., et al., *Functional analysis of a gene-edited mouse model to gain insights into the disease mechanisms of a titin missense variant.* Basic Res Cardiol, 2021. **116**(1): p. 14.
73. *Characteristics of Early and Late Adult C57BL/6NCrl Mice*. Charles River: https://www.criver.com/sites/default/files/resource-files/RM-C57BL6-Aged-Mouse-Ebook.pdf. p. 57.
74. Reynolds, T.H., et al., *The impact of age and sex on body composition and glucose sensitivity in C57BL/6J mice.* Physiol Rep, 2019. **7**(3): p. e13995.
75. Konhilas, J.P., et al., *Sex modifies exercise and cardiac adaptation in mice.* Am J Physiol Heart Circ Physiol, 2004. **287**(6): p. H2768-76.

76. Haroon, J., et al., *Gender differences in normal left ventricle of adult FVB/N mice due to variation in interleukins and natriuretic peptides expression levels.* Cytokine, 2015. **71**(1): p. 54-9.
77. Grison, M., et al., *α-Actinin/titin interaction: A dynamic and mechanically stable cluster of bonds in the muscle Z-disk.* Proc Natl Acad Sci U S A, 2017. **114**(5): p. 1015-1020.
78. Zhang, Z., et al., *Distinct subcellular mechanisms for the enhancement of the surface membrane expression of SK2 channel by its interacting proteins, α-actinin2 and filamin A.* J Physiol, 2017. **595**(7): p. 2271-2284.
79. Cukovic, D., et al., *A discrete amino terminal domain of Kv1.5 and Kv1.4 potassium channels interacts with the spectrin repeats of alpha-actinin-2.* FEBS Lett, 2001. **498**(1): p. 87-92.
80. Barber, R.D., et al., *GAPDH as a housekeeping gene: analysis of GAPDH mRNA expression in a panel of 72 human tissues.* Physiol Genomics, 2005. **21**(3): p. 389-95.
81. Taegtmeyer, H., S. Sen, and D. Vela, *Return to the fetal gene program: a suggested metabolic link to gene expression in the heart.* Ann N Y Acad Sci, 2010. **1188**: p. 191-8.
82. Razeghi, P., et al., *Metabolic gene expression in fetal and failing human heart.* Circulation, 2001. **104**(24): p. 2923-31.
83. Olivé, M., et al., *Expression of mutant ubiquitin (UBB+1) and p62 in myotilinopathies and desminopathies.* Neuropathol Appl Neurobiol, 2008. **34**(1): p. 76-87.
84. Selcen, D. and A.G. Engel, *Mutations in myotilin cause myofibrillar myopathy.* Neurology, 2004. **62**(8): p. 1363-71.
85. Sharma, S., P.G. Jackson, and J. Makan, *Cardiac troponins.* J Clin Pathol, 2004. **57**(10): p. 1025-6.
86. Hasler, S., et al., *Elevated high-sensitivity troponin T levels are associated with adverse cardiac remodelling and myocardial fibrosis in hypertrophic cardiomyopathy.* Swiss Med Wkly, 2016. **146**: p. w14285.
87. Apple, F.S., *Tissue specificity of cardiac troponin I, cardiac troponin T and creatine kinase-MB.* Clin Chim Acta, 1999. **284**(2): p. 151-9.
88. Martin, J.L., et al., *Small heat shock proteins and protection against ischemic injury in cardiac myocytes.* Circulation, 1997. **96**(12): p. 4343-8.
89. Mymrikov, E.V., A.S. Seit-Nebi, and N.B. Gusev, *Large potentials of small heat shock proteins.* Physiol Rev, 2011. **91**(4): p. 1123-59.
90. Herwig, M., et al., *Modulation of Titin-Based Stiffness in Hypertrophic Cardiomyopathy via Protein Kinase D.* Front Physiol, 2020. **11**: p. 240.
91. Schuldt, M., et al., *Sex-Related Differences in Protein Expression in Sarcomere Mutation-Positive Hypertrophic Cardiomyopathy.* Front Cardiovasc Med, 2021. **8**: p. 612215.
92. Wu, T., et al., *HSPB7 is indispensable for heart development by modulating actin filament assembly.* Proc Natl Acad Sci U S A, 2017. **114**(45): p. 11956-11961.
93. Hu, X., et al., *The protective role of small heat shock proteins in cardiac diseases: key role in atrial fibrillation.* Cell Stress Chaperones, 2017. **22**(4): p. 665-674.
94. Krief, S., et al., *Identification and characterization of cvHsp. A novel human small stress protein selectively expressed in cardiovascular and insulin-sensitive tissues.* J Biol Chem, 1999. **274**(51): p. 36592-600.

95. Liao, W.C., et al., *HSPB7 prevents cardiac conduction system defect through maintaining intercalated disc integrity.* PLoS Genet, 2017. **13**(8): p. e1006984.
96. Ehsan, M., et al., *Mutant Muscle LIM Protein C58G causes cardiomyopathy through protein depletion.* J Mol Cell Cardiol, 2018. **121**: p. 287-296.
97. Wu, J., et al., *Gender Differences in Cardiac Hypertrophy.* J Cardiovasc Transl Res, 2020. **13**(1): p. 73-84.
98. Mercer, E.J., et al., *Hspb7 is a cardioprotective chaperone facilitating sarcomeric proteostasis.* Dev Biol, 2018. **435**(1): p. 41-55.
99. Leinwand, L.A., *Sex is a potent modifier of the cardiovascular system.* J Clin Invest, 2003. **112**(3): p. 302-7.
100. Freeman, K., et al., *Progression from hypertrophic to dilated cardiomyopathy in mice that express a mutant myosin transgene.* Am J Physiol Heart Circ Physiol, 2001. **280**(1): p. H151-9.
101. Tardiff, J.C., et al., *Cardiac troponin T mutations result in allele-specific phenotypes in a mouse model for hypertrophic cardiomyopathy.* J Clin Invest, 1999. **104**(4): p. 469-81.
102. Lakdawala, N.K., et al., *Associations Between Female Sex, Sarcomere Variants, and Clinical Outcomes in Hypertrophic Cardiomyopathy.* Circ Genom Precis Med, 2021. **14**(1): p. e003062.
103. Ghiselli, L., et al., *Sex-related differences in exercise performance and outcome of patients with hypertrophic cardiomyopathy.* Eur J Prev Cardiol, 2020. **27**(17): p. 1821-1831.
104. Nováková, M., et al., *Mouse Model of Congenital Heart Defects, Dysmorphic Facial Features and Intellectual Developmental Disorders as a Result of Non-functional CDK13.* Front Cell Dev Biol, 2019. **7**: p. 155.
105. von Nandelstadh, P., et al., *Analysis of myotilin turnover provides mechanistic insight into the role of myotilinopathy-causing mutations.* Biochem J, 2011. **436**(1): p. 113-21.
106. Vignier, N., et al., *Nonsense-mediated mRNA decay and ubiquitin-proteasome system regulate cardiac myosin-binding protein C mutant levels in cardiomyopathic mice.* Circ Res, 2009. **105**(3): p. 239-48.
107. Park, J., et al., *Case Report: Novel Likely Pathogenic.* Front Pediatr, 2021. **9**: p. 609389.
108. Seto, J.T., et al., *Deficiency of α-actinin-3 is associated with increased susceptibility to contraction-induced damage and skeletal muscle remodeling.* Hum Mol Genet, 2011. **20**(15): p. 2914-27.
109. MacArthur, D.G., et al., *Loss of ACTN3 gene function alters mouse muscle metabolism and shows evidence of positive selection in humans.* Nat Genet, 2007. **39**(10): p. 1261-5.
110. O'Sullivan, L.R., M.R. Cahill, and P.W. Young, *The Importance of Alpha-Actinin Proteins in Platelet Formation and Function, and Their Causative Role in Congenital Macrothrombocytopenia.* Int J Mol Sci, 2021. **22**(17).
111. Xie, G.F., et al., *High ACTN1 Is Associated with Poor Prognosis, and ACTN1 Silencing Suppresses Cell Proliferation and Metastasis in Oral Squamous Cell Carcinoma.* Drug Des Devel Ther, 2020. **14**: p. 1717-1727.
112. Liu, X. and K.M. Chu, *α-Actinin-4 promotes metastasis in gastric cancer.* Lab Invest, 2017. **97**(9): p. 1084-1094.

113. Kakuya, T., et al., *Prognostic significance of gene amplification of ACTN4 in stage I and II oral tongue cancer.* Int J Oral Maxillofac Surg, 2017. **46**(8): p. 968-976.
114. Frank, D., et al., *Cardiac α-Actin (ACTC1) Gene Mutation Causes Atrial-Septal Defects Associated With Late-Onset Dilated Cardiomyopathy.* Circ Genom Precis Med, 2019. **12**(8): p. e002491.
115. Kumar, A., et al., *Rescue of cardiac alpha-actin-deficient mice by enteric smooth muscle gamma-actin.* Proc Natl Acad Sci U S A, 1997. **94**(9): p. 4406-11.
116. Man, J., P. Barnett, and V.M. Christoffels, *Structure and function of the Nppa-Nppb cluster locus during heart development and disease.* Cell Mol Life Sci, 2018. **75**(8): p. 1435-1444.
117. Sergeeva, I.A., et al., *A transgenic mouse model for the simultaneous monitoring of ANF and BNP gene activity during heart development and disease.* Cardiovasc Res, 2014. **101**(1): p. 78-86.
118. Izumo, S., B. Nadal-Ginard, and V. Mahdavi, *Protooncogene induction and reprogramming of cardiac gene expression produced by pressure overload.* Proc Natl Acad Sci U S A, 1988. **85**(2): p. 339-43.
119. Kuwahara, K., T. Nishikimi, and K. Nakao, *Transcriptional regulation of the fetal cardiac gene program.* J Pharmacol Sci, 2012. **119**(3): p. 198-203.
120. Chien, K.R., et al., *Regulation of cardiac gene expression during myocardial growth and hypertrophy: molecular studies of an adaptive physiologic response.* FASEB J, 1991. **5**(15): p. 3037-46.
121. Fang, X., et al., *cAMP induces hypertrophy and alters DNA methylation in HL-1 cardiomyocytes.* Am J Physiol Cell Physiol, 2015. **309**(6): p. C425-36.
122. Ciechanover, A., *Intracellular protein degradation: from a vague idea thru the lysosome and the ubiquitin-proteasome system and onto human diseases and drug targeting.* Biochim Biophys Acta, 2012. **1824**(1): p. 3-13.
123. Hassoun, R., et al., *Stress activated signalling impaired protein quality control pathways in human hypertrophic cardiomyopathy.* Int J Cardiol, 2021.
124. Zhang, X., et al., *Involvement of reductive stress in the cardiomyopathy in transgenic mice with cardiac-specific overexpression of heat shock protein 27.* Hypertension, 2010. **55**(6): p. 1412-7.
125. Liu, S., et al., *Effect of Hsp27 on early embryonic development in the mouse.* Reprod Biomed Online, 2013. **26**(5): p. 491-9.
126. Song, S., et al., *Filamin C in cardiomyopathy: from physiological roles to DNA variants.* Heart Fail Rev, 2021.
127. Mao, Z. and F. Nakamura, *Structure and Function of Filamin C in the Muscle Z-Disc.* Int J Mol Sci, 2020. **21**(8).
128. Swist, S., et al., *Maintenance of sarcomeric integrity in adult muscle cells crucially depends on Z-disc anchored titin.* Nat Commun, 2020. **11**(1): p. 4479.
129. Masui, S., et al., *Pluripotency governed by Sox2 via regulation of Oct3/4 expression in mouse embryonic stem cells.* Nat Cell Biol, 2007. **9**(6): p. 625-35.
130. Spray, D.C. and J.M. Burt, *Structure-activity relations of the cardiac gap junction channel.* Am J Physiol, 1990. **258**(2 Pt 1): p. C195-205.
131. Sallé, L. and F. Brette, *T-tubules: a key structure of cardiac function and dysfunction.* Arch Mal Coeur Vaiss, 2007. **100**(3): p. 225-30.

132. Lecker, S.H., A.L. Goldberg, and W.E. Mitch, *Protein degradation by the ubiquitin-proteasome pathway in normal and disease states.* J Am Soc Nephrol, 2006. **17**(7): p. 1807-19.
133. Du, D.T., et al., *Action potential morphology of human induced pluripotent stem cell-derived cardiomyocytes does not predict cardiac chamber specificity and is dependent on cell density.* Biophys J, 2015. **108**(1): p. 1-4.
134. Karbassi, E., et al., *Cardiomyocyte maturation: advances in knowledge and implications for regenerative medicine.* Nat Rev Cardiol, 2020. **17**(6): p. 341-359.
135. Leonard, A., et al., *Afterload promotes maturation of human induced pluripotent stem cell derived cardiomyocytes in engineered heart tissues.* J Mol Cell Cardiol, 2018. **118**: p. 147-158.
136. Morris, T.A., et al., *Striated myocyte structural integrity: Automated analysis of sarcomeric z-discs.* PLoS Comput Biol, 2020. **16**(3): p. e1007676.
137. Hill, C.L. and G.J. Stephens, *An Introduction to Patch Clamp Recording.* Methods Mol Biol, 2021. **2188**: p. 1-19.
138. Kamei, K., et al., *Comprehensive analyses of arrhythmogenic substrates and vulnerability to ventricular tachycardia in left ventricular hypertrophy in salt-sensitive hypertensive rats.* Circ J, 2007. **71**(3): p. 390-6.
139. Shipsey, S.J., S.M. Bryant, and G. Hart, *Effects of hypertrophy on regional action potential characteristics in the rat left ventricle: a cellular basis for T-wave inversion?* Circulation, 1997. **96**(6): p. 2061-8.
140. Anavekar, N.S. and J.K. Oh, *Doppler echocardiography: a contemporary review.* J Cardiol, 2009. **54**(3): p. 347-58.
141. Fennira, S., et al., *[Pulse-wave Doppler Tissue Imaging in the assessment of regional left ventricular diastolic function in patients with coronary artery disease].* Tunis Med, 2010. **88**(7): p. 492-6.
142. Reeder, G.S., et al., *Use of Doppler techniques (continuous-wave, pulsed-wave, and color flow imaging) in the noninvasive hemodynamic assessment of congenital heart disease.* Mayo Clin Proc, 1986. **61**(9): p. 725-44.